Transport and (bio)geochemical processes at cold seeps of the Makran convergent margin

Dissertation
zur Erlangung des Doktorgrades der Naturwissenschaften
(Dr. rer. nat.)

dem Fachbereich 5 (Geowissenschaften) der Universität
Bremen vorgelegt von

David Fischer

Bremen, November 2011

1. Gutachterin: Frau PD Dr. habil. Sabine Kasten

2. Gutachter: Herr Prof. Dr. Gerhard Bohrmann

PREFACE

This study was conducted in the framework of the Research Center/Cluster of Excellence “The Oceans in the Earth System” (MARUM) funded by the Deutsche Forschungsgemeinschaft as part of projects E1 “Structure and dynamics of cold seeps, associated communities and mineral precipitates” (previous funding period) and GB6 “Mineral authigenesis and organomineralization” (funding period July 2009-June 2013). Financial support was also provided by the Helmholtz Association (Alfred Wegener Institute for Polar and Marine Research, AWI, Bremerhaven). The present work is submitted as dissertation and was supervised by PD Dr. habil. Sabine Kasten (AWI).

With this thesis I wish to contribute to the understanding of the pore water and solid phase geochemistry and early diagenetic processes at marine hydrocarbon seeps. The thesis and involved laboratory work has been carried out jointly at the *MARUM-Center for Marine Environmental Sciences at the University of Bremen*, at the *Alfred Wegener Institute for Polar and Marine Research* in Bremerhaven and at the *University of Newcastle* between 2008 and 2011. In chapter 1 I give a detailed introduction into the scientific background related to the work discussed in later chapters. Chapters 2, 3, and 4 comprise three manuscripts that are in review with, submitted to, or in preparation for submission to international peer-reviewed journals, respectively. Chapter 5 lists the titles and abstracts of published co-author papers. Chapter 6 summarizes the main outcome of the present thesis and provides a brief outlook to what future scientific work in the field of cold seep biogeochemistry may be worth focusing on. Any published literature cited in this thesis appears in the references. In order to ease readability, all chapters close with an own reference section.

The thesis comprises three independent studies conducted on sediment and pore water samples collected during cruise M74/3 of the R/V METEOR in 2007. All studies presented here were designed and mainly written by myself (supervised by Sabine Kasten) and benefited from the contribution of the respective co-authors in discussion of data and/or writing. To the first study (chapter 2) I contributed sampling onboard ship and measurements of all discussed pore water parameters. Heiko Sahling and Heide Schulz-Vogt conducted identification of macrofauna. Kerstin Nöthen assisted in pore water modeling. The study is currently under peer-review with the journal "*Biogeosciences*" and has been published as a discussion paper in

"*Biogeosciences Discussions*". The second manuscript (chapter 3) deals with pore water data produced by myself and Matthias Zabel, and solid phase data that were produced by myself assisted by Rubén Alvaréz. The pore water model was set-up by José Mogollón with contributions of myself. Michael Strasser and Gerhard Bohrmann contributed to data interpretation and writing of the manuscript. The manuscript has been submitted for peer-review to the journal "*Nature Geoscience*". The third study (chapter 4) deals with an extended set of pore water data used in the second study and additional solid phase data. Sequential iron extractions were conducted by myself under supervision of Simon Poulton. TIC/TOC data were produced by Hella Buschhoff. The third study is currently in preparation for submission to the journal "*Chemical Geology*". Two further studies that I have contributed to as a co-author during the PhD-phase were published in the journals "*Biogeosciences*" in 2010 and "*Geochemistry, Geophysics and Geosystems*" in 2011. These co-author manuscripts were written by the respective first-authors and I contributed to sample collection onboard ship, pore water analyses, discussion of data and writing.

TABLE OF CONTENTS

Thesis Summary

Cold seeps are sites of upward transport and biogeochemical turnover of hydrocarbons, which leads to a condensed geochemical zonation in the pore water and influences element cycling in the shallow sub-surface sediment. Due to the upward transport and high concentrations of hydrocarbons dominated by methane, cold seeps often host shallow gas hydrates and unique chemosynthetic communities that thrive on redox-products released to the pore water by the microbial consumption of methane. At the same time, these redox-products (bicarbonate and hydrogen sulfide) foster mineral authigenesis which alters the sediment composition.

The present thesis focuses on pore water transport and geochemical processes including mineral authigenesis at hydrocarbon seeps of the Makran convergent margin, which is characterized by a stable oxygen minimum zone (OMZ) between depths of ~150-1000 m limiting oxygen availability for metazoan respiration. The local continental slope architecture comprises a set of near-parallel accretionary ridges. Four hydrocarbon seeps located along a downslope OMZ-transect and expelling gas bubbles into the water column were investigated to study the interaction of bottom water redox, methane seepage, and chemosynthetic communities. Seeps within the core-OMZ were devoid of metazoans. Thus, the so-called bioirrigation, which is a process understood as organisms irrigating bottom water into the upper sediment, was absent. In contrast, sites below the core-OMZ were characterized by vast communities of vesicomyid clams and ampharetid polychaetes. Rates of the counteracting transport processes fluid advection and bioirrigation were quantified using a numerical nonsteady state pore water model, which revealed that the biota most efficiently balance the upward advection of hydrogen sulfide-rich fluids by pumping oxic and sulfate-rich water into the sediment. This process steepens pore water gradients and hence amplifies rates of sulfate reduction via anaerobic oxidation of methane leading to the release of hydrogen sulfide at a defined depth. Hydrogen sulfide is toxic for metazoans, but it is needed for respiration by thiotrophic endosymbionts in the clams and polychaetes. The animals thus engineer their habitats by expanding the sulfate-zone deeper into the sediment and strongly control solute fluxes and

turnover. Geologically induced fluid advection is controlled by biological activity at the sea floor, provided that the bottom water is oxic and thus supports higher life.

Pore water modeling and bulk sediment analyses of gravity cores obtained from two sites at the youngest accretionary ridge (Nascent Ridge) at the Makran convergent margin were conducted. Calculations of the time necessary to form observed authigenic barium enrichments and nonsteady state pore water modeling revealed that the upward methane flux has drastically increased about 60-90 years before present. In 1945, which is 62 years before coring, the strongest and shallowest earthquake ever recorded for the northern Arabian Sea occurred at a distance of a few tens of kilometers to Nascent Ridge. The solid-phase barium enrichments and nonsteady state pore water profiles were interpreted to reflect a major event of gas injection into the shallow sub-surface that significantly shifted the sulfate/methane transition (SMT) towards the sediment surface and amplified, and triggered gas transfer from the sea floor into the water column. Further evidence for this event is based on the examined distribution of bulk iron species. Using a sequential extraction method, it was possible to discriminate between different iron species and it could be shown that although the pore water was sulfidic, relatively abundant iron bound as iron-(oxyhydr)oxides was present. If the pore water had been sulfidic for a longer time, most of the iron-(oxyhydr)oxides should have been converted into pyrite, which is the reduced end-member species in iron diagenesis. At one of the investigated sites at Nascent Ridge, a sulfidization front was found that clearly separated ferrimagnetic iron-(oxyhydr)oxides near the sediment surface from paramagnetic iron-sulfides below the reaction front. Considering published seismo-acoustic data obtained from Nascent Ridge the emerging synthesis of the above findings led to conclude, that the earthquake in 1945 exerted shear-stress and fractured sediments and gas hydrates that trapped free gas underneath. As soon as the capping layers were fractured, the gas ascended into the gas hydrate stability zone and crystallized as gas hydrates as long as interstitial water was available to form the clathrate cage. Further free gas migrated upwards along earthquake-induced pathways and punctually escaped into the water column, which we still observed 62 years after the event. During the described event, the SMT was rapidly pushed towards the sediment surface and released hydrogen sulfide in sediment intervals that had been located within the suboxic, i.e. non-sulfidic zone before, which led to the observed partial reduction of iron minerals. It is proposed that earthquakes can produce migration pathways for

free gas trapped underneath gas hydrates and should be considered in local and global budgets of atmospheric carbon, for example CO_2 and CH_4, which act as greenhouse gases.

Considering the functioning of the geochemistry at cold seeps, this thesis provides an improved understanding of counteracting pore water transport processes at the sediment/water interface and the activity of related chemosynthetic organisms. It further shows that the combination of calculated ages of authigenic barium enrichments together with nonsteady state pore water modeling can accurately document events of upward SMT migration. Finally, earthquakes fracturing gas hydrate-cemented sediments could be identified as a further trigger mechanism for seepage.

Kurzfassung

Kalte Quellen von kohlenwasserstoffreichen Fluiden, im Folgenden *cold seeps* genannt, sind durch den Aufstieg und biogeochemischen Umsatz von Methan in den obersten Stockwerken mariner Sedimente charakterisiert. Dies beeinflusst Elementkreisläufe und führt dazu, dass die geochemische Zonierung im Sediment kondensiert wird. Durch den aufwärtsgerichteten Transport von methanreichen Fluiden können cold seeps zum einen Gashydrate und zum anderen einzigartige chemosynthetische Gemeinschaften beherbergen, welche auf die Freisetzung von Redox-Produkten angewiesen sind, die beim Umsatz von Methan entstehen. Gleichzeitig können diese Produkte (Hydrogenkarbonat und Schwefelwasserstoff) zur Authigenese von Mineralen führen, was die Zusammensetzung des Sediments verändert.

Die vorliegende Dissertation beschäftigt sich mit Prozessen des Porenwasser-Transports, der Geochemie und der Mineralauthigenese in seep-beeinflussten Sedimenten des konvergenten Makran Kontinentalhanges. Dieser ist durch eine sehr stabile Sauerstoffminimumzone (OMZ) in einer Tiefe von ca. 150-1000 m in der Wassersäule charakterisiert, die die Verfügbarkeit von Sauerstoff für Metazoen stark einschränkt. Die lokale Hangarchitektur umfasst eine Anordnung küsten-paralleler Akkretionsrücken. Vier aktive cold seeps wurden entlang eines Transekts hangabwärts durch die OMZ untersucht, um die Interaktion von Bodenwasser Redox-Milieu, Methanausstoß und chemosynthetischen Gemeinschaften zu untersuchen. Seeps innerhalb der Kernzone der OMZ waren frei von Metazoen. Daher fand Bioirrigation, welche als aktives Spülen des oberen Sediments mit Bodenwasser durch Organismen beschrieben ist, nicht statt. Seeps unterhalb der Kernzone der OMZ waren jedoch durch vesicomyide Muscheln und ampharetide Polychäten in Form von großen Kolonien besiedelt. Die Raten der entgegengerichteten Transportprozesse Advektion und Bioirrigation wurden mit Hilfe eines numerischen nonsteady state Porenwassermodells quantifiziert. Es zeigte sich, dass die Organismen an der Sedimentoberfläche die aufwärtsgerichtete Advektion schwefelwasserstoffreicher Fluide sehr effizient ausgleichen, indem sie oxisches, sulfatreiches Bodenwasser ins Sediment pumpen. Dieser Prozess verstärkt durch die Versteilung der Porenwassergradienten den Umsatz von Sulfat im Zuge der anaeroben

Oxidation von Methan und führte zu einer definierten Tiefe der Schwefelwasserstoff Freisetzung. Schwefelwasserstoff ist für vielzelliges Leben zwar toxisch, wird aber von den chemosynthetischen Muscheln und Polychaeten an der Sedimentoberfläche benötigt, um ihre thiotrophen Symbionten zu versorgen. Die Tiere manipulieren auf diese Weise ihr Habitat, indem sie die Sulfatzone erweitern und kontrollieren gleichzeitig Fluss und Umsatz der gelösten Stoffe. Geologisch angetriebene Fluidadvektion wird durch biologische Aktivität am und im Meeresboden kompensiert, vorausgesetzt Sauerstoff ist verfügbar.

Porenwasser- und Festphasenanalysen wurden an Schwerelotkernen durchgeführt, die von zwei Stellen auf dem jüngsten akkretionären Rücken (Nascent Ridge) am konvergenten Makran Kontinentalhang gewonnen wurden. Die berechnete Zeit zur Bildung der gefundenen Bariumanreicherungen in der sedimentären Festphase und die Modellierung der Sulfatprofile zeigten, dass der aufwärtsgerichtete Methanfluss vor 60-90 Jahren drastisch zugenommen haben muss. Im Jahr 1945, das heißt 62 Jahre vor der Kerngewinnung, ereignete sich das stärkste und gleichzeitig flachste Erdbeben, dass je im nördlichen Arabischen Meer registriert wurde, nur wenige Zehner Kilometer von Nascent Ridge entfernt. Die Bariumanreicherungen und die Ergebnisse der Porenwassermodellierung wurden als Anzeiger für ein massives Gasmigrationsereignis interpretiert, welches die Sulfat/Methan Übergangszone (SMT) stark In Richtung Sedimentoberfläche verlagerte und das Austreten von freiem Gas am Meeresboden verstärkte, oder gar verursachte. Unterstützt wird diese These durch die untersuchte Verteilung von Eisen-Spezies in der Festphase an den oben genannten Stationen. Durch die Anwendung einer sequentiellen Eisenextraktion war es möglich, zwischen verschiedenen Eisenphasen zu unterscheiden und es konnte gezeigt werden, dass trotz sulfidischer Bedingungen im Porenwasser noch große Mengen an Eisen(oxyhydr)oxiden im Sediment vorhanden waren. Wäre das Porenwasser bereits für längere (geologische) Zeit sulfidisch gewesen, so hätten die meisten Eisen(oxyhydr)oxide bereits in Pyrit umgewandelt worden sein müssen, welches das reduzierte Endglied in der Eisendiagenese darstellt. Für einen weiteren Sedimentkern, der wenige km östlich gewonnen wurde, konnte ein ähnliches Szenario entwickelt werden. In diesem Kern wurde allerdings eine deutliche Sulfidisierungsfront gefunden, die ferrimagnetische Eisen(oxyhydr)oxide nahe der Sedimentoberfläche von paramagnetischen Eisensulfiden unterhalb der Front

trennte. Unter Berücksichtigung publizierter seismo-akustischer Daten, die genau im Untersuchungsgebiet gewonnen wurden, führte die Synthese aus den oben angeführten Funden zu dem Schluss, dass das Erdbeben im Jahr 1945 gashydrat-zementierte Sedimente zerscherte und dadurch unterliegendes freies Gas mobilisierte. Sobald die überlagernden Schichten zerschert waren, migrierte dieses Gas in die Gashydratstabilitätszone und bildete neues Gashydrat so lange ausreichend Wasser zur Bildung des Klathratkäfigs zur Verfügung stand. Darüber hinaus migrierte weiteres Gas entlang von vom Erdbeben verursachten Schwächezonen nach oben und entwich stellenweise in die Wassersäule, was wir 62 Jahre nach diesem Ereignis immer noch beobachten konnten. Während des beschriebenen Prozesses wurde die SMT sehr schnell nach oben verlagert und setzte Sedimente, die vorher lediglich in der suboxischen Zone lagen, dem Schwefelwasserstoff aus, was zur beobachteten, aber unvollständigen Reduktion von Eisenmineralen führte. Unter Berücksichtigung dieser Funde wird vorgeschlagen, dass das Erdbeben Migrationspfade für freies Gas bildete, welches vorher unter Gashydraten gefangen war. Aus diesem Grund sollte der Prozess der Kohlenwasserstoffmobilisierung durch Erdbeben in lokalen und globalen Bilanzen für atmosphärischen Kohlenstoff berücksichtigt werden, zum Beispiel von CO_2 und CH_4, welche als Treibhausgase fungieren.

Im Hinblick auf die geochemische Funktionsweise von cold seeps verbessern die Studien, die in dieser Dissertation dargestellt sind, unser Verständnis von einander entgegen gerichteten Porenwassertransportprozessen an der Sediment/Wasser Grenzschicht und der Aktivität der beteiligten chemosynthetischen Organismen. Des Weiteren zeigt die Arbeit, dass die Kombination von berechneten Bildungszeiten von authigen gebildeten Bariumanreicherungen in Verbindung mit der Modellierung von Porenwasserprofilen eine aufwärts gerichtete Migration der SMT dokumentieren können. Außerdem konnte gezeigt werden, dass Erdbeben einen weiteren Auslösemechanismus für cold seeps darstellen.

Chapter I – General Introduction: Setting the Scene

Although our planet is covered with water by around 70%, we call it "Earth". While research provided comprehensive insights into the geology of the continents since the early work of James Hutton, the "ocean in the earth-system" has not been systematically investigated in much detail until the mid-twentieth century. This was largely due to technical difficulties that simply made it impossible for ocean researchers to either dive to the deep-sea floor, or to retrieve samples. Based on this lack of information and knowledge, the deep-sea floor has been considered a life-hostile desert. With the discovery of very dynamic ecosystems and unique geological features such as hydrothermal vents and black smokers at the divergent plate boundary of the East Pacific Rise in the 1970s, marine-geological research was kick-started. A further important discovery, however, was the cool counter-part of hydrothermal vents: *Cold seeps*, locations at the sea floor, where low temperature fluids including gases are expelled from the sediments. Three major types of cold seeps are known: ground water-, brine-, and hydrocarbon seeps (cf. Judd and Hovland, 2007). This thesis, in general, deals with marine hydrocarbon seeps and the term *cold seep* will be used synonymously in the following. The importance of hydrocarbon transfer from marine sediments to the hydro- and atmosphere has been frequently highlighted in the scientific literature, because any source of hydrocarbons to the environment potentially contributes to the atmospheric carbon budget – and ultimately to the greenhouse effect (Denman et al., 2007). Cold seeps host unique and diverse ecosystems that rely on chemically stored energy transferred from the sediment to and across the sediment/water interface (Sibuet and Olu, 1998; Levin, 2005). As the energy is gained by microbes through oxidation of reduced compounds (for example hydrocarbons and hydrogen sulfide), cold seep ecosystems may be best described as chemosynthetic ecosystems. Where reduced sulfur and carbon species are oxidized, products accumulate that can be preserved in the geological record, if they precipitate as authigenic minerals. In the following, I will give a detailed introduction into the global distribution of cold seeps as well as modes of gas/fluid transport, (bio)geochemical processes and mineral authigenesis. The chapter closes with the motivation and objectives of this thesis.

1 Global distribution and trigger mechanisms of cold seeps

Marine hydrocarbon seepage across the sediment/water interface is a widespread phenomenon in marine sediments (Judd and Hovland, 2007). While most, if not all continental margins host cold seeps, irrespective of tectonic activity, some seeps are known from remote mid-ocean settings, which are, however, always related to tectonic activity (Judd and Hovland, 2007; Suess, 2010). It is therefore important to investigate where cold seeps occur and which driving forces trigger seepage of hydrocarbons from marine sediments. Since the first detailed reports on cold seeps comprising chemosynthetic communities, authigenic minerals and gas transfer into the water column (Suess et al., 1985; Kulm et al., 1986), numerous other cold seeps have been discovered and studied, as summarized in published global maps (Campbell, 2006; Suess, 2010). Suess (2010) recently provided an updated map of the global occurrence of cold seeps distinguishing between cold seeps located either at active or inactive continental margins. The majority of cold seeps studied so far were discovered at convergent and thus active continental margins involving subduction of oceanic plates under continental plates. In these settings, fluid and gas are mobilized due to compression or buoyancy forces (see next section). Perhaps the best-studied convergent margin hosting cold seeps is the Cascadia margin offshore Oregon (USA). Transform plate boundaries have been as well reported to host cold seeps, and mechanisms triggering seepage appear to be similar to convergent margins (Suess, 2010). Cold seeps unrelated to plate-tectonism were reported from passive continental margins, and well-studied examples of these were discovered for instance in the North Sea (e.g. Hovland, 1993; Hovland, 2007), along the western African continental margin (e.g. Gay et al., 2006; Sahling et al., 2008), at Blake Ridge offshore Florida (e.g. Holbrook et al., 2002; van Dover et al., 2003), and in the Black Sea (e.g. Ivanov et al., 1998; Bohrmann et al., 2003). Other important sites of hydrocarbon seepage are so-called mud volcanoes, which often evolve due to mud-, or salt-diapirism (Brown, 1990; Kopf, 2002; Kopf, 2003; Milkov et al., 2003; Niemann and Boetius, 2010). Mud volcanoes are not in focus of this study and will thus not be further discussed here.

2 Fluid transport processes at cold seeps

Typically, non-mud volcanic cold seeps are driven either by gas bubble buoyancy, by pore water advection, or by a combination of both. Furthermore, downward transport of bottom water into the sediment is an important process at cold seeps, because it introduces oxidized compounds into the reduced environment which can act as electron acceptors for early diagenetic transformation of organic matter in the upper sediment. It is thus mandatory to consider those transport processes in detail that control the distribution of bottom water, pore water, and/or free gas in seep sediments (Fig. 1).

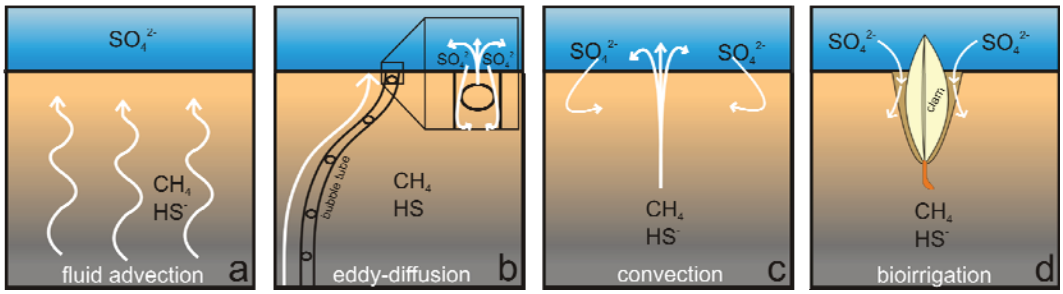

Figure 1: Schematic overview of different modes of pore water and/or gas transport at cold seeps. White arrows indicate transport pathways. Although not explicitly indicated in the figure, molecular diffusion takes place at any stage and in any scenario. The different scenarios (a-d) are discussed in the text.

Fluid advection: Pore water advection can be self-induced by methane dissolving in pore water (Park et al., 1990), because methane-rich pore water has, depending on its methane concentration, a lower specific density (<1 kg l^{-1}) than pure (pore) water (~1 kg l^{-1}). Thus, with increasing concentration of dissolved methane, the fluid gets less dense, *i.e.* relatively lighter, than ambient, methane-poor pore water and ascends due to positive buoyancy (Park et al., 1990). Consequently, even if free gas is present and ascends buoyantly, it is also the pore water that migrates upwards and thus transports dissolved compounds towards the sediment surface. This process is called pore water advection and it is schematically shown in Fig. 1a. Apart from density-driven flow of pore water, there is a further process that can lead to advection: sediment compaction either due to accumulation of sediment, or due to dewatering in geological stress zones, as for example convergent margins (Park et al., 1990).

Eddy diffusion and convection: In case the pore water is oversaturated with methane under the given pressure and temperature conditions, gas ebullition can

occur, and free gas bubbles rise through the sediment column. During ascent such bubbles can push overlying pore water and sediment towards and across the sediment surface. As a consequence, bubble ascent might lead to a draw-down of bottom water into the gas bubble migration tubes via turbulent mixing also described as eddy-diffusion (Fig. 1b; Haeckel et al., 2007). In addition, downward flow of bottom water into the sediment independent of gas tubes is also a well-known process and may lead to convective cycling of bottom water into the sediment and discharge of pore water from the sediment into the bottom water (Fig. 1c; O'Hara et al., 1995; Tryon et al., 2002). Based on simple volume-balance this process describes the escape of gas bubbles from the sediment through a central gas conduit that drives a downward flow of water into the sediment at a certain distance (Fig. 1c).

Bioirrigation: In Fig. 1d the process of bioirrigation is exemplified by clams, which often colonize cold seeps and host thiotrophic endosymbionts. In order to supply these endosymbionts with their energy source (reduced sulfur), the animals take up hydrogen sulfide from ambient pore water. However, the "formidable problem" (Childress et al., 1991) in this strategy lays in the fact that hydrogen sulfide is on the one hand needed for respiration by the microbial endosymbionts but is at the same time toxic to the host-organisms (cf. Childress et al., 1991). The clams circumvent this problem by irrigating and hence detoxifying ambient sediment with oxic bottom water and at the same time protruding their foot into sulfidic pore water (Childress et al., 1991; Wallmann et al., 1997). During this process the sulfate zone in the sediment is vertically expanded. The interaction of the related pore water transport processes described above is investigated in detail in chapter 2.

3 Gas hydrates

Under high hydrostatic pressure, low temperatures and salinity, oversaturation of low molecular-weight gases, particularly methane, leads to the formation of gas hydrates (Shipley et al., 1979; Hesse and Harrison, 1981; Bohrmann and Torres, 2006; Tréhu et al., 2006). In gas hydrates, guest molecules are trapped in crystallized cages (clathrates) of water molecules, held together by *van der Waals*-forces. The formation of gas hydrates leads to the exclusion of dissolved ions from the clathrate (Hesse and Harrison, 1981) resulting in ion-enrichments in

the pore water. Thus, even if gas hydrates partially dissociate *ex situ*, when brought outside of their stability field, e.g. due to pressure release during recovery of hydrate-bearing sediment cores, enrichment horizons of e.g. chloride in the pore water might hint to the presence of hydrates under *in situ* conditions (Haeckel et al., 2004). In fact, it was shown that the magnitude of chloride anomalies allows for an estimate of the *in situ* gas hydrate contents (e.g. Ussler and Paull, 1995; Haeckel et al., 2004; Tréhu et al., 2004).

At present, gas hydrates are in the focus of scientific and economic research due to two main reasons: (1) Gas hydrates trap large amounts of the greenhouse gas methane with a gas/hydrate volumetric ratio of approximately 160/1 (cm^3/cm^3) under standard temperature and pressure conditions; (2) Gas hydrates are considered to stabilize marine sediments, in particular slopes, and were suggested to cause geohazards, as for instance tsunamis, if they were to dissociate (Sultan et al., 2004). In the context of this thesis, the presence of gas hydrates plays a prominent role in the geochemistry at cold seeps. They may (1) trap hydrocarbons and act as a methane sink within the gas hydrate stability zone, or they may (2) release hydrocarbons to the environment and act as a methane source. It has further been shown, that gas hydrates can act as a physical barrier for free gas in the sediment. For example, Shipley et al. (1979) found a peculiar bottom-simulating seismic reflector (BSR), which was confirmed to represent the lower boundary of gas hydrate stability. Below this BSR free gas occurred which was trapped by gas hydrates. This phenomenon will be addressed in chapter 3.

4 (Bio)geochemical processes and mineral authigenesis at cold seeps

The fundamental works by Froelich et al. (1979) and (Berner, 1980) showed that, during microbial organic matter remineralization, a cascade of electron acceptors with consecutively decreasing energy yields establishes a typical redox zonation in marine sediments (Fig. 2). This redox zonation has been described from a thermodynamic point of view by Berner (1980) and was recently reviewed in great detail by Canfield and Thamdrup (2009), who suggested slightly different terminologies compared to those that have been used since Froelich´s work. Aerobic respiration of organic matter with sea water-derived oxygen provides the

highest standard free energy yield for respiration per mol of organic carbon (ΔG^0 -479 kJ mol^{-1} C). Where oxygen is depleted, denitrification (ΔG^0 -453 kJ mol^{-1} C), manganese- (ΔG^0 -349 kJ mol^{-1}) and iron-reduction (ΔG^0 -114 kJ mol^{-1} C) provide the next lower energy yields for microbes. During dissimilatory metal reduction, solid phase Fe(III) and Mn(IV) are reduced, and Fe^{2+} and Mn^{2+} are released to the pore water. The next lower energy yield for microbes remineralizing organic matter is by sulfate reduction (ΔG^0 -77 kJ mol^{-1} C). Organoclastic sulfate reduction usually occurs in sediments below the Fe(II)/Fe(III) redox boundary and above the methanic zone, although it was shown that the pore water redox zones can considerably overlap, and associated redox reactions are not necessarily spatially separated (e.g. Canfield et al., 1993; Postma and Jakobsen, 1996; Canfield and Thamdrup, 2009). The last step in organic matter degradation in marine sediments releases methane and higher hydrocarbon homologues to the environment. Methane (C_1) and higher homologues (C_{2+}) are produced via two different pathways: Thermogenic versus biogenic methanogenesis. Thermogenic methane is produced in the sediment within the so-called "catagenesis temperature window" at sediment depths of several hundreds of meters to kilometers, where organic matter encounters high temperatures caused by the geotherm (Claypool and Kaplan, 1974; Schoell, 1988). The thermocatalytic breakdown (`cracking´) of organic matter releases hydrocarbons that are dominated by methane but include significant amounts of C_{2+} compounds, for example ethane, propane, and iso-butane. Furthermore, the isotopic composition of thermogenic hydrocarbons is characterized by a relative enrichment in the heavy ^{13}C atoms which leads to high $\delta^{13}C$ values. Biogenic formation of hydrocarbons during organic matter degradation is performed by strictly anaerobic archaea below the sulfate-zone of the sediment and may proceed along two pathways, in which acetate (CH_3COOH; ΔG^0 -30 kJ mol^{-1} C), or carbon-dioxide (CO_2; ΔG^0 -135 kJ mol^{-1} C) are used by archaea to form dominantly methane (Claypool and Kaplan, 1974; Rice and Claypool, 1981; Whiticar et al., 1986). Biogenic methane is usually depleted in higher homologues (high C_1/C_{2+} ratios) and shows a very low $\delta^{13}C$ due to microbial isotope fractionation and hence the enrichment of light ^{12}C atoms (Claypool and Kaplan, 1974; Whiticar et al., 1986; Whiticar, 1999). A criterion to distinguish between both hydrocarbon production-pathways (thermogenic vs. biogenic) has been proposed, which is based on the comparison of the C_1/C_{2+} ratio and the carbon-isotopic composition of a given sample (Bernard et al., 1976). However,

recent findings compromise this method to a certain extent, because some methanogens were proven to also produce C_{2+} hydrocarbons (Hinrichs et al., 2006).

Barnes and Goldberg (1976) pointed out that sulfate reduction in marine sediments is often accompanied with a concomitant depletion in methane that diffuses up from the zone of methanogenesis. About 20 years later a final scenario was suggested, which explains the co-depletion of sulfate and methane (Hoehler et al., 1994, Hinrichs et al., 1999; Boetius et al., 2000). The reaction was termed the anaerobic oxidation of methane (AOM) with sulfate as the terminal electron acceptor (Eqn. 1), it is apparently conducted by a microbial consortium of sulfate reducing bacteria and methane-oxidizing archaea (Boetius et al., 2000), and it provides a very low energy yield (ΔG^0) on the order of -25 kJ mol^{-1} C.

$$CH_4 + SO_4^{2-} \rightarrow HCO_3^- + HS^- + H_2O \qquad \text{(Eqn. 1)}$$

anaerobic oxidation of methane with sulfate releases bicarbonate and hydrogen sulfide

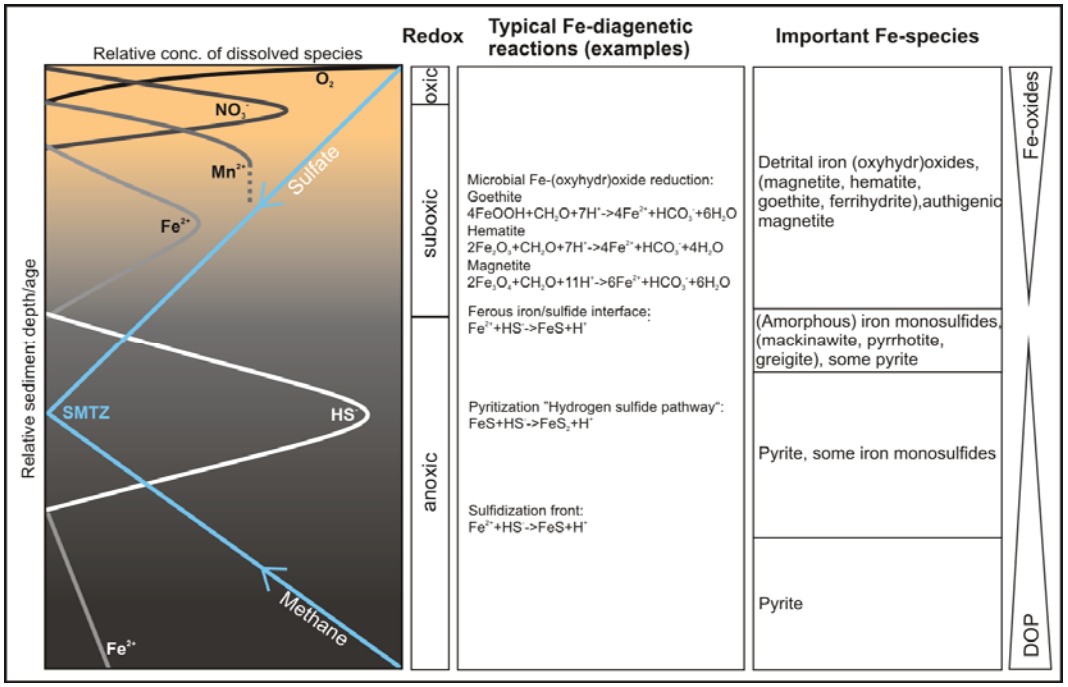

Figure 2: Schematic overview of the redox zonation in marine sediments (left). The column to the left shows the simplified distribution of dissolved species after Froelich et al. (1979). The third and fourth column from left shows the main geochemical reactions involving iron diagenesis and the most important iron species. The column to the right indicates a simplified distribution of Fe-oxides which are depleted towards, depth and the degree of pyritization (DOP) which increases towards depth. The composite figure was inspired by Kasten et al. (2003) and the redox zonation follows Berner (1980).

The products of AOM, bicarbonate (HCO_3^-) and hydrogen sulfide (HS^-), play an important role in the context of this thesis, because these anions can precipitate as authigenic minerals (carbonates and iron sulfides) and may accumulate in the sedimentary solid phase. Furthermore, hydrogen sulfide drives chemosynthetic ecosystems at cold seeps. Authigenic carbonates and iron sulfides are important sinks in the global cycles of the involved elements, particularly C, S, Ca, and Fe with minor significance for Mn, Sr, and Mg. Carbonate authigenesis has been widely documented at cold seeps worldwide and is reasonably well understood (e.g. Kulm et al., 1986; Ritger et al., 1987; Han and Suess, 1989; Jørgensen, 1992; von Rad et al., 1996; Bohrmann et al., 1998; Peckmann et al., 2001; Díaz-del-Río et al., 2003; Teichert et al., 2003; Aloisi et al., 2004b; Teichert et al., 2005a; Bayon et al., 2007; Naehr et al., 2007; Himmler et al., 2010; Nöthen and Kasten, 2011). In contrast to carbonates, the formation, distribution and stability of authigenic iron sulfides (Fig. 2) associated with gas hydrates, cold seeps, and other methane-rich sediments has only been marginally studied to date (e.g. Reynolds et al., 1990; Housen and Musgrave, 1996; Kasten et al., 1998; Jørgensen et al., 2004; Neretin et al., 2004; Novosel et al., 2005; Riedinger et al., 2005; Larrasoaña et al., 2007; März et al., 2008). The formation of sedimentary pyrite was first described in detail by Berner (1970, 1984). It is agreed that pyrite formation most often involves a number of intermediate iron sulfide species (Canfield et al., 1986; Canfield, 1989; Rickard et al., 1995; Rickard, 1997; Rickard and Luther, 1997; Schippers and Jørgensen, 2002; Rickard and Morse, 2005; Jørgensen and Kasten, 2006; Rickard and Luther, 2007; Holmkvist et al., 2011). According to Berner (1970), aqueous ferrous iron (Fe^{2+}), which is released during dissimilatory iron reduction below the Fe(II)/Fe(III) redox boundary (Fig. 2), reacts with hydrogen sulfide to form amorphous (i.e. non-crystalline) iron monosulfides or mackinawite (Eqn. 2)

$$Fe^{2+} + HS^- \rightarrow FeS + H^+ \qquad \text{(Eqn. 2)}$$

precipitation of mackinawite

Mackinawite is unstable in the presence of hydrogen sulfide. According to the hydrogen sulfide pathway (Rickard and Luther, 1997), mackinawite builds aqueous FeS-clusters, which react with hydrogen sulfide to form pyrite (Eqn. 3). This process is relevant at cold seeps, which are usually characterized by high hydrogen sulfide contents due to AOM.

$$FeS + HS^- \rightarrow FeS_2 + H^+ \quad \text{(Eqn. 3)}$$

pyritization of mackinawite

The various authigenic iron sulfides are characterized by different magnetic properties. This topic demands consideration here, because the occurrence and distribution of different Fe-sulfides can be traced by rock-magnetic methods. Diagenetic pyritization of Fe-minerals overprints the original record of magnetic susceptibility, if magnetic Fe-(oxyhydr)oxides are converted into paramagnetic Fe-sulfides (e.g. Novosel et al., 2005; Riedinger et al., 2005; Larrasoaña et al., 2007; Fu et al., 2008; März et al., 2008). While pyrite and mackinawite are paramagnetic, metastable pyrrhotite and greigite are ferrimagnetic. It is this property and its association with gas hydrate occurrence that has brought greigite into scientific focus over the last years (e.g. Housen and Musgrave, 1996; Larrasoaña et al., 2007; Fu et al., 2008). For example, Housen and Musgrave (1996) speculated that greigite may act as a proxy for (hydrogen sulfide-bearing) gas hydrates in marine sediments. Larrasoaña et al. (2007) suggested that greigite may be used as mineralogical indicator for moderate methane fluxes. Processes related to this topic will be investigated in chapter 4.

A further authigenic mineral typically found in cold seep sediments is barite ($BaSO_4$). Barium (Ba) arrives at and is buried in the sea floor as microcrystalline biogenic barite, Ba-rich biogenic carbonates and bound in alumosilicates (Dehairs et al., 1980). In case the pore water is sulfate-depleted, for example due to AOM, the solubility of barite is significantly increased and barite dissolves. The released barium ion (Ba^{2+}) diffuses up into sulfate-containing sediments and reprecipitates upon contact with sulfate to from authigenic barite just above the SMT. This phenomenon has been documented for numerous locations including cold seeps (Torres et al., 1996a; Torres et al., 1996b; Dickens, 2001; Torres et al., 2002; Aloisi et al., 2004a; Castellini et al., 2006; Riedinger et al., 2006; Snyder et al., 2007; Feng and Roberts, 2011; Nöthen and Kasten, 2011). Authigenic barite fronts have previously been used as proxies for shifting SMT depths, to estimate methane fluxes, or to document pulses of fluid flow (Dickens, 2001; Riedinger et al., 2006; Snyder et al., 2007; Feng and Roberts, 2011) and will be dealt with in chapter 3.

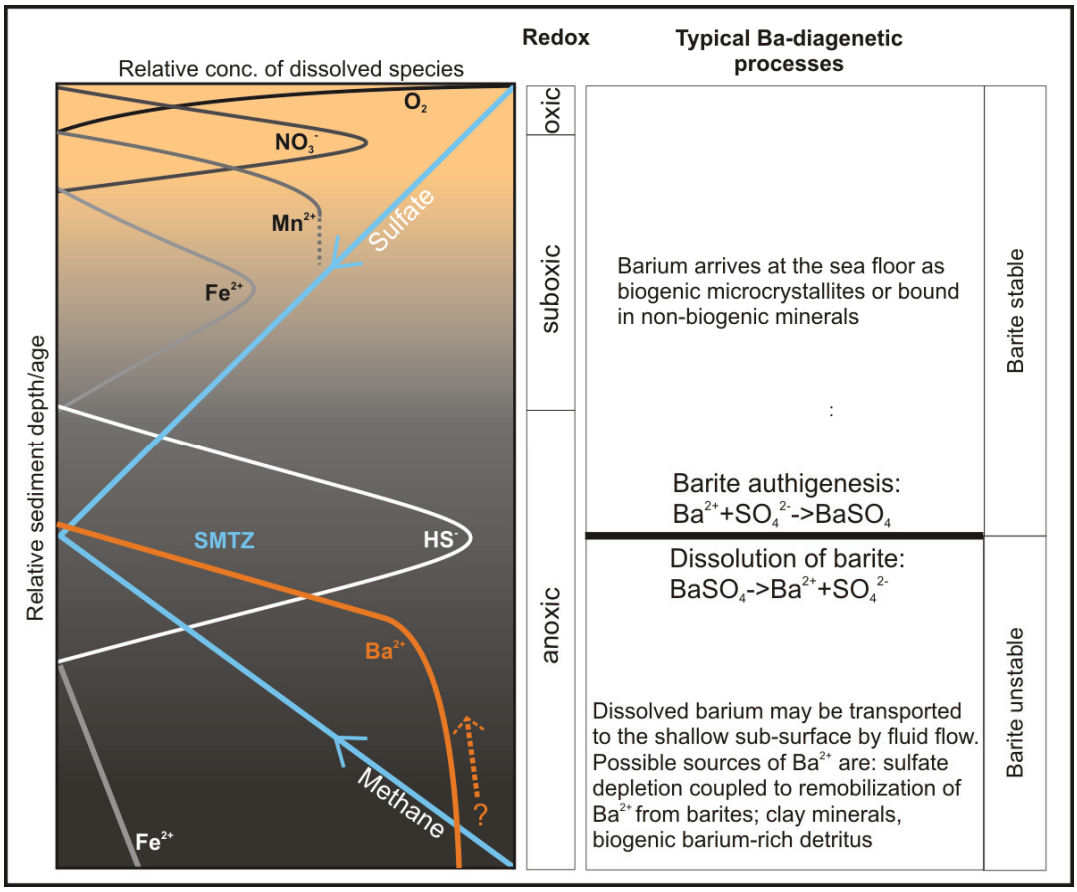

Figure 3: Modified version of Fig. 2 with focus on Ba diagenesis. The composite figure was inspired by Kasten et al. (2003) and the redox zonation follows Berner (1980).

However, barite fronts are only preserved in the sediment and can thus only provide information on the depth of sulfate-depletion, if the SMT has not migrated upwards. If the SMT would migrate above the authigenic barite enrichment, any authigenic barite that precipitated above the former SMT-depth would then be located within the zone of sulfate-depletion, and would thus be prone to dissolution.

5 Motivation and objectives

James Hutton was the first to realize, that: *"Understanding the geological past provides the base for predicting the future"* (modified after Hutton, 1788). Furthermore, Hutton´s "principle of actualism" implies that: *"Geological processes observed today must have been active in the same way in the past"* (modified after Hutton, 1788). Thus, the **general questions** in researching cold seeps include, whether solid phase records such as authigenic minerals or gas hydrates at contemporary seeps provide information on (a) environmental conditions during formation, (b) the (geological) time-frame of seepage, or (c) the extent, intensity, and trigger-mechanisms of seepage. Furthermore, the role of chemosynthetic organisms in controlling pore water fluxes and element cycling at the sediment/water interface of cold seeps is only poorly understood. Few studies addressed the above questions. For example, Wallmann et al. (1997) and Haese et al. (2003; 2006) investigated the complex interactions and consequences of fluid advection and bioirrigation at modern cold seeps in the Aleutian subduction zone and Mediterranean Sea. Campbell (2006) collected a wealth of information on fossil seeps and seep carbonates from the literature that allow for the interpretation of the paleo-environment during the time of seepage. Furthermore, Luth et al. (1999) and Peckmann et al. (2001) showed that the different morphotypes of authigenic carbonates may indicate the redox state of the respective environment and water column during the time of formation. Nöthen and Kasten (2011) analyzed the pore water and solid phase of Congo Fan sediments by means of Sr/Ca and Mg/Ca ratios and reconstructed changes in seep-activity. In a study of rare earth elements in authigenic carbonates of the Makran convergent margin, Himmler et al. (2010) found that the chemical signature of the seeping pore water is preserved. Furthermore, Bohrmann et al. (1998, 2002) and Teichert et al. (2005b) reported on carbonates with a gas bubble fabric (clathrites) and suggested that the occurrence of clathrites indicates the presence of free gas and gas hydrates at shallow sediment depth. Yet, the questions remain, whether other authigenic minerals, for example iron sulfides or barite, bear a similar diagnostic potential compared to seep carbonates, and whether fluid transport processes and trigger mechanisms of fluid seepage can be reconstructed by analyzing the geochemistry of modern seeps.

In order to contribute to the scientific understanding of cold seep geochemistry, pore water transport processes, and the diagnostic potential of authigenic seep

minerals found in the geological record, three **specific questions** will be addressed in this thesis:

I How do fluid advection, water column redox and benthic chemosynthetic communities interact on small scales at different cold seep-habitats?

II Which mechanisms potentially trigger episodic seep events and can geochemical proxies or pore water modeling be used to reconstruct the evolution of such events?

III Are authigenic minerals suitable to provide information on the geochemical and/or transport processes at cold seeps?

References

Aloisi, G., Wallmann, K., Bollwerk, S. M., Derkachev, A., Bohrmann, G. and Suess, E.: The effect of dissolved barium on biogeochemical processes at cold seeps, Geochim. Cosmochim. Acta, 68, 1735-1748, 2004a.

Aloisi, G., Wallmann, K., Haese, R. R. and Saliège, J. F.: Chemical, biological and hydrological controls on the ^{14}C content of cold seep carbonate crusts: numerical modeling and implications for convection at cold seeps, Chem. Geol., 213, 359-383, 2004b.

Barnes, R. O. and Goldberg, E. D.: Methane production and consumption in anoxic marine sediments, Geology, 4, 297-300, 1976.

Bayon, G., Pierre, C., Etoubleau, J., Voisset, M., Cauquil, E., Marsset, T., Sultan, N., Le Drezen, E. and Fouquet, Y.: Sr/Ca and Mg/Ca ratios in Niger Delta sediments: Implications for authigenic carbonate genesis in cold seep environments, Mar. Geol., 241, 93-109, 2007.

Bernard, B. B., Brooks, J. M. and Sackett, W. M.: Natural gas seepage in the Gulf of Mexico, Earth. Planet. Sci. Lett., 31, 48-54, 1976.

Berner, R. A.: Sedimentary pyrite formation, Am. J. Sci., 268, 1-23, 1970.

Berner, R. A.: Early Diagenesis - A Theoretical Approach, Princeton University Press, Princeton, 1980.

Berner, R. A.: Sedimentary pyrite formation: An update, Geochim. Cosmochim. Acta, 48, 605-615, 1984.

Boetius, A., Ravenschlag, K., Schubert, C. J., Rickert, D., Widdel, F., Gieseke, A., Amann, R., Jørgensen, B. B., Witte, U. and Pfannkuche, O.: A marine microbial consortium apparently mediating anaerobic oxidation of methane, Nature, 407, 623-626, 2000.

Bohrmann, G., Greinert, J., Suess, E. and Torres, M.: Authigenic carbonates from the Cascadia subduction zone and their relation to gas hydrate stability, Geology, 26, 647-650, 1998.

Bohrmann, G., Ivanov, M., Foucher, J. P., Spiess, V., Bialas, J., Greinert, J., Weinrebe, W., Abegg, F., Aloisi, G., Artemov, Y., Blinova, V., Drews, M., Heidersdorf, F., Krabbenhöft, A., Klaucke, I., Krastel, S., Leder, T., Polikarpov, I., Saburova, M., Schmale, O., Seifert, R., Volkonskaya, A. and Zillmer, M.: Mud volcanoes and gas hydrates in the Black Sea: new data from Dvurechenskii and Odessa mud volcanoes, Geo-Mar. Lett., 23, 239-249, 2003.

Bohrmann, G., Suess, E., Greinert, J., Teichert, B. and Naehr, T.: Gas Hydrate Carbonates from Hydrate Ridge, Cascadia Convergent Margin:Indicators of near-seafloor clathrate deposits, Proceedings of the Fourth International Conference on Gas Hydrates, Yokohama, Japan, 2002.

Bohrmann, G. and Torres, M. E.: Gas hydrates in marine sediments, in: Marine geochemistry, edited by: Schulz, H. D., and Zabel, M., Springer Verlag, Berlin, Heidelberg, New York, 418–512, 2006.

Brown, K. M.: The nature and hydrogeologic significance of mud diapirs and diatremes for accretionary systems, Journal of Geophysical Research-Solid Earth and Planets, 95, 8969-8982, 1990.

Campbell, K. A.: Hydrocarbon seep and hydrothermal vent paleoenvironments and paleontology: Past developments and future research directions, Palaeogeography, Palaeoclimatology, Palaeoecology, 232, 362-407, 2006.

Canfield, D. E.: Reactive iron in marine sediments, Geochim. Cosmochim. Acta, 53, 619-632, 1989.

Canfield, D. E., JÃ¸rgensen, B. B., Fossing, H., Glud, R., Gundersen, J., Ramsing, N. B., Thamdrup, B., Hansen, J. W., Nielsen, L. P. and Hall, P. O. J.: Pathways of organic carbon oxidation in three continental margin sediments, Mar. Geol., 113, 27-40, 1993.

Canfield, D. E., Raiswell, R., Westrich, J. T., Reaves, C. M. and Berner, R. A.: The use of chromium reduction in the analysis of reduced inorganic sulfur in sediments and shales, Chem. Geol., 54, 149-155, 1986.

Canfield, D. E. and Thamdrup, B.: Towards a consistent classification scheme for geochemical environments, or, why we wish the term ‘suboxic’ would go away, Geobiology, 7, 385-392, 2009.

Castellini, D. G., Dickens, G. R., Snyder, G. T. and Ruppel, C. D.: Barium cycling in shallow sediment above active mud volcanoes in the Gulf of Mexico, Chem. Geol., 226, 1-30, 2006.

Childress, J. J., Fisher, C. R., Favuzzi, J. A. and Sanders, N. K.: Sulfide and carbon dioxide uptake by the hydrothermal vent clam, *Calyptogena magnifica*, and its chemoautotrophic symbionts, Physiol. Zool., 64, 1444-1470, 1991.

Claypool, G. E. and Kaplan, I. R.: The origin and distribution of methane in marine sediments., in: Natural gases in marine sediments, edited by: Kaplan, I. R., Plenum Publishing Corporation, New York, 1974.

Dehairs, F., Chesselet, R. and Jedwab, J.: Discrete suspended particles of barite and the barium cycle in the open ocean, Earth. Planet. Sci. Lett., 49, 528-550, 1980.

Denman, K. L., Brasseur, G., Chidthaisong, A., Ciais, P., Cox, P. M., Dickinson, R. E., Hauglustaine, D., Heinze, C., Holland, E., Jacob, D., Lohmann, U., Ramachandran, S., da Silva Dias, P. L., Wofsy, S. C. and Zhang, X.: Couplings between changes in the climate system and biogeochemistry, in: Climate Change 2007: The Physical Science Basis. Contribution of Working Group I to the Fourth Assessment Report of the Intergovernmental Panel on Climate Change, edited by: Solomon, S., Qin, D., Manning, M., Chen, Z., Marquis, M., Averyt, K. B., Tignor, M., and Miller, H. L., Cambridge University Press, Cambrige, New York, 2007.

Díaz-del-Río, V., Somoza, L., Martínez-Frias, J., Mata, M. P., Delgado, A., Hernandez-Molina, F. J., Lunar, R., Martín-Rubí, J. A., Maestro, A., Fernández-Puga, M. C., León, R., Llave, E., Medialdea, T. and Vázquez, J. T.: Vast fields of hydrocarbon-derived carbonate chimneys related to the accretionary wedge/olistostrome of the Gulf of Cádiz, Mar. Geol., 195, 177-200, 2003.

Dickens, G. R.: Sulfate profiles and barium fronts in sediment on the Blake Ridge: present and past methane fluxes through a large gas hydrate reservoir, Geochim. Cosmochim. Acta, 65, 529-543, 2001.

Feng, D. and Roberts, H. H.: Geochemical characteristics of the barite deposits at cold seeps from the northern Gulf of Mexico continental slope, Earth. Planet. Sci. Lett., 309, 89-99, 2011.

Froelich, P. N., Klinkhammer, G. P., Bender, M. L., Luedtke, N. A., Heath, G. R., Cullen, D., Dauphin, P., Hammond, D., Hartman, B. and Maynard, V.: Early oxidation of organic matter in pelagic sediments of the eastern equatorial Atlantic: suboxic diagenesis, Geochim. Cosmochim. Acta, 43, 1075-1090, 1979.

Fu, Y., von Dobeneck, T., Franke, C., Heslop, D. and Kasten, S.: Rock magnetic identification and geochemical process models of greigite formation in Quaternary marine sediments from the Gulf of Mexico (IODP Hole U1319A), Earth. Planet. Sci. Lett., 275, 233-245, 2008.

Gay, A., Lopez, M., Cochonat, P., Séranne, M., Levaché, D. and Sermondadaz, G.: Isolated seafloor pockmarks linked to BSRs, fluid chimneys, polygonal

faults and stacked Oligocene-Miocene turbiditic palaeochannels in the Lower Congo Basin, Mar. Geol., 226, 25-40, 2006.

Haeckel, M., Boudreau, B. P. and Wallmann, K.: Bubble-induced porewater mixing: A 3-D model for deep porewater irrigation., Geochim. Cosmochim. Acta, 71, 5135-5154, 2007.

Haeckel, M., Suess, E., Wallmann, K. and Rickert, D.: Rising methane gas bubbles form massive hydrate layers at the seafloor, Geochim. Cosmochim. Acta, 68, 4335-4345, 2004.

Haese, R. R., Hensen, C. and de Lange, G. J.: Pore water geochemistry of eastern Mediterranean mud volcanoes: Implications for fluid transport and fluid origin, Mar. Geol., 225, 191-208, 2006.

Haese, R. R., Meile, C., Van Cappellen, P. and De Lange, G. J.: Carbon geochemistry of cold seeps: Methane fluxes and transformation in sediments from Kazan mud volcano, eastern Mediterranean Sea, Earth. Planet. Sci. Lett., 212, 361-375, 2003.

Han, M. W. and Suess, E.: Subduction-induced pore fluid venting and the formation of authigenic carbonates along the cascadia continental margin: Implications for the global Ca-cycle, Palaeogeography, Palaeoclimatology, Palaeoecology, 71, 97-118, 1989.

Hesse, R. and Harrison, W. E.: Gas hydrates (clathrates) causing pore-water freshening and oxygen isotope fractionation in deep-water sedimentary sections of terrigenous continental margins, Earth. Planet. Sci. Lett., 55, 453-462, 1981.

Himmler, T., Bach, W., Bohrmann, G. and Peckmann, J.: Rare earth elements in authigenic methane-seep carbonates as tracers for fluid composition during early diagenesis, Chem. Geol., 277, 126-136, 2010.

Hinrichs, K.-U., Hayes, J. M., Bach, W., Spivack, A. J., Hmelo, L. R., Holm, N. G., Johnson, C. G. and Sylva, S. P.: Biological formation of ethane and propane in the deep marine subsurface, Proceedings of the National Academy of Sciences, 103, 14684-14689, 2006.

Hinrichs, K.-U., Hayes, J. M., Sylva, S. P., Brewer, P. G. and DeLong, E. F.: Methane-consuming archaebacteria in marine sediments, Nature, 398, 802-805, 1999.

Hoehler, T., Alperin, M. J., Albert, D. B. and Martens, C.: Field and laboratory studies of methane oxidation in an anoxic marine sediment: evidence for a

methanogen-sulfate reducer consortium., Global Biogeochem. Cycles, 8, 451-463, 1994.

Holbrook, W. S., Lizarralde, D., Pecher, I. A., Gorman, A. R., Hackwith, K. L., Hornbach, M. and Saffer, D.: Escape of methane gas through sediment waves in a large methane hydrate province, Geology, 30, 467-470, 2002.

Holmkvist, L., Ferdelman, T. G. and Jørgensen, B. B.: A cryptic sulfur cycle driven by iron in the methane zone of marine sediment (Aarhus Bay, Denmark), Geochim. Cosmochim. Acta, 75, 3581-3599, 2011.

Housen, B. A. and Musgrave, R. J.: Rock-magnetic signature of gas hydrates in accretionary prism sediments, Earth. Planet. Sci. Lett., 139, 509-519, 1996.

Hovland, M.: Submarine gas seepage in the North Sea and adjacent areas, Geological Society, London, Petroleum Geology Conference series, 4, 1333-1338, 1993.

Hovland, M.: Discovery of prolific natural methane seeps at Gullfaks, northern North Sea, Geo-Mar. Lett., 27, 197-201, 2007.

Hutton, J.: Theory of the Earth; or an investigation of the laws observable in the composition, dissolution, and restoration of land upon the globe, Trans. Roy. Soc. Edinburgh: Earth Sci., 1, 209-304, 1788.

Ivanov, M. K., Liminov, A. F. and Woodside, J. M.: Extensive deep fluid flux through the sea floor on the Crimean continental margin (Black Sea). in: Gas hydrates: Relevance to world margin stability and Climate Change., edited by: Henriet, J.-P., and Mienert, J., Geological Society of London, London, 196-213, 1998.

Jørgensen, B. B., Böttcher, M. E., Lüschen, H., Neretin, L. N. and Volkov, I. I.: Anaerobic methane oxidation and a deep H_2S sink generate isotopically heavy sulfides in Black Sea sediments, Geochim. Cosmochim. Acta, 68, 2095-2118, 2004.

Jørgensen, B. B. and Kasten, S.: Sulfur cycling and methane oxidation, in: Marine Geochemistry, edited by: Schulz, H. D., and Zabel, M., Springer-Verlag, Berlin, Heidelberg, 271-309, 2006.

Jørgensen, N. O.: Methane-derived carbonate cementation of marine sediments from the Kattegat, Denmark: Geochemical and geological evidence, Mar. Geol., 103, 1-13, 1992.

Judd, A. G. and Hovland, M.: Seabed fluid flow: the impact on geology, biology, and the marine environment, Cambridge University Press, Cambridge, 2007.

Kasten, S., Freudenthal, T., Gingele, F. X. and Schulz, H. D.: Simultaneous formation of iron-rich layers at different redox boundaries in sediments of the Amazon deep-sea fan, Geochim. Cosmochim. Acta, 62, 2253-2264, 1998.

Kasten, S., Zabel, M., Heuer, V. and Hensen, C.: Processes and signals of nonsteady-state diagenesis in deep-sea sediments and their pore waters, in: The South Atlantic in the Late Quaternary: Reconstruction of Material Budget and Current Systems, edited by: Wefer, G., Mulitza, S., and Ratmeyer, V., Springer-Verlag, Heidelberg, 431-459, 2003.

Kopf, A.: Global methane emission through mud volcanoes and its past and present impact on the Earth's climate, Int. J. Earth Sci., 92, 806-816, 2003.

Kopf, A. J.: Significance of mud volcanism, Rev. Geophys., 40, 1005, 2002.

Kulm, L. D., Suess, E., Moore, J. C., Carson, B., Lewis, B. T., Ritger, S. D., Kadko, D. C., Thornburg, T. M., Embley, R. W., Rugh, W. D., Massoth, G. J., Langseth, M. G., Cochrane, G. R. and Scamman, R. L.: Oregon subduction zone - venting, fauna, and carbonates, Science, 231, 561-566, 1986.

Larrasoaña, J. C., Roberts, A. P., Musgrave, R. J., Gràcia, E., Piñero, E., Vega, M. and Martínez-Ruiz, F.: Diagenetic formation of greigite and pyrrhotite in gas hydrate marine sedimentary systems, Earth. Planet. Sci. Lett., 261, 350-366, 2007.

Levin, L. A.: Ecology of cold seep sediments: interactions of fauna with flow, chemistry and microbes., Oceanogr. Mar. Biol. Annu. Rev., 43, 1-46, 2005.

Luth, C., Luth, U., Gebruk, A. V. and Thiel, H.: Methane gas Seeps Along the Oxic/Anoxic Gradient in the Black Sea: Manifestations, Biogenic Sediment Compounds and Preliminary Results on Benthic Ecology, Mar. Ecol., 20, 221-249, 1999.

März, C., Hoffmann, J., Bleil, U., de Lange, G. J. and Kasten, S.: Diagenetic changes of magnetic and geochemical signals by anaerobic methane oxidation in sediments of the Zambezi deep-sea fan (SW Indian Ocean), Mar. Geol., 255, 118-130, 2008.

Milkov, A. V., Sassen, R., Apanasovich, T. V. and Dadashev, F. G.: Global gas flux from mud volcanoes: a significant source of fossil methane in the atmosphere and the ocean, Geophys. Res. Lett., 30, 1029, 2003.

Naehr, T. H., Eichhubl, P., Orphan, V. J., Hovland, M., Paull, C. K., Ussler Iii, W., Lorenson, T. D. and Greene, H. G.: Authigenic carbonate formation at hydrocarbon seeps in continental margin sediments: A comparative study, Deep Sea Res. Part II, 54, 1268-1291, 2007.

Neretin, L. N., Böttcher, M. E., Jørgensen, B. B., Volkov, I. I., Lüschen, H. and Hilgenfeldt, K.: Pyritization processes and greigite formation in the advancing sulfidization front in the upper Pleistocene sediments of the Black Sea, Geochim. Cosmochim. Acta, 68, 2081-2093, 2004.

Niemann, H. and Boetius, A.: Mud Volcanoes, in: Handbook of Hydrocarbon and Lipid Microbiology, edited by: Timmis, K. N., Springer Berlin Heidelberg, 205-214, 2010.

Nöthen, K. and Kasten, S.: Reconstructing changes in seep activity by means of pore water and solid phase Sr/Ca and Mg/Ca ratios in pockmark sediments of the Northern Congo Fan, Mar. Geol., 287, 1-13, 2011.

Novosel, I., Spence, G. D. and Hyndman, R. D.: Reduced magnetization produced by increased methane flux at a gas hydrate vent, Mar. Geol., 216, 265-274, 2005.

O'Hara, S. C. M., Dando, P. R., Schuster, U., Bennis, A., Boyle, J. D., Chui, F. T. W., Hatherell, T. V. J., Niven, S. J. and Taylor, L. J.: Gas seep induced interstitial water circulation: observations and environmental implications, Cont. Shelf Res., 15, 931-948, 1995.

Park, A., Dewers, T. and Ortoleva, P.: Cellular and oscillatory self-induced methane migration, Earth-Sci. Rev., 29, 249-265, 1990.

Peckmann, J., Reimer, A., Luth, U., Luth, C., Hansen, B. T., Heinicke, C., Hoefs, J. and Reitner, J.: Methane-derived carbonates and authigenic pyrite from the northwestern Black Sea, Mar. Geol., 177, 129-150, 2001.

Postma, D. and Jakobsen, R.: Redox zonation: Equilibrium constraints on the Fe(III)/SO4-reduction interface, Geochim. Cosmochim. Acta, 60, 3169-3175, 1996.

Reynolds, R. L., Fishman, N. S., Wanty, R. and Goldhaber, M. B.: Iron sulfide minerals at Cement oil field, Oklahoma: Implications for magnetic detection of oil fields, Geol. Soc. Am. Bull., 102, 368-380, 1990.

Rice, D. D. and Claypool, G. E.: Biogenic gas - requirements for generation,accumulation-ressource potential evaluation, Oil & Gas Journal, 79, 258-&, 1981.

Rickard, D.: Kinetics of pyrite formation by the H2S oxidation of iron (II) monosulfide in aqueous solutions between 25 and 125 °C: The rate equation, Geochim. Cosmochim. Acta, 61, 115-134, 1997.

Rickard, D. and Luther, G. W.: Kinetics of pyrite formation by the H2S oxidation of iron (II) monosulfide in aqueous solutions between 25 and 125 °C: The mechanism, Geochim. Cosmochim. Acta, 61, 135-147, 1997.

Rickard, D. and Luther, G. W.: Chemistry of Iron Sulfides, Chem. Rev., 107, 514-562, 2007.

Rickard, D. and Morse, J. W.: Acid volatile sulfide (AVS), Mar. Chem., 97, 141-197, 2005.

Rickard, D., Schoonen Martin, A. A. and Luther, G. W.: Chemistry of Iron Sulfides in Sedimentary Environments, in: Geochemical Transformations of Sedimentary Sulfur, ACS Symposium Series, American Chemical Society, 168-193, 1995.

Riedinger, N., Kasten, S., Gröger, J., Franke, C. and Pfeifer, K.: Active and buried authigenic barite fronts in sediments from the Eastern Cape Basin, Earth. Planet. Sci. Lett., 241, 876-887, 2006.

Riedinger, N., Pfeifer, K., Kasten, S., Garming, J. F. L., Vogt, C. and Hensen, C.: Diagenetic alteration of magnetic signals by anaerobic oxidation of methane related to a change in sedimentation rate, Geochim. Cosmochim. Acta, 69, 4117-4126, 2005.

Ritger, S., Carson, B. and Suess, E.: Methane-derived authigenic carbonates formed by subduction-induced pore-water expulsion along the Oregon/Washington margin, Geol. Soc. Am. Bull., 98, 147-156, 1987.

Sahling, H., Bohrmann, G., Spiess, V., Bialas, J., Breitzke, M., Ivanov, M., Kasten, S., Krastel, S. and Schneider, R.: Pockmarks in the Northern Congo Fan area, SW Africa: Complex seafloor features shaped by fluid flow, Mar. Geol., 249, 206-225, 2008.

Schippers, A. and Jørgensen, B. B.: Biogeochemistry of pyrite and iron sulfide oxidation in marine sediments, Geochim. Cosmochim. Acta, 66, 85-92, 2002.

Schoell, M.: Multiple origins of methane in the Earth, Chem. Geol., 71, 1-10, 1988.

Shipley, T. H., Houston, M. H., Buffler, R. T., Shaub, F. J., McMillen, K. J., Ladd, J. W. and Worzel, J. L.: Seismic evidence for widespread possible gas hydrate horizons on continental slopes and rises, AAPG Bull., 63, 2204-2213, 1979.

Sibuet, M. and Olu, K.: Biogeography, biodiversity and fluid dependence of deep-sea cold-seep communities at active and passive margins, Deep Sea Res. Part II, 45, 517-567, 1998.

Snyder, G. T., Dickens, G. R. and Castellini, D. G.: Labile barite contents and dissolved barium concentrations on Blake Ridge: New perspectives on barium cycling above gas hydrate systems, J. Geochem. Explor., 95, 48-65, 2007.

Suess, E.: Marine Cold Seeps, in: Handbook of Hydrocarbon and Lipid Microbiology, edited by: Timmis, K. N., McGenity, T., van derMeer, J. R., and de Lorenzo, V., Springer Berlin, Heidelberg, 185-203, 2010.

Suess, E., Carson, B., Ritger, S. D., Moore, J. C., Jones, M. L., Kulm, G. R. and Cochrance, G. R.: Biological communities at vent sites along the subduction zone off Oregon., Bulltein of the Biological Society of Washington, 6, 475-484, 1985.

Sultan, N., Cochonat, P., Foucher, J. P. and Mienert, J.: Effect of gas hydrates melting on seafloor slope instability, Mar. Geol., 213, 379-401, 2004.

Teichert, B. M. A., Bohrmann, G. and Suess, E.: Chemoherms on Hydrate Ridge -- Unique microbially-mediated carbonate build-ups growing into the water column, Palaeogeography, Palaeoclimatology, Palaeoecology, 227, 67-85, 2005a.

Teichert, B. M. A., Eisenhauer, A., Bohrmann, G., Haase-Schramm, A., Bock, B. and Linke, P.: U/Th systematics and ages of authigenic carbonates from Hydrate Ridge, Cascadia Margin: recorders of fluid flow variations, Geochim. Cosmochim. Acta, 67, 3845-3857, 2003.

Teichert, B. M. A., Gussone, N., Eisenhauer, A. and Bohrmann, G.: Clathrites: Archives of near-seafloor pore-fluid evolution ($\delta^{44/40}$Ca, δ^{13}C, δ^{18}O) in gas hydrate environments, Geology, 33, 213-216, 2005b.

Torres, M. E., Bohrmann, G. and Suess, E.: Authigenic barites and fluxes of barium associated with fluid seeps in the Peru subduction zone, Earth. Planet. Sci. Lett., 144, 469-481, 1996a.

Torres, M. E., Brumsack, H. J., Bohrmann, G. and Emeis, K. C.: Barite fronts in continental margin sediments: a new look at barium remobilization in the

zone of sulfate reduction and formation of heavy barites in diagenetic fronts, Chem. Geol., 127, 125-139, 1996b.

Torres, M. E., McManus, J. and Huh, C.-A.: Fluid seepage along the San Clemente Fault scarp: basin-wide impact on barium cycling, Earth. Planet. Sci. Lett., 203, 181-194, 2002.

Tréhu, A. M., Long, P. E., Torres, M. E., Bohrmann, G., Rack, F. R., Collett, T. S., Goldberg, D. S., Milkov, A. V., Riedel, M., Schultheiss, P., Bangs, N. L., Barr, S. R., Borowski, W. S., Claypool, G. E., Delwiche, M. E., Dickens, G. R., Gracia, E., Guerin, G., Holland, M., Johnson, J. E., Lee, Y. J., Liu, C. S., Su, X., Teichert, B., Tomaru, H., Vanneste, M., Watanabe, M. and Weinberger, J. L.: Three-dimensional distribution of gas hydrate beneath southern Hydrate Ridge: constraints from ODP Leg 204, Earth. Planet. Sci. Lett., 222, 845-862, 2004.

Tréhu, A. M., Ruppel, C., Holland, M., Dickens, G. R., Torres, M. E., Collett, T. S., Goldberg, D., Riedel, M. and Schultheiss, P.: Gas hydrates in marine sediments: Lessons from scientific ocean drilling, Oceanography, 19, 124–142, 2006.

Tryon, M. D., Brown, K. M. and Torres, M. E.: Fluid and chemical flux in and out of sediments hosting methane hydrate deposits on Hydrate Ridge, OR, II: Hydrological processes, Earth. Planet. Sci. Lett., 201, 541-557, 2002.

Ussler, W. and Paull, C. K.: Effects of ion exclusion and isotopic fractionation on pore-water geochemistry during gas hydrate formation and decomposition, Geo-Mar. Lett., 15, 37-44, 1995.

van Dover, C. L., Aharon, P., Bernhard, J. M., Caylor, E., Doerries, M., Flickinger, W., Gilhooly, W., Goffredi, S. K., Knick, K. E., Macko, S. A., Rapoport, S., Raulfs, E. C., Ruppel, C., Salerno, J. L., Seitz, R. D., Sen Gupta, B. K., Shank, T., Turnipseed, M. and Vrijenhoek, R.: Blake Ridge methane seeps: characterization of a soft-sediment, chemosynthetically based ecosystem, Deep Sea Res. Part I, 50, 281-300, 2003.

von Rad, U., Rösch, H., Berner, U., Geyh, M., Marchig, V. and Schulz, H.: Authigenic carbonates derived from oxidized methane vented from the Makran accretionary prism off Pakistan, Mar. Geol., 136, 55-77, 1996.

Wallmann, K., Linke, P., Suess, E., Bohrmann, G., Sahling, H., Schlüter, M., Dählmann, A., Lammers, S., Greinert, J. and von Mirbach, N.: Quantifying fluid flow, solute mixing, and biogeochemical turnover at cold vents of the

eastern Aleutian subduction zone, Geochim. Cosmochim. Acta, 61, 5209-5219, 1997.

Whiticar, M. J.: Carbon and hydrogen isotope systematics of bacterial formation and oxidation of methane, Chem. Geol., 161, 291-314, 1999.

Whiticar, M. J., Faber, E. and Schoell, M.: Biogenic methane formation in marine and freshwater environments: CO2 reduction vs. acetate fermentation--Isotope evidence, Geochim. Cosmochim. Acta, 50, 693-709, 1986.

Chapter II – Manuscript 1

Interaction between hydrocarbon seepage, chemosynthetic communities and bottom water redox at cold seeps of the Makran accretionary prism: Insights from habitat-specific pore water sampling and modeling

D. Fischer[1], H. Sahling[1], K. Nöthen[2], G. Bohrmann[1], M. Zabel[1] and S. Kasten[2]

[1] MARUM – Center for Marine Environmental Sciences and Department of Geosciences, University of Bremen, Klagenfurter Strasse, D-28334 Bremen, Germany

[2] Alfred Wegener Institute for Polar and Marine Research, Am Handelshafen 12, D-27570 Bremerhaven, Germany

(Manuscript in review with "Biogeosciences")

Abstract

The interaction between fluid seepage, bottom water redox, and chemosynthetic communities was studied at cold seeps across one of the world's largest oxygen minimum zones (OMZ) located at the Makran convergent continental margin. Push cores were obtained from seeps within and at the lower boundary of the core-OMZ with a remotely operated vehicle. Extracted pore water was analyzed for sulfide and sulfate contents. Depending on oxygen availability, seeps were either colonized by microbial mats or by mats and macrofauna. The latter, including ampharetid polychaetes and vesicomyid clams, occurred in distinct benthic habitats which were arranged in a concentric fashion around gas orifices. At most sites colonized by microbial mats, hydrogen sulfide was exported into the bottom water. Where macrofauna was widely abundant, hydrogen sulfide was consumed within the sediment.

Numerical modeling of pore water profiles was performed in order to assess rates of fluid advection and bioirrigation. While the magnitude of upward fluid flow decreased from 11 cm yr^{-1} to <1 cm yr^{-1} and the sulfate/methane transition zone (SMTZ) deepened with increasing distance from the central gas orifice, the fluxes of sulfate into the SMTZ did not significantly differ (6.6-9.3 mol m^{-2} yr^{-1}). Depth-integrated rates of bioirrigation increased from 120 cm yr^{-1} in central habitats characterized by microbial mats and sparse macrofauna to 297 cm yr^{-1} in habitats of large and small vesicomyid clams. These results reveal that chemosynthetic macrofauna inhabiting the outer seep habitats at the lower boundary of the OMZ efficiently bioirrigate and thus transport sulfate into the upper 10 to 15 cm of the sediment. In this way bioirrigation compensates for the lower upward flux of methane in outer habitats and stimulates rates of anaerobic oxidation of methane (AOM) with sulfate high enough to provide sulfide for chemosynthesis. Through bioirrigation macrofauna engineer their geochemical environment and fuel upward sulfide flux via AOM. Due to the introduction of oxygenated bottom water into the sediment via bioirrigation the depth of the sulfide sink gradually deepens towards outer habitats. We therefore suggest that – in addition to the oxygen levels in the water column which determine whether macrofaunal communities can develop or not - it is rather the depth of the SMTZ and thus of sulfide production that determines which chemosynthetic communities are able to exploit the sulfide at depth. Moreover, large vesicomyid clams most efficiently expand

the sulfate zone in the sediment and cut off smaller or immobile organisms from the sulfide source.

1 Introduction

Cold seep sites at the seafloor are created by the focused upward migration of both dissolved and/or gaseous hydrocarbons. Seeps are found at passive and active continental margins and generally show strong temporal and spatial variations in fluid flux (e. g. Wallmann et al., 1997; Suess et al., 1998; Tryon et al., 1999; Wallmann et al., 2006; Sahling et al., 2008; Niemann et al., 2009; Reitz et al., 2011). The upward supply of hydrocarbons towards and across the sediment/water interface produces steep geochemical gradients in the pore water and typically stimulates high rates of anaerobic oxidation of methane (AOM) and other hydrocarbons with sulfate close to the sediment surface (Borowski et al., 1996). The process of AOM which is performed by a consortium of archaea and sulfate-reducing bacteria (Hoehler et al., 1994; Hinrichs et al., 1999; Boetius et al., 2000) releases hydrogen sulfide and bicarbonate into the pore water at the so-called sulfate/methane transition zone (SMTZ). Hence, AOM fuels microbial and macrofaunal chemosynthetic life and generates a significant carbon sink through carbonate authigenesis (Ritger et al., 1987). Numerous studies have demonstrated that the flux of methane and sulfide towards the sediment/water interface determines the microbial and faunal community composition at cold seeps (e.g. Dando and Hovland, 1992; Barry et al., 1997; Sibuet and Olu, 1998; Sahling et al., 2002; Levin et al., 2003; van Dover et al., 2003; Arvidson et al., 2004; Levin, 2005; de Beer et al., 2006; Niemann et al., 2009; Lichtschlag et al., 2010a).

The convergent continental margin off Pakistan is referred to as the "Makran accretionary prism" after the Makran coastal desert. Cold seeps off Pakistan and their properties as habitats for chemosynthetic microbial and faunal life were described earlier (Faber et al., 1994; von Rad et al., 1996; von Rad et al., 2000; Schmaljohann et al., 2001). Von Rad et al. (2000) found signs for gas seepage mostly on the upper slope (< 1000 m) which they explained to result from local tectonic uplift and hence a destabilization of gas hydrates trapped within the gas hydrate stability zone at greater depth. These authors found that the occurrence of *Thioploca sp*. and/or *Beggiatoa sp*. mats in the area is confined to sites punctually expelling free gas or sites of drift-wood or other large pieces of organic matter on the sea floor (von Rad et al. 2000). It has been suggested that local variations in the spatial distribution of benthic, chemosynthetic macrofauna in the study area may be co-induced by the depth of AOM-derived sulfide supply and

oxygen availability in the bottom water (von Rad et al., 1995; von Rad et al., 1996; von Rad et al., 2000; Schmaljohann et al., 2001).

The influence of bioirrigation and bioturbation on solute distribution and fluxes in marine sediments has been investigated in detail (e. g. Aller, 1980; Aller, 1984; Aller and Aller, 1998; Meile et al., 2001). However, only a few studies have quantified the influence of the activity of chemosynthetic biota on benthic fluxes at cold seeps (Wallmann et al., 1997; Haese, 2002; Haese et al., 2006). Bioirrigation, described as pumping of pore water by benthic fauna through their environment, is a prominent transport process at cold seeps as these sites are often densely colonized by chemosynthetic macrofauna. Wallmann et al. (1997) proposed that seep biota settling on and within the sulfidic seep sediments need to detoxify their habitats from high sulfide concentrations and do so by flushing their immediate surrounding with bottom water thereby introducing sulfate into the methanic zone of the sediment. On the other hand, macrofauna can only gain access to the sulfide pool needed for chemosymbiosis by digging down into the sediment. Besides sulfide removal by reaction with reactive (towards sulfide) iron phases (Berner, 1970), the distribution of sulfide within seep sediments and a potential sulfide export into the water column are controlled by both, the depths and rates of AOM as well as the activity of macrofauna colonizing the sediment surface. Due to the location of the “Makran” cold seeps within and below the core-OMZ and thus the distinct distribution of oxygen-dependent, bioirrigating/bioturbating (macrofauna) and anaerobic, non-irrigating (microbial mats) seep communities on the sediment surface the study area is ideal for exploring the interaction of water column redox, rates of upward fluid/gas migration, and bioirrigation in cold seep habitats.

In this study we investigate and quantify transport processes in different benthic seep-habitats of the Makran accretionary prism. The particular aim of this work is to elucidate the interaction between the intensity of fluid flux, oxygen levels in the bottom water, colonization with chemosynthetic biota, and solute fluxes towards and across the sediment/water interface. For this purpose we have carried out a visual examination (high definition camera) and video-targeted sediment sampling of distinct seep habitats within and below the core-OMZ by means of a remotely operated vehicle (ROV). We quantify pore water flow caused by advection and bioirrigation by means of 1-D modeling of pore water profiles. We show how seep-dependent macrofauna inhabiting the sediment surface actively

shape their geochemical environment and thus control solute fluxes within the sediment and across the sediment/water interface.

2 Geological setting and local oceanography

At the Makran subduction zone oceanic crust of the Arabian plate and the Omara micro-plate dips northward underneath the Eurasian plate to form the Makran accretionary prism (Fig. 4). The deformation front of the Makran prism is located south of the first accretionary ridge at about 3000 m water depth and strikes West to East, parallel to the coastline of Pakistan (Kukowski et al., 2000; Kukowski et al., 2001; Ding et al., 2010).

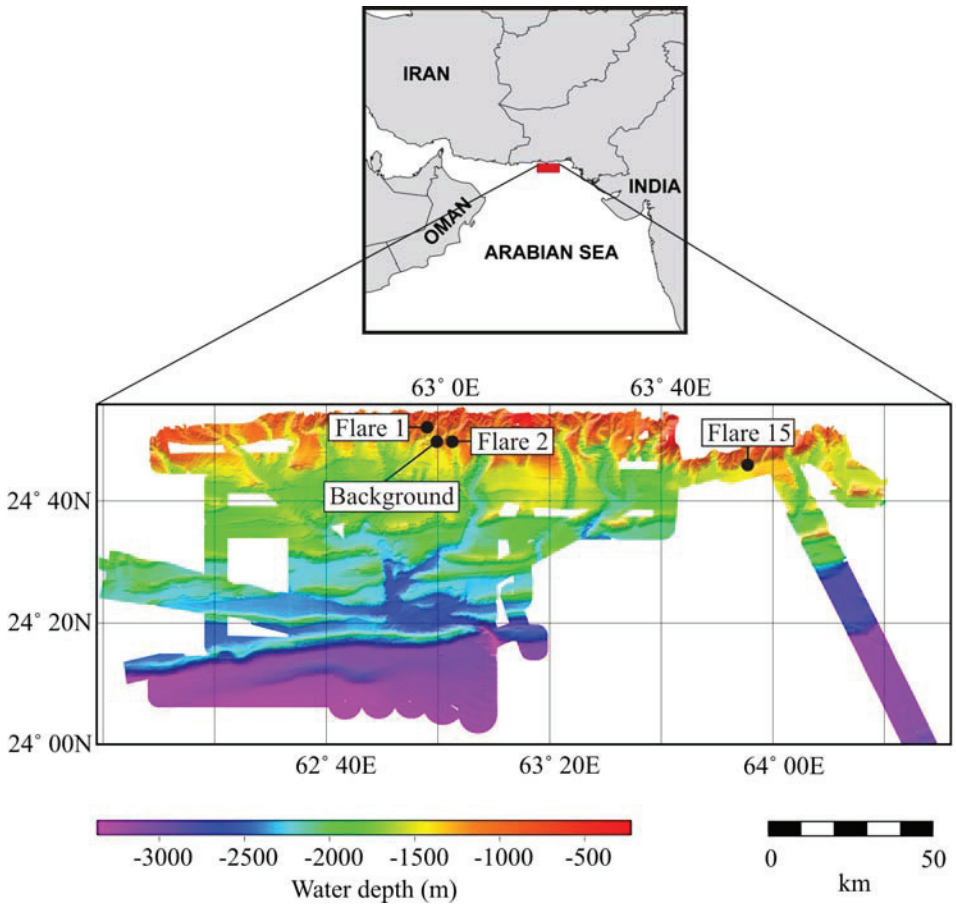

Figure 4: Overview map of the northern Arabian Sea and detailed bathymetric map of the working area off the coast of Pakistan. Dots indicate investigated sites.

Convergence rates range from 36.5-42 mm yr^{-1} (Kukowski et al., 2001). A sediment package of 5-7 km thickness accumulated on top of the oceanic crust

which is subject to subduction since at least the Oligocene (Schlüter et al., 2002). Kukowski et al. (2001) pointed out that sediments above the décollement are being accreted by imbricate thrusting forming well defined coast-parallel accretionary ridges. This N-S cascade of accretionary ridges was mapped in 1997 (Kukowski et al., 2000) and a distinct bottom simulating seismic reflector indicative for the phase boundary between free gas below and solid gas hydrates above has been described for the area (Kaul et al., 2000; von Rad et al., 2000; Ding et al., 2010).

The water column off Pakistan is characterized by a pronounced OMZ with oxygen concentrations < 2 µM between 100 m and 1000 m water depth (Wyrtki, 1973). The OMZ is, however, subject to temporal variations in its vertical extent (Wyrtki, 1973; Olson et al., 1993). The thickness of the OMZ off Pakistan is controlled by the combined effects of moderate to high rates of aerobic degradation of organic matter in the water column and a sluggish supply with warm and saline intermediate waters derived from marginal seas as e. g. the Red Sea and the Persian Gulf (Olson et al., 1993).

3 Materials and Methods

Sampling took place in the inter-monsoonal period in November 2007 during R/V METEOR cruise M 74/3 (Bohrmann et al., 2008). The main instrument of the cruise was the ROV MARUM-QUEST 4000. It was deployed at sites of gas discharge into the water column as recorded by echosounder gas flare imaging. Discrete sampling of individual seep habitats as visually identified based on different chemosynthetic microbial and macrobenthic communities was performed by ROV-operated push cores (PCs). Sampling included both the central as well as the surrounding habitats. We strictly avoided taking PCs in the immediate vicinity (< 5 cm) of gas orifices. Push cores were taken from the different habitats of two seep sites located within the core-OMZ (site GeoB 12320 at “Flare 1”, 551 m water depth, and site GeoB 12353 at “Flare 15”, 732 m water depth) and two seep sites found at the lower boundary of the core-OMZ (site GeoB 12315, 1025 m water depth, and site GeoB 12313, 1038 m water depth – both at “Flare 2”). In addition to the habitat-specific sampling of these four seep sites two sediment cores from background sites unaffected by hydrocarbon seepage were retrieved with a TV-guided Multiple Corer (TV-MUC). The exact

locations and characteristics of all sampling sites including the dominant chemosynthetic benthic communities of the individual habitats are listed in Table 1.

Table 1: Station list of all examined cores.

Flare	GeoB-Station	Gear	Position	Water depth (m)	GHSZ*	Habitat, seep community	Bottom water redox
1	12320-9	PC	24°53.634 N 63°01.404 E	551	-	Habitat 1, orange microbial mat	Core-OMZ
1	12320-4	PC	24°53.634N 63°01.404 E	551	-	Habitat 2, white microbial mat	Core-OMZ
	12312-3	MUC	24°53.072 N 63°01.641 E	654	-	Background	Core-OMZ
15	12353-5	PC	24°48.458 N 63°59.649 E	732	-	Habitat 1, orange microbial mat	Core-OMZ
15	12353-3	PC	24°48.457 N 63°59.649 E	732	-	Habitat 2, white microbial mat	Core-OMZ
	12309-3	MUC	24°52.322 N 62°59.859 E	962	+	Background	Core-OMZ
2	12315-9	PC	24°50.753 N 63°01.439 E	1025	+	Habitat 1, white/rose microbial mat, sparse polychaetes	Lower boundary of OMZ
2	12315-4	PC	24°50.753 N 63°01.439 E	1025	+	Habitat 2, polychaetes and small clams	Lower boundary of OMZ
2	12313-6	PC	24°50.828 N 63°01.419 E	1038	+	Habitat 1, white/rose microbial mat, sparse polychaetes	Lower boundary of OMZ
2	12313-12	PC	24°50.828 N 63°01.419 E	1038	+	Habitat 2, polychaetes and small clams	Lower boundary of OMZ
2	12313-13	PC	24°50.829 N 63°01.419 E	1038	+	Habitat 3, small and large clams	Lower boundary of OMZ

* Gas hydrate stability zone

3.1 Water column characteristics

Gas flare imaging was conducted with the ship-mounted parametric echosounder system ATLAS PARASOUND as described by Nikolovska et al. (2008). In this study the notation "Flare", as it has been adopted from onboard echosounder identification of potential sampling targets, will be used to specify a major locality. In that, a "Flare" usually comprises a seafloor area of several tens of square

meters including sites where more than one actual gas bubble stream was detected in the water column and where hydrocarbon seepage appeared bundled on the sea floor. Water column oxygen concentrations, temperature and salinity were determined with a Seabird 911+ CTD equipped with an SBE 43 (Seabird Electronics) oxygen sensor and temperature and salinity probes. These data were used as input parameters for geochemical modeling and flux calculations.

3.2 Identification of organisms

The ROV MARUM-QUEST 4000 was equipped with a 3 Mega-pixel photo camera and two video cameras, one of them in HD quality. Images of these three systems were used for visual interpretation of seep habitats (Fig. 5). A tentative differentiation between *Beggiatoa spp.*-dominated and *Marithioploca spp.*-dominated (formerly known as *Thioploca spp.*; cf. Salman et al., 2011)) microbial mats was achieved by means of the ROV-cameras. Admitting that this approach is rather weak compared to molecular biological techniques it may be stated that mats of both genera often appear in different shapes and structures. *Marithioploca spp*. were reported to appear as lawn-like, white filaments of sufficient length of several cm to sway in turbulent bottom waters and in a mat-thickness of several cm (Fossing et al., 1995; Schulz et al., 1996; Schulz and Jørgensen, 2001; Teske and Nelson, 2006; Salman et al., 2011). *Beggiatoa spp*. mats in contrast were often described to appear as white and/or orange-colored thin skins on the sediment surface with a mat thickness of less than one cm (Nelson et al., 1986; Robinson et al., 2004; Teske and Nelson, 2006; Salman et al., 2011).

Macrofauna (used here as the collective term for clams, polychaetes) specimens were obtained by an ROV-operated net or collected onboard from retrieved PCs and immediately stored in vials filled with 96% ethanol. In the following the central habitat of a seep site is termed “Habitat 1” and all successively occurring concentrically arranged habitats are termed “Habitat 2” and “Habitat 3”.

3.3 Pore water sampling and analyses

After arrival of the ROV and the TV-MUC on deck the sediment cores were immediately transferred into the cold room (4°C) of the ship and pore water was extracted within one hour by means of rhizons (Seeberg-Elverfeld et al., 2005). The average pore size of the rhizons is 0.1 µm and sampling resolution was 1 cm

for the PC and 1-2 cm for the TV-MUC cores, respectively. Data shown at zero depth in this study represent bottom water concentration. Pore water aliquots for sulfate determination were diluted 1:100 and stored at -20°C until analysis. Sulfate concentrations were measured by ion chromatography (IC) with an Advanced Compact IC 861 (METROHM). Subsamples for the analysis of total dissolved sulfide (ΣH_2S = H_2S + HS^- + S^{2-}) were fixed in a 5% Zn-acetate solution, kept at 4°C and measured photometrically according to the methylene-blue method after Cline (1969). The reproducibility the above methods was checked by analyzing replicates of standards. The accuracy of all measurements was within ± 3%.

3.4 Diffusive flux calculations

Diffusive fluxes of sulfate and sulfide were determined according to Fick´s first law of diffusion according to Eqn. (4):

$$J_{(species)} = -\Phi \times D_{sed} \times \frac{\delta C}{\delta X} \qquad \text{(Eqn. 4)}$$

where $J_{(species)}$ is the diffusive flux of the dissolved species, Φ represents sediment porosity (estimated 0.85), D_{sed} is the sediment diffusion coefficient in m^2 a^{-1} which was calculated for ambient bottom water temperature as determined by the CTD temperature sensor and corrected for tortuosity (Boudreau, 1997), and δC/δX is the concentration gradient of the dissolved species in mol m^{-3} m^{-1}. Concentration gradients of sulfide and sulfate were derived from measured pore water profiles obtained for the individual seep habitats. Sulfate fluxes at site GeoB 12313 (Flare 2) were calculated from concentration gradients generated by modeled profiles.

3.5 Geochemical modeling with "CoTReM"

Pore water profiles obtained for PCs taken from the three distinct successive habitats of seep site GeoB 12313 (Flare 2; 1038 m water depth) located at the lower boundary of the OMZ were modeled with the computer software CoTReM. The aim of this simulation was to assess rates of fluid advection and bioirrigation. Site GeoB 12313 was chosen for simulation runs because gas hydrates were found within 40-100 cm sediment depth in the area of Flare 2 (Bohrmann et al. 2008) and thus the lower boundary concentration of methane in equilibrium with gas hydrates (85 mM) could be estimated in the model following Tishchenko et

al. (2005). This approach is consistent, for example, with estimates of in situ methane concentrations used for pore water modeling at gas hydrate-bearing cold seeps on Hydrate Ridge off Oregon, USA (Torres et al., 2002) and at the Hikurangi Margin off New Zealand (Dale et al., 2010). Moreover, the spatial resolution was highest at site GeoB 12313 with three PCs obtained from adjacent habitats.

CoTReM is a one dimensional numerical, non-steady-state transport and reaction model based on an operator splitting approach. The software has been described in great detail elsewhere (e. g. Adler et al., 2000; Adler et al., 2001; Wenzhöfer et al., 2001; Pfeifer et al., 2002). Notably, CoTReM has already been successfully applied to model transport processes and geochemical reactions in other seep systems, namely mud volcanoes of the Eastern Mediterranean, by Haese et al. (2003) (simulation of AOM and advection rates) and Haese et al. (2006) (simulation of advection and bioirrigation rates).

Table 2: Input parameters used for pore water modeling of three cores at Flare 2.

Input parameters	Value
Length of modeled sediment column	50 cm
Porosity (upper to lower model boundary)	0.9 - 0.8
Temperature	12.3 °C
Sulfate concentrations at upper model boundary	26.3-31.6 mM (see text)
Methane concentrations at lower model boundary	85 mM (see text)
Fixed sulfide concentration at lower model boundary (only GeoB 12313-6)	14 mM

A model sediment column of 50 cm was chosen which was subdivided into cells of 1 mm thickness. The results are only displayed for the upper 30 cm of the sediment approximately corresponding to the length of the investigated PCs. Porosity was assumed to decrease from 0.9 at the sediment surface to 0.8 at a depth of 50 cm (lower model boundary). The time step to fulfill numerical stability was set to 10^{-4} yr. Bioirrigation was accounted for by implementing non-local mixing coefficients in the range of published values (e. g. Haese et al., 2006) until best-fit to measured sulfate profiles. Sedimentation rate was ignored due to the simulation of very short time scales. Measured bottom water concentrations of the chemical species involved define the upper boundary conditions. For

methane, and at site GeoB 12313-6 (Habitat 1 at Flare 2) also for sulfide, fixed concentrations were defined at the lower model boundary that created the gradients necessary to simulate the respective fluxes into the model area from below. The only chemical reaction considered in the simulations was AOM with sulfate. Pre-defined maximum rates for AOM (0.5 mol dm^{-3} yr^{-1}) were used by the model as long as the educt species were available in sufficient amounts to create a narrow SMTZ. As soon as the concentrations decreased, the rates were automatically reduced to match the available amount of reactants in each cell in order to avoid negative concentrations. A compilation of input parameters for the simulation runs is given in Table 2.

In a second modeling approach we explored how an initially diffusion-dominated sediment/pore water system responds to upward advection and/or bioirrigation at different rates (see section 5.4). The main question behind this simulation was to elucidate to which extent advective pore water flow – either through upward advection, or downward bioirrigation, or a combination of both – affects the depth of the SMTZ and fluxes of sulfate into the SMTZ. Boundary conditions chosen for the different scenarios were as described above, however in this approach we implemented the different transport processes consecutively in independent "scenarios".

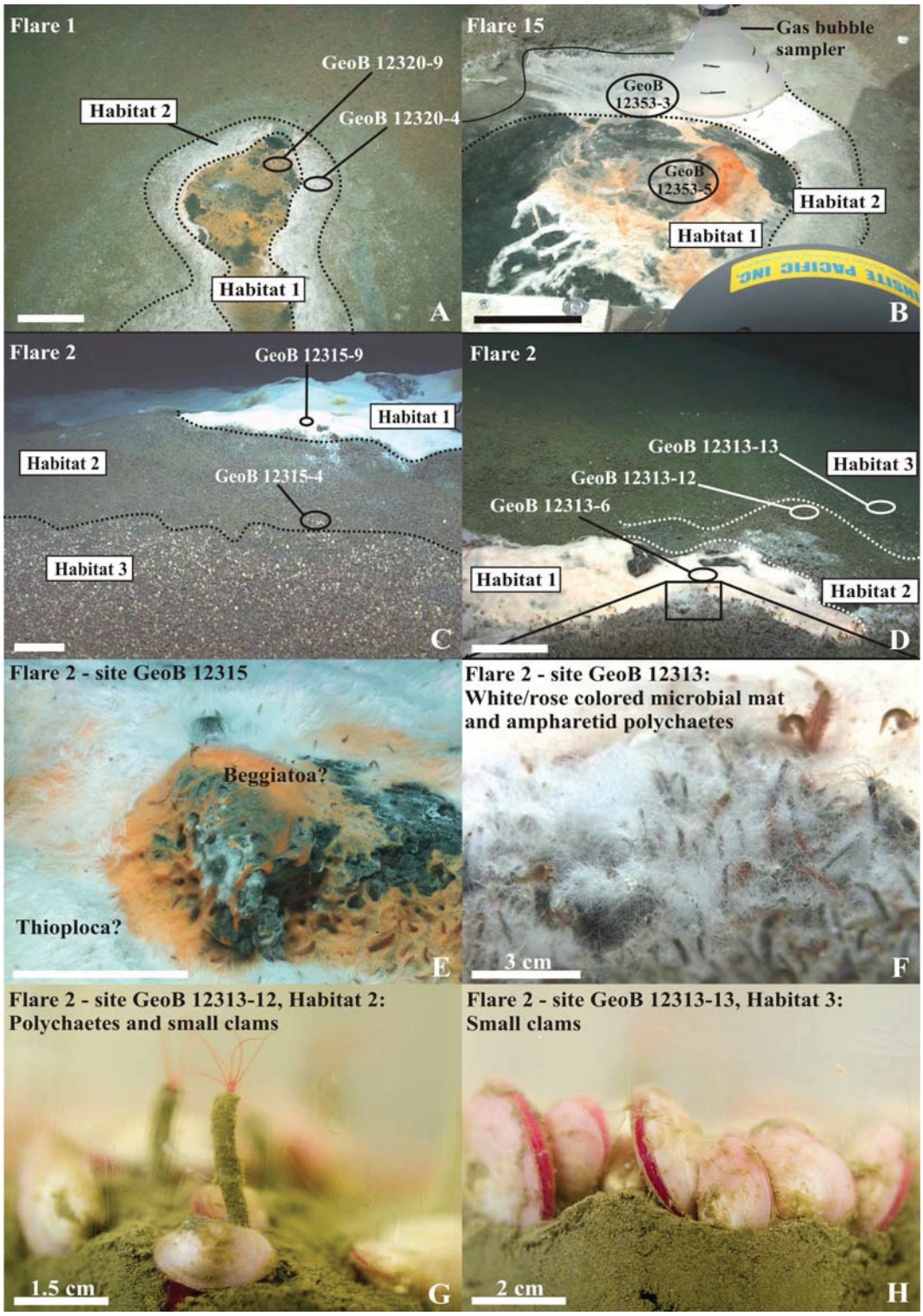

Figure 5: ROV still images (A-F) and images of retrieved cores (G-H). A-D: Major habitats at all sites are encircled by stippled lines and PC positions are denoted by circles. E: Close-up of Habitat 1 at site GeoB 12315, where we found microbial mats of distinctly different appearance (see text). F: Close-up of the transition from Habitat 1 to Habitat 2 in D. G Appearance of Habitat 2 in the retrieved PC GeoB 12313-12. H: Appearance of Habitat 3 in the retrieved PC GeoB 12313-13. Scale bar is 18 cm if not denoted otherwise.

4 Results

4.1 Background sites

Sulfate concentration profiles were obtained for two sites (TV-MUC cores GeoB 12309-3 and GeoB 12312-3) that were unaffected by gas release and did not show a colonization by chemosynthetic communities at the sediment surface. The sulfate profiles were linear at both sites and concentrations only slightly decreased with depth from bottom water values of 31 mM to about 29 mM at a depth of 20 cm in core GeoB 12309-3 and 26 mM at a depth of 23 cm in core GeoB 12312-3 (Fig. 6).

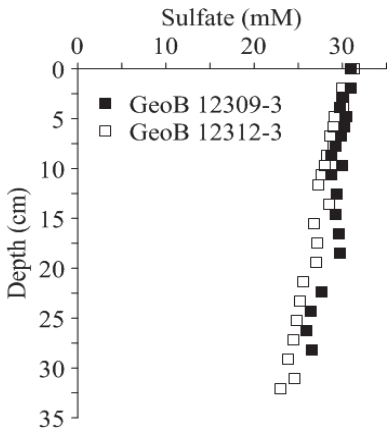

Figure 6: Pore water sulfate profiles of non-seep reference TV-MUC cores.

4.2 Gas seepage

At all four seep sites investigated in this study gas bubble ebullition from distinct gas orifices in the center of the seeps was observed. The gas orifices were about 1 cm in diameter. At the time of sampling gas flux at the shallower sites Flare 1 and Flare 15 (551 m and 732 m water depth) was generally lower than at Flare 2 (1025 m and 1038 m water depth; M. Römer, unpubl. data). At the latter, which was located well within the GHSZ, gas bubbles emanating from the sea floor were immediately surrounded by skins of gas hydrate (M. Römer, unpubl. data).

4.3 Seeps within the core-OMZ

The two seep sites GeoB 12320 (Flare 1, 551 m water depth; Fig. 5A) and GeoB 12353 (Flare 15, 732 m water depth; Fig. 5B) were located within the core-OMZ (oxygen concentrations < 1 µM; Bohrmann et al. 2008) and above the GHSZ. Seep communities at both sites exclusively consisted of orange-colored microbial mats in the center (Habitat 1) surrounded by white/rose-colored microbial mats (Habitat 2; Figs. 5A and 5B). The overall diameter of these microbial mats was about 40 cm at Flare 1 (GeoB 12320) and about 60 cm at Flare 15 (GeoB 12353). Microbial mats at both sites were up to 1 cm thick and appeared chaotic and interwoven (Figs. 5A and 5B). Microbial mat coverage of the sediment surface was heterogeneous and single filaments could not be resolved with the

HD camera. We tentatively identified the orange and white colored microbial mats at Flare 1 and 15 as *Beggiatoa spp*. or close relatives. Gas bubble emanation occurred from three distinct orifices within the orange mat at Flare 1 and from two orifices within the orange mat at Flare 15. Central, orange mats were always associated with dark-gray to black surface sediments (Figs. 5A and 5B) and we could observe blackish sediment grains entrained by gas bubbles ascending from the orifices. Bubble escape from the surrounding white/rose-colored mats was not observed. Authigenic carbonates of a very porous and brittle fashion were found in the surface sediments at Flare 1 and Flare 15. They exclusively occurred below microbial mats at gas vents. Pore water data obtained for the central habitats at Flares 1 and 15 (GeoB 12320-9 and GeoB 12353-5, respectively; "Habitat 1" in Figs. 5A and 5B) show that sulfate concentrations were already well below sea water values close to the sediment surface (6.77 mM in core GeoB 12320-9 and 11.85 mM in core GeoB 12353-5) and further decreased with depth to minimum concentrations of 0.16 mM in GeoB 12320-9 and 0.92 mM in GeoB 12353-5 (Figs. 7A and 8A). Sulfide contents in the seep centers (Habitat 1) were

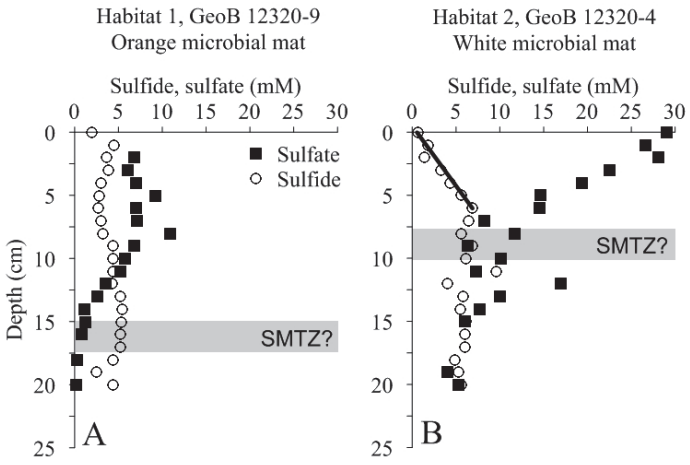

Figure 7: Pore water profiles of sulfide and sulfate of PCs obtained for Flare 1, site GeoB 12320. The assumed depth of the SMTZ is marked by a grey box. Coring positions are marked in Fig. 4 and sampling coordinates are given in Table 1.

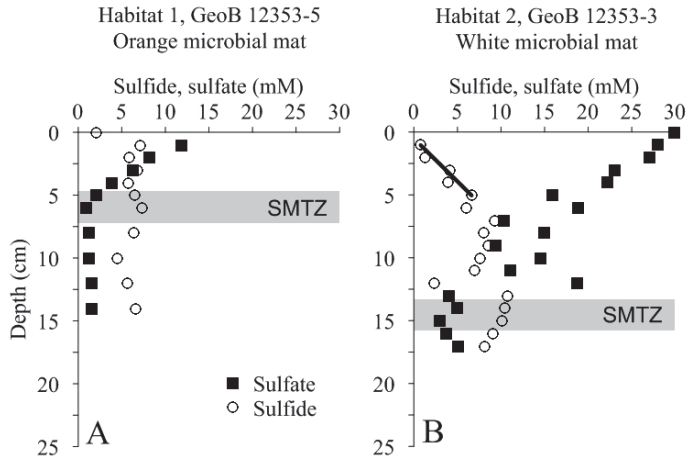

Figure 8: Pore water profiles of sulfide and sulfate of PCs obtained for Flare 15, site GeoB 12353. See caption of Fig. 7 for further details.

relatively constant over depth and fluctuated between 5 and 6 mM, respectively (Figs. 7A and 8A). A concentration gradient of sulfide into the overlying bottom water was observed at both sites. Sulfate profiles determined for the surrounding Habitats 2 at Flares 1 and 15 (GeoB 12320-4 and GeoB 12353-3 in Figs. 7B and 8B) show a steep, almost linear downward decrease from seawater values at the sediment surface to lowest concentrations fluctuating around 5 mM at 19 cm and 15 cm, respectively. Sulfide concentrations in both cores increase with depth along steep gradients to maximum values of 9.6 mM at 11 cm (GeoB 12320-4) and 10.7 mM at 13 cm (GeoB 12353-3). In these surrounding Habitats 2 of Flares 1 and 15 a sulfide concentration gradient into the bottom water was not observed.

4.4 Seeps at the lower boundary of the OMZ

The two seep locations situated at the lower boundary of the core-OMZ at Flare 2 (site GeoB 12315 at 1025 m and site GeoB 12313 at 1038 m water depth; Figs. 5C and 5D) were characterized by slightly elevated bottom-water oxygen concentrations (> 1 µM; Bohrmann et al. 2008) and abundant macrofaunal life both in the water column and at the sea floor. The sediment surface within both central habitats at Flare 2 was draped with m^2-sized patches of white/rose-colored microbial mats surrounding sites of active gas ebullition (Figs. 5C and 5D). The microbial mats (Habitat 1) at Flare 2 were about 1 m (GeoB 12313) and 5 m (GeoB 12315) in diameter, in places more than 5 cm thick and appeared as a lawn-like cover on the sediment surface. The mats at both central habitats at

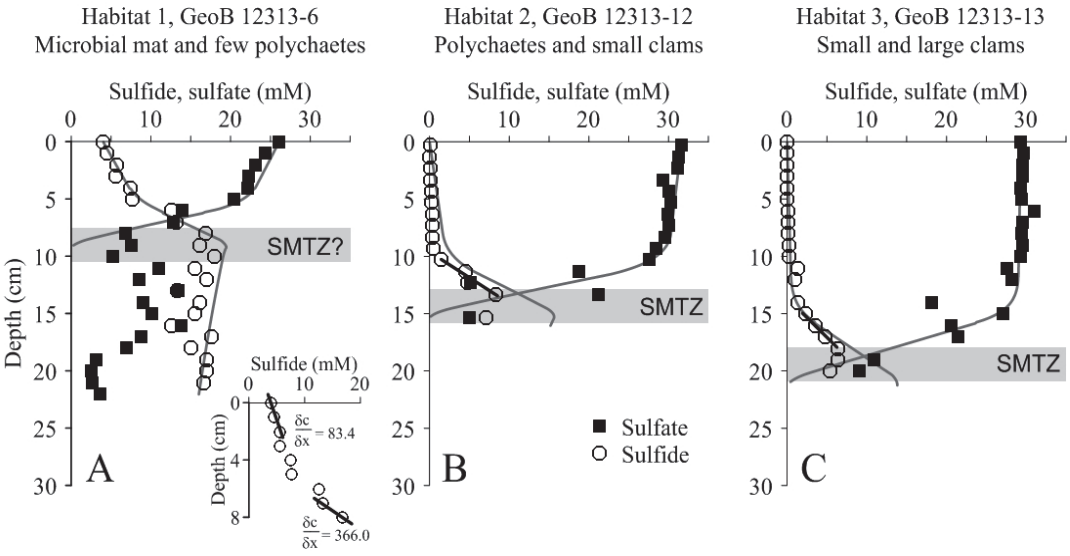

Figure 9: Pore water profiles of measured (symbols) and modeled (lines) solutes of PCs obtained for Flare 2, site GeoB 12313. See caption of Fig. 7 for further details.

Flare 2 occurred around dm-sized cracks and fissures in the sediment. We could resolve single microbial filaments by means of the HD camera (Figs. 5E and 5F). However, filament diameter could not be estimated based on these photographs. At site GeoB 12315 we found the central microbial mats in Habitat 1 to be accompanied with and underlain by a cm^2-sized mat of orange-colored microbial filaments that showed a distinctly different appearance with a smaller mat thickness of about 1 cm (Fig. 5E). Due to the distinctly different filament lengths and pigmentation of both observed mat types we tentatively suggest that they belong to different species. The central small mat at site GeoB 12315 resembles *Beggiatoa spp*.-type filaments or close relatives (Fig. 5E) whereas the thick and vast white mats occurring at site GeoB 12313 and GeoB 12315 resemble *Marithioploca spp*. or close relatives (Figs. 5E and 5F).

The central microbial mats at Flare 2 were always surrounded by concentrically arranged habitats of chemosynthetic or grazing/filtering macrofauna (Habitats 2 and 3). The transition from Habitat 1 to Habitat 2 at the Flare 2 sites was marked by the co-occurrence of microbial mats associated with few small vesicomyid clams (cf. *Isorropodon sp*.) and abundant ampharetid polychaetes (Fig. 5F). Habitat 2 at both Flare 2 sites was generally dominated by the ampharetid polychaete *Pavelius uschakovi* (Kuznetsov and Levenshtein, 1988) and small (< 3 cm) vesicomyid clams both decreasing in abundance in outward direction. The outermost Habitat 3 at both Flare 2 sites was dominated by small (<3 cm) and in places by larger vesicomyid clams. In contrast to the seep sites at Flares 1 and 15 (core-OMZ) a ubiquitous feature at both Flare 2 sites was the occurrence of massive authigenic carbonates that were up to a few dm in diameter. The carbonates were often but not exclusively found close to the gas orifices associated with microbial mats.

Pore water data were obtained for two PCs from seep site GeoB 12315 (Fig. 10) and for three PCs from seep site GeoB 12313 (Figs. 9). PC sampling of the central Habitat 1 sediments (GeoB 12315-9 and GeoB 12313-6) was partly complicated by the presence of massive authigenic carbonates. Sulfate concentration profiles obtained for these cores indicated that sulfate contents in the bottom water were depleted compared to bottom water at the background sites depicted in Fig. 6 and only showed a slight decrease down to a depth of about 5 cm (Figs. 9A and 10A). Below this depth sulfate concentrations sharply decreased to 8 mM (GeoB 12315-9) at 11 cm and 5 mM (GeoB 12313-6) at

10 cm sediment depth. In the central Habitat 1 of site GeoB 12313 sulfate concentrations increased again below 10 cm to reach values of 15 mM between 13 and 17 cm and then decreased downcore to reach values of about 2 mM at the base of the PC (Figure 10A). Sulfide concentrations for the two Habitat 1 cores showed a steep downward increase from 1.5 mM at 1 cm depth to 16.5 mM at 13 cm depth (GeoB 12315-9, Fig. 9A) and from 4 mM at the surface to 17.5 mM at a depth of 10 cm (GeoB 12313-6, Fig. 10A).

Sulfate profiles of the Habitat 2 PCs GeoB 12315-4 (Figure 9B) and GeoB 12313-12 (Fig. 10B) showed background concentrations at the sediment surface and a slight downward decrease within the first 6 and 10 cm, respectively. Below these depths, sulfate concentrations steeply dropped to 3 mM at a depth of 16 cm (GeoB 12315-4) and to 5 mM at a depth of 15 cm (GeoB 12313-12). Sulfide concentrations in both cores fluctuated between 0-2 mM in the upper 5-10 cm and increased along steep gradients to maximum values of 14 mM (GeoB 12315-4) and 8.5 mM (GeoB 12313-12) at 11 cm and 13 cm, respectively (Figs. 10B and 9B). In core GeoB 12313-13 obtained from Habitat 3 rather constant sulfate concentrations were measured from the sediment surface down to a depth of 15 cm below which sulfide showed a maximum of 6.4 mM at 19 cm and decreased downwards (Fig. 9C). In general, the depth of the distinct kink in the sulfate pore water profiles at both Flare 2 sites deepened with increasing distance to Habitat 1.

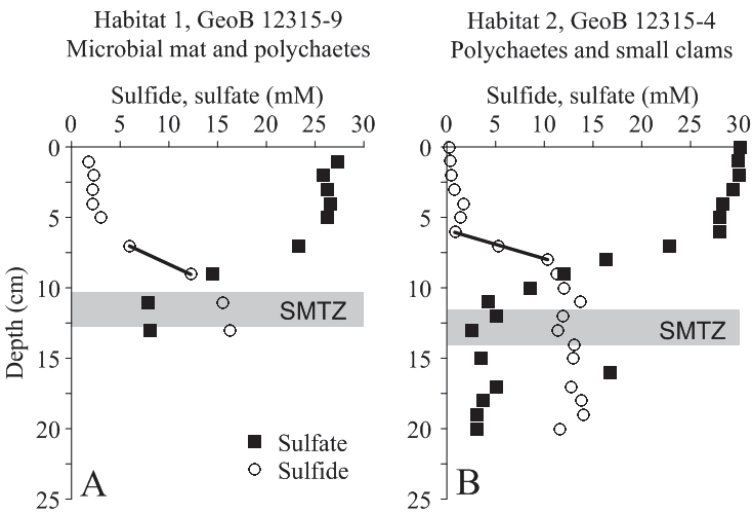

Figure 10: Pore water profiles of sulfide and sulfate of PCs obtained for Flare 2, site GeoB 12315. See caption of Fig. 7 for further details.

5 Discussion

5.1 Sulfate profiles and the depth of the SMTZ

Although displaying different profile shapes the interstitial sulfate concentrations at all investigated seep habitats decrease with depth indicating that AOM occurs close to the sediment surface. In contrast, sulfate contents at the two background sites GeoB 12309 and GeoB 12312 (Fig. 6) barely decrease over the sampled sediment interval and represent the “normal” pore water situation in the area which is governed by diffusion and neither affected by hydrocarbon seepage nor shallow AOM. The bottom water concentration of sulfate measured in the study area amounts to 31 mM (Fig. 6) and is thus slightly higher than average seawater sulfate values of ~28 mM (Claypool and Kaplan, 1974). Similarly high bottom-water sulfate concentrations were also reported by Schmaljohann et al. (2001) for sediment cores retrieved from comparable water depths on the Makran accretionary prism. A reasonable explanation for the elevated bottom water sulfate concentrations in the study area is the inflow of more saline intermediate water masses from marginal seas as e.g. the Red Sea and the Persian Gulf as has been proposed by Olson et al. (1993).

Sulfate profiles obtained for the core-OMZ sites (Flares 1 and 15, Figs. 7 and 8) depict distinctly different shapes compared to those obtained for the lower OMZ-boundary locations (Flare 2, Figs. 9 and 10). At the core-OMZ sites we found sulfate contents well below measured ambient bottom water values (~ 31 mM) at the sediment surface in the central habitats colonized by orange microbial mats (GeoB 12320-9, GeoB 12353-5). Following the interpretation by Niemann et al. (2006), the low sulfate concentrations at the sediment surface in the central habitats may be caused by fluid advection inhibiting the diffusion of sulfate into the sediment. Advection usually produces a concave-down curved sulfate profile which was found to a minor extent at the core-OMZ site GeoB 12353-5 (Fig. 8A). For the outer habitats ("Habitat 2") of Flares 1 and 15, which were colonized by white microbial mats, we determined linear sulfate profiles that suggest a diffusion-controlled depth of the SMTZ (Figs. 7B and 8B).

In contrast to the core-OMZ sites, sulfate profiles obtained for all habitats at Flare 2 located at the lower boundary of the OMZ uniformly show distinct "kink-type" or “irrigation-type” profiles (Aller, 1980; Aller and Aller, 1998; Hensen et al., 2003) several cm below the sediment surface (Figs. 9 and 10). Kink-type sulfate profiles suggest intense irrigation of the sediment surface with sulfate-rich bottom

water by polychaetes and clams colonizing these habitats (e.g. Fossing et al., 2000; Haese et al., 2006). Yet, based on the limited bottom water oxygenation at Flare 2, we suggest the polychaete and clam communities can only be sustained if the OMZ in the water column either shrinks or shifts periodically and in that way provides enough oxygen for these communities. In fact, it has been stated earlier that the vertical extent of the OMZ off Makran is not stable and undergoes monsoon-forced fluctuations (Wyrtki, 1973; Brand and Griffiths, 2009). It is thus likely that Flare 2 is periodically flushed with oxygen-rich bottom water sustaining the observed macrofauna.

The strong depletion in sulfate observed at a depth of several cm in all Habitat 1 cores indicates that the SMTZ was recovered in the sampled sediment intervals and is usually located between 5 and 15 cm (Figs. 7A, 8A, 9A and 10A). At all Habitat 2 and 3 sites the approximate depth of the SMTZ is located slightly deeper between 10 and 20 cm (Figs. 7B, 8B, 9B and 9C, 10B). At site GeoB 12313, where three PCs were retrieved, we found that the depth of the SMTZ progressively deepens from the center towards the outer habitats (Fig. 9).

It is difficult to identify the exact depths of the SMTZ at the four investigated seep sites because sulfate concentrations in all habitats except for site GeoB 12313-6 approach relatively constant concentrations around a few millimoles below the assumed depth of the SMTZ and do not completely vanish in the reaction zone. Some possible scenarios were suggested to explain similar observations at other seeps, including mixing of bottom water into the sediment due to ex situ degassing based on pressure release (Wallace et al., 2000) or ebullition of free gas in situ (Haeckel et al., 2007). Particularly the latter process needs to be considered in all Habitat 1 sites where bubble escape was observed. Oxidation of sulfide to sulfate during sample handling and storage has been discussed in several studies (Luff and Wallmann, 2003; Leloup et al., 2007) but may be of minor significance here due to immediate dilution and freezing of sulfate samples onboard ship. "Cryptic sulfur cycling" based on disproportionation of intermediate sulfur species releasing sulfate within the methane zone was identified by Holmkvist et al. (2011) to explain low sulfate contents in sediments of the Black Sea. We cannot exclude this process; however, sulfate concentrations reported here are much higher than those shown by Holmkvist and co-workers. Threshold sulfate concentrations up to 2 mM constraining bioenergetics for bacterial sulfate reduction (Leloup et al., 2007; Knab et al., 2008) and AOM (Dale et al., 2010)

were suggested to explain sulfate tailing below the SMTZ which may be of significance at sites GeoB 12315-4 and GeoB 12353-5 where we measured near-constant sulfate levels around 2 mM below the SMTZ. For sites close to in situ gas bubble ebullition (Habitats 1 in this study) a lateral flow of sulfate-rich pore water towards the gas bubble conduit involving convection-like pore water cycling was proposed which would lead to sulfate transport into a discrete layer below the SMTZ (O'Hara et al., 1995; Tryon et al., 2002; Haeckel and Wallmann, 2008). It was shown in detail by O`Hara et al. (1995) that a draw-down of bottom water into the sediment occurs at gas seeps off Denmark within a lateral distance of up to 20 cm from the gas orifice. Habitat 1 core GeoB 12313-6 provides strong evidence for this kind of convective flow because the sulfate profile displays a peak between 10 and 20 cm pointing at a source of sulfate to the pore water in this depth interval (Fig. 9A). The core was obtained within a distance of <30 cm from the gas orifice (Fig. 5D) and could thus be affected by convection of bottom water through the sediment (O`Hara et al. 1995). Habitats 2 and 3 cores at Flare 2, however, were obtained from sites several m away from the orifice (Fig. 5D) and may thus not be influenced by a draw-down of bottom water into the sediment which is supported by the absence of pronounced sulfate peaks below the SMTZ (Figs. 9B and 9C). In contrast, Habitat 2 cores at Flares 1 and 15 (Figs 5A and 5B) were retrieved within a radius of only 20 cm around the respective gas orifices and indeed show minor increases in sulfate contents at 12 cm (GeoB 12320-4) and 17 cm (12353-3) which suggest lateral flow of sulfate-rich bottom water into the sediment (Figs. 7B and 8B). Our interpretation of convection-like cycling of pore and bottom water is in accord with the study by O`Hara et al. (1995) stating that convective cycling of pore and bottom water at gas seeps is an important transport mechanism at sites close to the gas orifice and may influence rates of biogeochemical turnover of dissolved species as e. g. sulfate.

5.2 Hydrogen sulfide fluxes and chemosynthetic communities

Concentration gradients used for flux calculations are indicated as black lines in Figs. 7, 8, 9 and 10. Upward sulfide fluxes were calculated for the Habitat 2 sites at Flare 1 and Flare 15 (GeoB 12320-4 and GeoB 12353-3) which were not affected by gas bubble escape at the time of sampling. An export of sulfide into the bottom water is not indicated by pore water profiles at both sites (Figs. 7B and 8B). The sulfide flux at these sites amounts to 4.9 and 3.3 mol m^{-2} yr^{-1}, respectively, and is directed towards the sediment surface where white microbial

mats were observed (Table 3). The calculated sulfide flux is in the lower range of published values for comparable microbial mat habitats for example at the Cascadia margin (Sahling et al., 2002) and at the Håkon Mosby Mud Volcano (de Beer et al., 2006; Lichtschlag et al., 2010a). In fact, Lichtschlag et al. (2010a) found that a sulfide flux of 2.5 mol m^{-2} yr^{-1} represents the lower threshold for *Beggiatoa* mats which is well below the fluxes calculated for the Habitat 2 cores at Flares 1 and 15. In agreement with Gilhooly et al. (2007) we found at the core-OMZ sites that orange microbial mats (Habitat 1) seem to tolerate high sulfide concentrations and fluxes towards and across the sediment/water interface, whereas white microbial mats (Habitat 2) tolerate only moderate to low sulfide concentrations.

Table 3: Fluxes of dissolved sulfide and sulfate, as well as depth of steepest sulfide gradient at all seep sites. Fluxes derived from modeled pore water profiles are marked.

	Flare 2, Habitat 1 (below core OMZ)	Flare 2, Habitat 2 (below core OMZ)	Flare 2, Habitat 3 (below core OMZ)	Flare 1, 15; Habitat 2 (within core OMZ)
Organisms	White/rose colored mat, sparse polychaetes	Polychaetes, small clams	Small and large clams	White/rose colored mat
Core ID	GeoB 12315-9 GeoB 12313-6	GeoB 12315-4 GeoB 12313-12	GeoB 12313-13	GeoB 12320-4 GeoB 12353-3
Upward sulfide flux (mol m^{-2} yr^{-1})	8.0 9.2	11.0 5.7	2.8	4.9 3.3
Depth of steepest sulfide gradient	7-8 cm 3-7 cm	6-8 cm 10-13 cm	15-18 cm	2-6 cm 1-5 cm
Sulfate flux into SMTZ (mol m^{-2} yr^{-1})	9.3 9 (modeled)	8.0 8.4 (modeled)	6.6 (modeled)	7.1 4.5

At the microbial mat site GeoB 12313-6 (Habitat 1, Flare 2, lower boundary of OMZ) a sulfide flux across the sediment/water interface is indicated by the sulfide profile (Fig. 9A, inset). The sulfide export into the bottom water amounts to 1.3 mol m^{-2} yr^{-1}. We have observed numerous microbial filaments that were attached to carbonate chunks or polychaete tubes exposed above the sediment surface and that were thus cut off from the interstitial sulfide pool in the sediment (Fig. 5F). Apparently, the sulfide flux across the sediment/water interface is sufficient to nourish these microbes at site GeoB 12313-6 and probably at the comparable Habitat 1 site GeoB 12315-9 (Flare 2). A similar observation has been reported from cold seeps on the Hikurangi Margin (Sommer et al., 2010) which indicates that thiotrophic microbes do not necessarily depend on direct access to the pore

water sulfide pool as long as the sulfide export into the bottom water meets their sulfide demand.

Apart from the sulfide flux across the sediment/water interface in Habitat 1 at site GeoB 12313 we determined the "deep" upward sulfide flux from the SMTZ to depths of 5 to 15 cm at all Flare 2 sites. In general we found that the "deep" sulfide flux amounts to 8.0 and 9.2 mol m^{-2} yr^{-1} at the microbial mat sites (Habitat 1, GeoB 12313-6 and GeoB 12315-9) while fluxes of 5.7 and 11.0 mol m^{-2} yr^{-1} were determined for the polychaete and clam sites GeoB 12313-12 and GeoB 12315-4 (Habitat 2). The lowest flux of 3.9 mol m^{-2} yr^{-1} was obtained for the large clam site GeoB 12313-13 in Habitat 3 (Table 3). Despite the rather high flux at site GeoB 12315-4 (Habitat 1), the sulfide flux in general decreases slightly towards outer habitats at Flare 2. This pattern resembles findings by Sahling et al. (2002) who calculated a high sulfide flux of 23 mol m^{-2} yr^{-1} below a *Beggiatoa* mat and a lower flux of 6.6 mol m^{-2} yr^{-1} below a clam bed (large *Calyptogena*) at Hydrate Ridge cold seeps.

Table 4: Modeled rates of advection and bioirrigation obtained for three cores at Flare 2.

	Advection rate (cm yr^{-1})	Depth-integrated bioirrigation rate (cm yr^{-1}); at a depth of (cm)
Habitat 1, GeoB 12313-6	11	120; 4.1 - 5.9
Habitat 2, GeoB 12313-12	8	210; 8.0 - 11.5
Habitat 3, GeoB 12313-13	< 1	297; 11.8 - 15.7
Comparable approach using CoTReM by Haese et al. (2006)	5 - 30	max. 300; 8-11

Upward sulfide fluxes have been widely used in recent publications to describe the geochemical environment of chemosynthetic communities at cold seeps (e. g. Sahling et al., 2002; de Beer et al., 2006; Niemann et al., 2009; Lichtschlag et al., 2010b). It needs to be stressed that the sulfide profiles measured in sediments inhabited by chemosynthetic organisms are already influenced by the metazoan sulfide uptake and thus calculated fluxes may be a result rather than a prerequisite for chemosynthesis. In Table 3 we show the depth intervals of the steepest sulfide gradients for the three cores at site GeoB 12313. The depths gradually increase towards the outer habitats from 3-7 cm near the gas orifice

(GeoB 12313-6) to 15-18 cm in the outermost Habitat 3 (GeoB 12313-13) where abundant large and small vesicomyid clams were observed. The clams, although depending on a certain sulfide flux for their symbionts (e. g. Grehan and Juniper, 1996; Sahling et al., 2005), ventilate sulfide-free bottom water into the sediment and at the same time remove sulfide from the pore water for respiration. Our data show that the magnitude of the upward sulfide flux alone does not determine the colonization of the sediment by chemosynthetic organisms exploiting the sulfide pool and does thus not accurately describe their geochemical environment. It is rather the combination of sulfide flux, the depth of sulfide release (SMTZ) and the depth into which the flux occurs, i. e. the depth where sulfide is depleted either due to mineral authigenesis or uptake by organisms which determines the colonization of seeps by thiotrophic and/or chemosynthetic communities.

5.3 Quantifying transport processes – modeling results

The computer model CoTReM has been applied to the three habitats of site GeoB 12313 at Flare 2 below the core-OMZ. 3D-modeling of pore water profiles considering the seep including all habitats as a continuum would be favorable at the study site Flare 2. However, such an approach would require a much higher sampling density than was achieved during the cruise. For example, the pore water profiles used for modeling derive from three PCs obtained from distinctly different habitats at Flare 2 selected by eye. The investigated habitats in total covered an area of more than 25 m^2 which is estimated based on observed colonization with chemosynthetic communities. Thus, the pore water profiles of a single PC would represent an area of more than 8 m^2 which is not sufficient for 3D-modeling. We therefore considered each PC to be representative for its respective habitat and applied the 1D-model in order to estimate the magnitude pore water transport processes. Simulated profiles of sulfate and sulfide at site GeoB 12313 are depicted as solid lines in Fig. 9 and advection and bioirrigation rates are given in Table 4.

Advective flow velocity is highest (11 cm yr^{-1}) in core GeoB 12313-6 in the vicinity of the gas orifice and decreases with increasing distance to the orifice in cores GeoB 12313-12 (8 cm yr^{-1}) and GeoB 12313-13 (< 1 cm yr^{-1}). Few published pore water flow velocities of 10 cm yr^{-1} (Linke et al., 2005), 3-50 cm yr^{-1} (Haese et al., 2003; Haese et al., 2006) and 1-28 cm yr^{-1} (Han and Suess, 1989) determined for cold seeps on the Cascadia margin and mud volcanoes on the Costa Rica

margin and in the Mediterranean Sea compare well to the rates determined here. Yet, the majority of studies depicts much higher velocities of up to several meters yr^{-1} (e. g. Linke et al., 1994; Wallmann et al., 1997; Lichtschlag et al., 2010b). The low advection rates determined here may be due to the fact that cold seeps that are not associated with mud volcanism emit fluids and gas rather continuously and fluid flow is generally slow. In contrast, mud volcanoes, expel mixtures of gas, fluid and mud at high velocities during eruptive phases (cf. Kopf, 2002).

Depth-integrated rates of bioirrigation increase from 120 cm yr^{-1} in Habitat 1 to 210 cm yr^{-1} in Habitat 2 and 297 cm yr^{-1} in Habitat 3 including nonlocal mixing coefficients of 100-120 yr^{-1} (Table 4). The rates correspond exceptionally well with those obtained for a Mediterranean mud volcano by Haese et al. (2006) with a similar approach using CoTReM. Depth-integrated bioirrigation rates of up to 900 cm yr^{-1} were obtained by Wallmann et al. (1997) to simulate bioirrigation at active cold seeps in the Aleutian subduction zone. The higher values used by these authors are probably linked to the fact that the pore water advection obtained by Wallmann et al (1997) is with 340 cm yr^{-1} much higher than the maximum velocity determined in this study (11 cm yr^{-1}). Therefore, organisms responsible for bioirrigation at the Aleutian margin seeps had to counteract a much higher advective flow velocity in order to detoxify their habitat from too high sulfide concentrations.

The pore water model produces considerably higher maximum concentrations of hydrogen sulfide than those measured in cores GeoB 12313-12 and GeoB 12313-13 (Fig. 9). The deviation of modeled maximum sulfide concentrations compared to measured values is attributed to the fact that the model in our configuration neglects the various processes of sulfide consumption e.g. sulfide uptake by organisms (e. g. Arp et al., 1984), precipitation of iron sulfides (e. g. Berner, 1970) or sulfurization of organic matter (e. g. Brüchert, 1998). Regarding the formation of iron sulfide minerals, the availability of reactive Fe(III) species may play an important role: The Habitat 1 site GeoB 12313-6 is interpreted to be subject to most intense and shallowest production of sulfide via AOM due to highest rates of advective transport of methane-rich fluids. In theory, prolonged production of sulfide through AOM would result in a continuous reduction and removal of reactive iron (oxyhydr)oxides via reaction with hydrogen sulfide until most of the Fe(III) minerals are transformed into iron monosulfides and pyrite (Berner, 1970). Consequently, sites GeoB 12313-12 and GeoB 12313-13, which

are subject to lower rates of AOM and sulfide release than the central site GeoB 12313-6, may have experienced a less intense reduction of iron (oxyhydr)oxides. Thus, due to the fact that the only chemical reaction we used in CoTReM is AOM, one would expect that the overestimation of hydrogen sulfide concentrations by the model would be greater in distant sites (Habitats 2-3) than in the central one (Habitat 1) which is well supported by our data (Fig. 9).

5.4 Schematic evolution of the depth of the SMTZ and sulfate fluxes – unraveling the relative importance of different transport processes

The studies by Wallmann et al. (1997) and Haese et al. (2006) demonstrated that the interaction of the transport processes bioirrigation and advection significantly influences pore water profiles and solute fluxes at cold seeps. In this chapter we contribute further insights into the magnitude and importance of the complex interplay of up- and downward transport processes based on habitat-specific pore water modeling: Figure 11 depicts a simulated stepwise development of the pore water profiles at site GeoB 12313 from a purely diffusion-controlled system towards the present measured state including upward advection and downward bioirrigation. The initial setting for the simulation includes molecular diffusion as the only transport process (Fig. 11, scenario A). It is obvious that the shapes of the sulfate profiles, sulfate fluxes and the depths of the SMTZ in Fig. 11, scenario A do not match the measured ones depicted in scenario D. Upward advection was thus simulated for the three habitats at different rates in order to approach the observed sulfate gradients (and fluxes) into and the depths of the SMTZ (Fig. 11, scenario B). We have discussed earlier that the pore water profiles at site GeoB 12313 are likely influenced by a convection-like pore water flow, where the central Habitat 1 experiences lateral inflow of bottom water balancing the focused gas escape (O`Hara et al. 1995). Although the model does not consider lateral advection, it was possible to simulate the sulfate concentration gradients and particularly the respective depths of the SMTZs in both cores of Habitat 2 and 3 with upward advection. We therefore suggest that an upward advective flow of pore water is present in all modeled habitats at Flare 2. The onset of advective pore water flow pushes the SMTZ towards the sediment surface in all cores and significantly increases sulfate fluxes into the SMTZ in all habitats (Fig. 11, scenario B). The upward-shifted SMTZ leads to a shallower sulfide release via AOM and thus triggers an increase in sulfide flux towards the sediment surface in

all habitats. In Habitat 1 where the SMTZ is shallowest (Fig. 11, scenario B) the sulfide flux towards the sediment surface is highest and it decreases towards outer habitats because the sulfate fluxes into the reaction zone decrease in the same direction. Thus, the high advection of pore water in Habitat 1 triggers sulfide flux to the sediment surface that meets the high sulfide demand of microbial mats (de Beer et al., 2006). In contrast, the lower advection in Habitats 2 and 3 leads to a weaker upward sulfide flux that meets the demand of chemosynthetic macrofauna, for example clams and polychaetes (Sahling et al., 2005). We assume that scenario B in Fig. 11 represents the first step in seep colonization which determines whether the sediment surface is colonized by microbial mats in the center (highest sulfide flux) or by chemosynthetic macrofauna (lower sulfide flux in Habitats 2 and 3). Consequently, simulating the colonization of the seep with chemosynthetic organisms, non-local mixing coefficients (bioirrigation at different rates, Table 4) were implemented into the model to account for bioirrigation (Fig. 11, scenario D). Implementation of bioirrigation as a further transport process leads to the distinct gradient changes ("kink-type") that we observed in the measured sulfate profiles and at the same time shifts the SMTZ to greater depths due to introduction of sulfate-rich bottom water into the sediment (Fig. 11, scenario D). To test, if the depth of the SMTZ, sulfate fluxes, and shapes of the sulfate profiles can be sufficiently simulated considering only diffusion and bioirrigation without upward advection, we started a separate run (Fig. 11, scenario C). In this case the general sulfate profile shapes more or less match those of measured profiles, yet the depths of the SMTZ and sulfate fluxes do not, which highlights the importance of upward advection for the three examined sites.

The development of the sulfate fluxes in the different habitats and in the different model scenarios needs further consideration, because the sulfate input into the SMTZ determines the concentration and flux of released sulfide, which is essential for chemosynthetic communities. In Fig. 11 (scenario D, "present state") the sulfate fluxes into the SMTZ are given as bold numbers. The fluxes slightly decrease from 9.3 mol m^{-2} yr^{-1} in the center to 7.7 mol m^{-2} yr^{-1} and 6.6 mol m^{-2} yr^{-1} in the outer Habitats 2 and 3. When considering only advection (Fig. 11, scenario B) sulfate fluxes decrease stronger in the same direction, whereas sulfate fluxes stay similar when considering only bioirrigation (Fig. 11, scenario C). This shows that the combined transport processes advection and bioirrigation produce a mixed signal in the fluxes of sulfate into the SMTZ. Thus, the ventilating

macrofauna counteract upward advection by shifting the SMTZ to greater depth but at the same time lead to comparably high sulfate fluxes (and high rates of sulfide production) in all three habitats. The stepwise simulation in Fig. 11 shows that it is the combination of upward advection and counteracting downward transport of bottom water by chemosynthetic macrofauna that resulted in the best fit of the depth of the SMTZ, sulfate fluxes into the reaction zone and the general shapes of the sulfate profiles in all three habitats at Flare 2. Compared to earlier studies (e. g. Wallmann et al., 1997; Haese et al., 2006) targeted sampling of distinct seep-habitats enabled us to quantify the complex interplay of bioirrigation and advection and their impact on solute fluxes in the three different habitats at Flare 2.

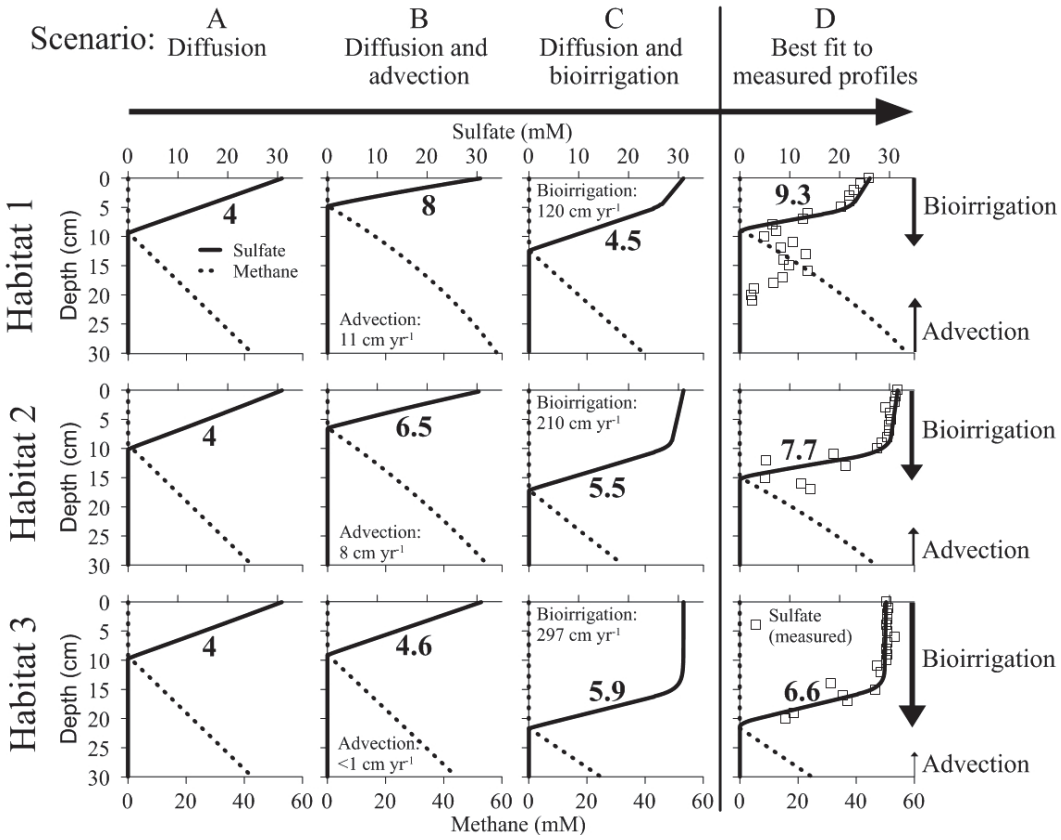

Figure 11: Stepwise development of modeled sulfate and methane concentration profiles from a diffusively controlled system towards the observed state including advection and bioirrigation. Columns A-D indicate different "scenarios" whereas rows indicate the three different habitats at site GeoB 12313. Bold numbers next to concentration profiles depict modeled fluxes of sulfate into the SMTZ. The arrows on the right indicate the relative magnitude of the indicated transport processes.

5.5 The mutual interaction of geochemistry and chemosynthetic communities

Comparing core-OMZ seeps (Flare 1 and 15) to those at the lower boundary of the OMZ (Flare 2) the most prominent feature is that oxygen levels in the bottom water determine whether a cold seep is colonized exclusively by microbial mats or by mats and surrounding chemosynthetic macrofauna including ampharetid polychaetes and vesicomyid clams. We could show that the macrofauna - most probably the observed clams - compensate for lower upward advection in outer habitats compared to the microbial mat habitat by shifting the SMTZ to greater depth which induces high sulfate fluxes and intense sulfide release. This is summarized in the conceptual model given in Fig. 12. This figure shows how animals ventilating the sediment surface with bottom water lead to an extended sulfate zone and thus provide oxic (or at least non-sulfidic) conditions (Fig. 12B). Seeps within the OMZ lack colonization by metazoans which allows a very shallow SMTZ to develop (Fig. 12A). The fact that clams shift the SMTZ to greater depth implies that they may gradually proceed towards the seep-center attracted by the shallow and high sulfide flux and may at the same time undermine and thus cut off smaller organisms (cf. Habitat 1-2 in this study) from the sulfide source (Figs. 11 and 12). In that way the clams progressively broaden the sulfate zone and thus eventually dominate the respective habitats. It is important to note that the irrigating activity of (large) clams does not only help to detoxify their own habitat from too high sulfide concentrations (Wallmann et al., 1997) but could be an opportunistic means in order to gain advantage over competitive, smaller organisms in accessing the sulfide pool in the sediment. Sommer et al. (2008; 2010) argued that ampharetid polychaete habitats at cold seeps (cf. Habitats 2 at Flare 2 in this study) may represent an early stage of seep-colonization by metazoans. Based on our findings we wish to expand upon this idea by suggesting that the occurrence of large clams in the vicinity of gas orifices and without "transient" habitats of medium-sized organisms such as polychaetes or smaller clams may indicate a mature stage of a cold seep-ecosystem, where polychaete and small clam communities have been undermined and cut off from the sulfide source in the sediment by the opportunistic and dominant large clams. This statement is further supported by the observation of cold seeps at greater depth (~ 1850 m) in the Makran area which are almost exclusively colonized by large (< 10 cm) vesicomyid clams in the vicinity of gas orifices lacking any distinct microbial mat, polychaete or small

clams habitats ("Flare 6", cf. Bohrmann et al. 2008). It is striking in this respect that these sites are additionally characterized by massive pavements of authigenic carbonates at the sea floor. In contrast to the deeper Flare 6 (cf. Bohrmann et al. 2008) sites within and at the lower boundary of the core-OMZ investigated in this study may represent rather young/juvenile seep ecosystems. This is suggested by vast "transient" habitats of small chemosynthetic clams and polychaetes (Flare 2) and the sparse occurrence of authigenic carbonates (Flares 1, 2 and 15).

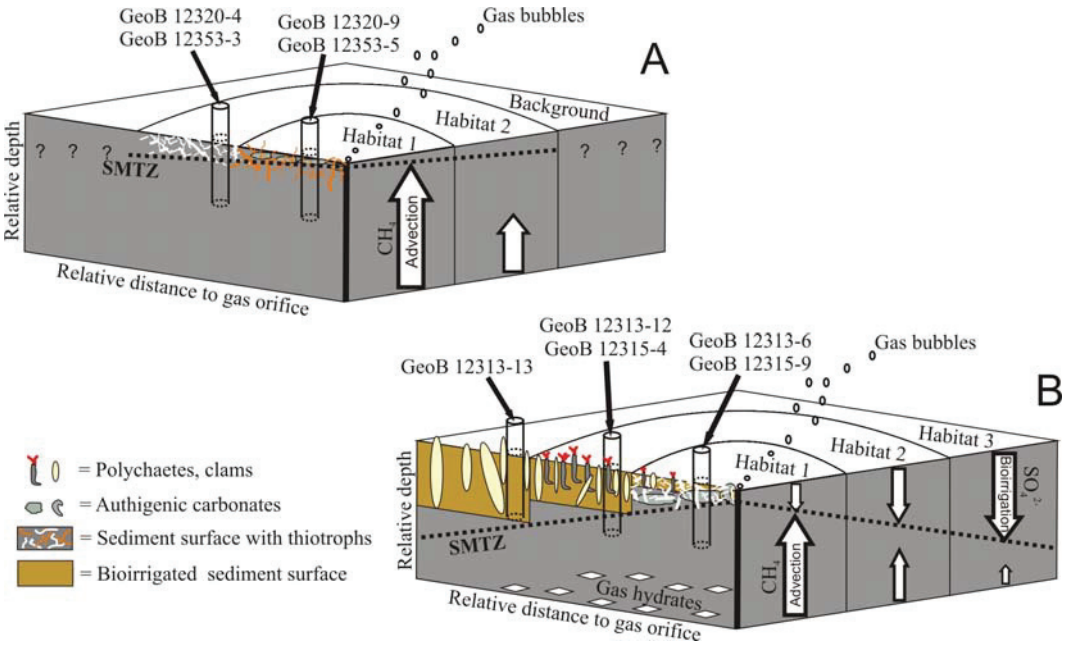

Figure 12: Schematic illustration of the investigated seeps indicating how chemosynthetic communities determine the depth of the SMTZ. A: Situation within the core-OMZ. Oxygen deficiency in the bottom water does not allow for metazoan life and thus microbial mats are the only organisms observed at Flares 1 and 15. The microbes do not irrigate the sediment surface. Advection is expected at least in Habitat 1 where bubble escape was observed and where sulfate profiles are curved concave-down. B: Situation at the lower boundary of the OMZ. Slightly increased oxygen contents sustain chemosynthetic communities represented by the observed polychaetes and clams at Flare 2. Compared to the core-OMZ sites intense bioirrigation leads to a downward shift of the SMTZ due to high fluxes of sulfate into the sediment and thus compensates upward advection in all habitats.

6 Summary and conclusions

This is one of the first studies which examined the interplay of bioirrigation and advection in defined cold seep habitats across a marine oxygen minimum zone (OMZ). We performed targeted push core sampling with a remotely operated vehicle and conducted pore water analyses in different habitats at four seep-

sites. Sites within the core-OMZ are characterized by linear sulfate profiles and the absence of metazoan life. Sites at the lower boundary of the OMZ depict pronounced kink-type sulfate profiles and are characterized by at least three distinct habitats arranged in a concentric fashion around the gas orifice that are dominated by microbial mats, ampharetid polychaetes, or vesicomyid clams. Pore water modeling was conducted for a seep at Flare 2 at the lower boundary of the OMZ. The simulation revealed that upward advection is highest near the gas orifice and decreases towards the outer habitats, whereas depth-integrated rates of bioirrigation increase in the same direction due to changes in the chemosynthetic communities. Hydrogen sulfide fluxes towards the sediment surface at all sites only slightly decrease towards outer habitats. A sulfide export into the bottom water was found in three of four central habitats colonized by microbial mats, whereas sulfide is depleted at or below the sediment surface in the other habitats. It appears that chemosynthetic macrofauna in outer habitats, here polychaetes and/or clams, compensate for lower supply with sulfide triggered by low advection rates, i. e. methane flux, by introducing oxygenated and sulfate-rich bottom water into the sediment. Furthermore, bioirrigation considerably shifts the SMTZ towards greater depths. At the same time steep gradients and comparably high fluxes of sulfate into the SMTZ are established in all three habitats which fuel hydrogen sulfide release via anaerobic oxidation of methane. We could thus show that chemosynthetic communities dominated by clams and polychaetes actively shape their geochemical environment by shifting the SMTZ towards depth and gain selective advantage over passive or immobile organisms (e. g. thiotrophic microbes) competing for sulfide in the sediment. Taking into account that macrofauna depend on oxygen supply we propose that it is the mutual influence of bottom water redox geochemistry and burrowing chemosynthetic organisms that determines the depth of the SMTZ at cold seeps.

Acknowledgements

We are indebted to the captain, crew and the shipboard scientific party of RV Meteor cruise M 74/3 for excellent support and cooperation. André Gaßner and Karsten Enneking (University of Bremen) are thanked for laboratory assistance onboard ship as well as onshore. We would like to thank K. Zonneveld (University of Bremen) for conducting CTD casts and oxygen measurements during the cruise. H. N. Schulz-Vogt (MPI for Marine Microbiology, Bremen)

greatly helped with the identification of seep-organisms. Matthias Haeckel (IFM-GEOMAR, Kiel), Jörn Peckmann (MARUM, Bremen; now University of Vienna), and Michael Schlüter (AWI, Bremerhaven) are thanked for numerous valuable discussions. Thanks to Dieter Fiege (Senckenberg Forschungsinstitut) for polychaete identification. This study was funded through the DFG-Research Center/ Cluster of Excellence ”The Ocean in the Earth System" (MARUM). We acknowledge further financial support from the Helmholtz Association (AWI, Bremerhaven). All data are available on the database Pangaea (http://www.pangaea.de).

References

Adler, M., Hensen, C., Kasten, S. and Schulz, H. D.: Computer simulation of deep sulfate reduction in sediments of the Amazon Fan, Int. J. Earth Sci., 88, 641-654, 2000.

Adler, M., Hensen, C., Wenzhöfer, F., Pfeifer, K. and Schulz, H. D.: Modeling of calcite dissolution by oxic respiration in supralysoclinal deep-sea sediments, Marine Geology, 177, 167-189, 2001.

Aller, R. C.: Quantifying solute distributions in the bioturbated zone of marine sediments by defining an average microenvironment, Geochim. Cosmochim. Acta, 44, 1955-1965, 1980.

Aller, R. C.: The importance of relict burrow structures and burrow irrigation in controlling sedimentary solute distributions, Geochim. Cosmochim. Acta, 48, 1929-1934, 1984.

Aller, R. C. and Aller, J. Y.: The effect of biogenic irrigation intensity and solute exchange on diagenetic reaction rates in marine sediments, J. Mar. Res., 56, 905-936, 1998.

Arp, A. J., Childress, J. J. and Fisher, C. R., Jr.: Metabolic and blood gas transport characteristics of the hydrothermal vent bivalve calyptogena magnifica, Physiol. Zool., 57, 648-662, 1984.

Arvidson, R. S., Morse, J. W. and Joye, S. B.: The sulfur biogeochemistry of chemosynthetic cold seep communities, Gulf of Mexico, USA, Mar. Chem., 87, 97-119, 2004.

Barry, J. P., Kochevar, R. E. and Baxter, C. H.: The influence of pore-water chemistry and physiology on the distribution of vesicomyid clams at cold seeps in Monterey Bay: Implications for patterns of chemosynthetic community organization, Limnol. Oceanogr., 42, 318-328, 1997.

Berner, R. A.: Sedimentary pyrite formation, Am. J. Sci., 268, 1-23, 1970.

Boetius, A., Ravenschlag, K., Schubert, C. J., Rickert, D., Widdel, F., Gieseke, A., Amann, R., Jørgensen, B. B., Witte, U. and Pfannkuche, O.: A marine microbial consortium apparently mediating anaerobic oxidation of methane, Nature, 407, 623-626, 2000.

Bohrmann, G., Bahr, A., Brinkmann, F., Brüning, M., Buhmann, S., Diekamp, V., Enneking, K., Fischer, D., Gassner, A., von Halem, G., Huettich, D., Kasten, S., Klapp, S., Nasir, M., Nowald, N., Ochsenhirt, W.-T., Pape, T., Ratmeyer, V., Rehage, R., Rethemeyer, J., Reuter, M., Rossel, P., Saleem, M., Schmidt, W., Seiter, C., Stephan, S., Thomanek, K.,

Wittenberg, N., Yoshinaga, M. and Zonneveld, K.: Report and preliminary results of R/V Meteor cruise M74/3, Fujairah-Male, 30 October-28 November, 2007. Cold seeps of the Makran subduction zone (Continental margin off Pakistan), Berichte, Fachbereich 5, Universität Bremen, edited by: Bohrmann, G., and Ohling, G., Bremen, 161 pp., 2008.

Borowski, W. S., Paull, C. K. and Ussler, W., III: Marine pore-water sulfate profiles indicate in situ methane flux from underlying gas hydrate, Geology, 24, 655-658, 1996.

Boudreau, B. P.: Diagenetic models and their implementations., Springer-Verlag, New York, 1997.

Brand, T. D. and Griffiths, C.: Seasonality in the hydrography and biogeochemistry across the Pakistan margin of the NE Arabian Sea, Deep Sea Res. Part II, 56, 283-295, 2009.

Brüchert, V.: Early diagenesis of sulfur in estuarine sediments: the role of sedimentary humic and fulvic acids, Geochim. Cosmochim. Acta, 62, 1567-1586, 1998.

Claypool, G. E. and Kaplan, I. R.: The origin and distribution of methane in marine sediments., in: Natural gases in marine sediments, edited by: Kaplan, I. R., Plenum Publishing Corporation, New York, 1974.

Cline, J. D.: Spectrophotometric determination of hydrogen sulfide in natural waters, Limnol. Oceanogr., 14, 454-458, 1969.

Dale, A. W., Sommer, S., Haeckel, M., Wallmann, K., Linke, P., Wegener, G. and Pfannkuche, O.: Pathways and regulation of carbon, sulfur and energy transfer in marine sediments overlying methane gas hydrates on the Opouawe Bank (New Zealand), Geochim. Cosmochim. Acta, 74, 5763-5784, 2010.

Dando, P. R. and Hovland, M.: Environmental effects of submarine seeping natural gas, Cont. Shelf Res., 12, 1197-1207, 1992.

de Beer, D., Sauter, E., Niemann, H., Kaul, N., Foucher, J.-P., Witte, U., Schlüter, M. and Boetius, A.: In situ fluxes and zonation of microbial activity in surface sediments of the Håkon Mosby Mud Volcano, Limnol. Oceanogr., 51, 1315-1331, 2006.

Ding, F., Spiess, V., Fekete, N., Murton, B., Brüning, M. and Bohrmann, G.: Interaction between accretionary thrust faulting and slope sedimentation at the frontal Makran accretionary prism and its implications for hydrocarbon

fluid seepage, J. Geophys. Res., 115, B08106, doi:10.1029/2008JB006246, 2010.

Faber, E., Gerling, P., Berner, U. and Sohns, E.: Methane in ocean waters: Concentrations and carbon isotope variability at East Pacific Rise and the Arabian Sea, Environ. Monit. Assess., 31, 139-144, 1994.

Fossing, H., Ferdelman, T. G. and Berg, P.: Sulfate reduction and methane oxidation in continental margin sediments influenced by irrigation (South-East Atlantic off Namibia), Geochim. Cosmochim. Acta, 64, 897-910, 2000.

Fossing, H., Gallardo, V. A., Jørgensen, B. B., Hüttel, M., Nielsen, L. P., Schulz, H., Canfield, D. E., Forster, S., Glud, R. N., Gundersen, J. K., Küver, J., Ramsing, N. B., Teske, A., Thamdrup, B. and Ulloa, O.: Concentration and transport of nitrate by the mat-forming sulphur bacterium *Thioploca*., Nature, 374, 713-715, 1995.

Gilhooly III, W. P., Carney, R. S. and Macko, S. A.: Relationships between sulfide-oxidizing bacterial mats and their carbon sources in northern Gulf of Mexico cold seeps, Org. Geochem., 38, 380-393, 2007.

Grehan, A. J. and Juniper, S. K.: Clam distribution and subsurface hydrothermal processes at Chowder Hill (Middle Valley), Juan de Fuca Ridge, Mar. Ecol. Prog. Ser., 130, 105-115, 1996.

Haeckel, M., Boudreau, B. P. and Wallmann, K.: Bubble-induced porewater mixing: A 3-D model for deep porewater irrigation., Geochim. Cosmochim. Acta, 71, 5135-5154, 2007.

Haeckel, M. and Wallmann, K.: Indications for convective flow induced by focussed fluid venting at bacterial mats, Geochim. Cosmochim. Acta, 72, A339-A405, 2008.

Haese, R. R.: Macrobenthic activity and its effects on biogeochemical reactions and fluxes, in: Ocean Margin Systems, edited by: Wefer, G., Billet, D., Hebbeln, D., Jørgensen, B. B., Schlüter, M., and Van Weering, T., Springer Verlag, Berlin, Heidelberg, 219-234, 2002.

Haese, R. R., Hensen, C. and de Lange, G. J.: Pore water geochemistry of eastern Mediterranean mud volcanoes: Implications for fluid transport and fluid origin, Mar. Geol., 225, 191-208, 2006.

Haese, R. R., Meile, C., Van Cappellen, P. and De Lange, G. J.: Carbon geochemistry of cold seeps: Methane fluxes and transformation in sediments from Kazan mud volcano, eastern Mediterranean Sea, Earth. Planet. Sci. Lett., 212, 361-375, 2003.

Han, M. W. and Suess, E.: Subduction-induced pore fluid venting and the formation of authigenic carbonates along the cascadia continental margin: Implications for the global Ca-cycle, Palaeogeography, Palaeoclimatology, Palaeoecology, 71, 97-118, 1989.

Hensen, C., Zabel, M., Pfeifer, K., Schwenk, T., Kasten, S., Riedinger, N., Schulz, H. D. and Boetius, A.: Control of sulfate pore-water profiles by sedimentary events and the significance of anaerobic oxidation of methane for the burial of sulfur in marine sediments, Geochimica et Cosmochimica Acta, 67, 2631-2647, 2003.

Hinrichs, K.-U., Hayes, J. M., Sylva, S. P., Brewer, P. G. and DeLong, E. F.: Methane-consuming archaebacteria in marine sediments, Nature, 398, 802-805, 1999.

Hoehler, T., Alperin, M. J., Albert, D. B. and Martens, C.: Field and laboratory studies of methane oxidation in an anoxic marine sediment: evidence for a methanogen-sulfate reducer consortium., Global Biogeochem. Cycles, 8, 451-463, 1994.

Holmkvist, L., Ferdelman, T. G. and Jørgensen, B. B.: A cryptic sulfur cycle driven by iron in the methane zone of marine sediment (Aarhus Bay, Denmark), Geochim. Cosmochim. Acta, 75, 3581-3599, 2011.

Kaul, N., Rosenberger, A. and Villinger, H.: Comparison of measured and BSR-derived heat flow values, Makran accretionary prism, Pakistan., Mar. Geol., 164, 37-51, 2000.

Knab, N. J., Dale, A. W., Lettmann, K., Fossing, H. and Jørgensen, B. B.: Thermodynamic and kinetic control on anaerobic oxidation of methane in marine sediments, Geochim. Cosmochim. Acta, 72, 3746-3757, 2008.

Kopf, A. J.: Significance of mud volcanism, Rev. Geophys., 40, 1005, doi:10.1029/2000RG000093, 2002.

Kukowski, N., Schillhorn, T., Flueh, E. R. and Huhn, K.: Newly identified strike-slip plate boundary in the northeastern Arabian Sea, Geology, 28, 355-358, 2000.

Kukowski, N., Schillhorn, T., Huhn, K., von Rad, U., Husen, S. and Flueh, E. R.: Morphotectonics and mechanics of the central Makran accretionary wedge off Pakistan, Mar. Geol., 173, 1-19, 2001.

Kuznetsov, A. P. and Levenshtein, R. Y.: Pavelius uschakovi gen. et sp. n. (Polychaeta, Ampharetidae) from the area of the Paramushir gas hydrate

vent in the Sea of Okhotsk., Zoologicheskiy zhurnal (in russian), 6, 819-825, 1988.

Leloup, J., Loy, A., Knab, N. J., Borowski, C., Wagner, M. and Jorgensen, B. B.: Diversity and abundance of sulfate-reducing microorganisms in the sulfate and methane zones of a marine sediment, Black Sea, Environ. Microbiol., 9, 131-142, 2007.

Levin, L., Ziebis, W., Mendoza, G. F., Growney, V. A., Tryon, M., Brown, K. M., Mahn, C., Gieskes, J. M. and Rathburn, A. E.: Spatial heterogeneity of macrofauna at northern California methane seeps: influence of sulfide concentration and fluid flow, Mar. Ecol. Prog. Ser., 265, 123-139, 2003.

Levin, L. A.: Ecology of cold seep sediments: interactions of fauna with flow, chemistry and microbes., Oceanogr. Mar. Biol. Annu. Rev., 43, 1-46, 2005.

Lichtschlag, A., Felden, J., Brüchert, V., Boetius, A. and deBeer, D.: Geochemical processes and chemosynthetic primary production in different thiotrophic mats of the Håkon Mosby Mud Volcano (Barents Sea) Limnol. Oceanogr., 55, 931-949, 2010a.

Lichtschlag, A., Felden, J., Wenzhöfer, F., Schubotz, F., Ertefai, T. F., Boetius, A. and de Beer, D.: Methane and sulfide fluxes in permanent anoxia: In situ studies at the Dvurechenskii mud volcano (Sorokin Trough, Black Sea), Geochim. Cosmochim. Acta, 74, 5002-5018, 2010b.

Linke, P., Suess, E., Torres, M., Martens, V., Rugh, W. D., Ziebis, W. and Kulm, L. D.: In situ measurement of fluid flow from cold seeps at active continental margins, Deep Sea Res. Part I, 41, 721-739, 1994.

Linke, P., Wallmann, K., Suess, E., Hensen, C. and Rehder, G.: In situ benthic fluxes from an intermittently active mud volcano at the Costa Rica convergent margin, Earth. Planet. Sci. Lett., 235, 79-95, 2005.

Luff, R. and Wallmann, K.: Fluid flow, methane fluxes, carbonate precipitation and biogeochemical turnover in gas hydrate-bearing sediments at Hydrate Ridge, Cascadia Margin: numerical modeling and mass balances, Geochim. Cosmochim. Acta, 67, 3403-3421, 2003.

Meile, C., Koretsky, C. and van Cappellen, P.: Quantifying bioirrigation in aquatic sediments: an inverse modeling approach., Limnol. Oceanogr., 46, 164-177, 2001.

Nelson, D. C., Jorgensen, B. B. and Revsbech, N. P.: Growth pattern and yield of a chemoautotrophic Beggiatoa sp. in oxygen-sulfide microgradients, Appl. Environ. Microbiol., 52, 225-233, 1986.

Niemann, H., Fischer, D., Graffe, D., Knittel, K., Montiel, A., Heilmayer, O., Nöthen, K., Pape, T., Kasten, S., Bohrmann, G., Boetius, A. and Gutt, J.: Biogeochemistry of a low-activity cold seep in the Larsen B area, western Weddell Sea, Antarctica, Biogeosciences, 6, 2383-2395, 2009.

Niemann, H., Lösekann, T., de Beer, D., Elvert, M., Nadalig, T., Knittel, K., Amann, R., Sauter, E. J., Schlüter, M., Klages, M., Foucher, J. P. and Boetius, A.: Novel microbial communities of the Haakon Mosby mud volcano and their role as a methane sink, Nature, 443, 854-858, 2006.

Nikolovska, A., Sahling, H. and Bohrmann, G.: Hydroacoustic methodology for detection, localization, and quantification of gas bubbles rising from the seafloor at gas seeps from the eastern Black Sea, Geochem. Geophys. Geosyst., 9, Q10010, doi:10.1029/2008GC002118, 2008.

O'Hara, S. C. M., Dando, P. R., Schuster, U., Bennis, A., Boyle, J. D., Chui, F. T. W., Hatherell, T. V. J., Niven, S. J. and Taylor, L. J.: Gas seep induced interstitial water circulation: observations and environmental implications, Cont. Shelf Res., 15, 931-948, 1995.

Olson, D. B., Hitchcock, G. L., Fine, R. A. and Warren, B. A.: Maintenance of the low-oxygen layer in the central Arabian Sea, Deep-Sea Research Part II - Topical Studies in Oceanography, 40, 673-685, 1993.

Pfeifer, K., Hensen, C., Adler, M., Wenzhöfer, F., Weber, B. and Schulz, H. D.: Modeling of subsurface calcite dissolution, including the respiration and reoxidation processes of marine sediments in the region of equatorial upwelling off Gabon, Geochim. Cosmochim. Acta, 66, 4247-4259, 2002.

Reitz, A., Pape, T., Haeckel, M., Schmidt, M., Berner, U., Scholz, F., Liebetrau, V., Aloisi, G., Weise, S. M. and Wallmann, K.: Sources of fluids and gases expelled at cold seeps offshore Georgia, eastern Black Sea, Geochim. Cosmochim. Acta, 75, 3250-3268, 2011.

Ritger, S., Carson, B. and Suess, E.: Methane-derived authigenic carbonates formed by subduction-induced pore-water expulsion along the Oregon/Washington margin, Geol. Soc. Am. Bull., 98, 147-156, 1987.

Robinson, C. A., Bernhard, J. M., Levin, L. A., Mendoza, G. F. and Blanks, J. K.: Surficial Hydrocarbon Seep Infauna from the Blake Ridge (Atlantic Ocean, 2150 m) and the Gulf of Mexico (690-2240m), Mar. Ecol., 25, 313-336, 2004.

Sahling, H., Bohrmann, G., Spiess, V., Bialas, J., Breitzke, M., Ivanov, M., Kasten, S., Krastel, S. and Schneider, R.: Pockmarks in the Northern

Congo Fan area, SW Africa: Complex seafloor features shaped by fluid flow, Mar. Geol., 249, 206-225, 2008.

Sahling, H., Rickert, D., Lee, R. W., Linke, P. and Suess, E.: Macrofaunal community structure and sulfide flux at gas hydrate deposits from the Cascadia convergent margin, NE Pacific, Mar. Ecol. Prog. Ser., 231, 121-138, 2002.

Sahling, H., Wallmann, K., Dählmann, A., Schmaljohann, R. and Petersen, S.: The physicochemical habitat of Sclerolinum sp. at Hook Ridge hydrothermal vent, Bransfield Strait, Antarctica, Limnol. Oceanogr., 50, 598-606, 2005.

Salman, V., Amann, R., Girnth, A.-C., Polerecky, L., Bailey, J. V., Høgslund, S., Jessen, G., Pantoja, S. and Schulz-Vogt, H. N.: A single-cell sequencing approach to the classification of large, vacuolated sulfur bacteria, Syst. Appl. Microbiol., 34, 243-259, 2011.

Schlüter, H. U., Prexl, A., Gaedicke, C., Roeser, H., Reichert, C., Meyer, H. and von Daniels, C.: The Makran accretionary wedge: sediment thicknesses and ages and the origin of mud volcanoes, Mar. Geol., 185, 219-232, 2002.

Schmaljohann, R., Drews, M., Walter, S., Linke, P., Rad, U. v. and Imhoff, J. F.: Oxygen-minimum zone sediments in the northeastern Arabian Sea off Pakistan: a habitat for the bacterium Thioploca, Mar. Ecol. Prog. Ser., 211, 27-42, 2001.

Schulz, H. N., Jorgensen, B. B., Fossing, H. A. and Ramsing, N. B.: Community Structure of Filamentous, Sheath-Building Sulfur Bacteria, Thioploca spp., off the Coast of Chile, Appl. Environ. Microbiol., 62, 1855-1862, 1996.

Schulz, H. N. and Jørgensen, B. B.: Big Bacteria, Annu. Rev. Microbiol., 55, 105-137, 2001.

Seeberg-Elverfeld, J., Schlüter, M., Feseker, T. and Kölling, M.: Rhizon sampling of porewaters near the sediment-water interface of aquatic systems, Limnol. Oceanogr. Methods, 3, 361-371, 2005.

Sibuet, M. and Olu, K.: Biogeography, biodiversity and fluid dependence of deep-sea cold-seep communities at active and passive margins, Deep Sea Res. Part II, 45, 517-567, 1998.

Sommer, S., Linke, P., Pfannkuche, O., Bowden, D. A., Haeckel, M., Greinert, J. and Thurber, A. R.: Novel cold Seep Habitat along the Hikurangi Margin (New Zealand), Geophys. Res. Abstr., 10, EGU2008-A-02387, 2008.

Sommer, S., Linke, P., Pfannkuche, O., Niemann, H. and Treude, T.: Benthic respiration in a seep habitat dominated by dense beds of ampharetid polychaetes at the Hikurangi Margin (New Zealand), Mar. Geol., 272, 223-232, 2010.

Suess, E., Bohrmann, G., von Huene, R., Linke, P., Wallmann, K., Lammers, S., Sahling, H., Winckler, G., Lutz, R. A. and Orange, D.: Fluid venting in the eastern Aleutian subduction zone, J. Geophys. Res., 103, 2597-2614, 1998.

Teske, A. and Nelson, D.: The Genera Beggiatoa and Thioploca, in: Dworkin, M., Stanley, F., Rosenberg, E., Schleifer, K.-H., Stackebrand, E., (eds.) The Prokaryotes, Springer-Verlag, Berlin, 784-810, 2006.

Tishchenko, P., Hensen, C., Wallmann, K. and Wong, C. S.: Calculation of the stability and solubility of methane hydrate in seawater, Chem. Geol., 219, 37-52, 2005.

Torres, M. E., McManus, J., Hammond, D. E., de Angelis, M. A., Heeschen, K. U., Colbert, S. L., Tryon, M. D., Brown, K. M. and Suess, E.: Fluid and chemical fluxes in and out of sediments hosting methane hydrate deposits on Hydrate Ridge, OR, I: Hydrological provinces, Earth. Planet. Sci. Lett., 201, 525-540, 2002.

Tryon, M. D., Brown, K. M. and Torres, M. E.: Fluid and chemical flux in and out of sediments hosting methane hydrate deposits on Hydrate Ridge, OR, II: Hydrological processes, Earth. Planet. Sci. Lett., 201, 541-557, 2002.

Tryon, M. D., Brown, K. M., Torres, M. E., Trehu, A. M., McManus, J. and Collier, R. W.: Measurements of transience and downward fluid flow near episodic methane gas vents, Hydrate Ridge, Cascadia, Geology, 27, 1075-1078, 1999.

van Dover, C. L., Aharon, P., Bernhard, J. M., Caylor, E., Doerries, M., Flickinger, W., Gilhooly, W., Goffredi, S. K., Knick, K. E., Macko, S. A., Rapoport, S., Raulfs, E. C., Ruppel, C., Salerno, J. L., Seitz, R. D., Sen Gupta, B. K., Shank, T., Turnipseed, M. and Vrijenhoek, R.: Blake Ridge methane seeps: characterization of a soft-sediment, chemosynthetically based ecosystem, Deep Sea Res. Part I, 50, 281-300, 2003.

von Rad, U., Berner, U., Delisle, G., Doose-Rolinski, H., Fechner, N., Linke, P., Lückge, A., Roeser, H. A., Schmaljohann, R., Wiedicke, M., Parties, S. S., Parties, S. S., Block, M., Damm, V., Erbacher, J., Fritsch, J., Harazim, B., Poggenburg, J., Scheeder, G., Schreckenberger, B., von Mirbach, N.,

Drews, M., Walter, S., Ali Khan, A., Inam, A., Tahir, M., Tabrez, A. R., Cheema, A. H., Pervaz, M. and Ashraf, M.: Gas and fluid venting at the Makran accretionary wedge off Pakistan, Geo-Mar. Lett., 20, 10-19, 2000.

von Rad, U., Rösch, H., Berner, U., Geyh, M., Marchig, V. and Schulz, H.: Authigenic carbonates derived from oxidized methane vented from the Makran accretionary prism off Pakistan, Mar. Geol., 136, 55-77, 1996.

von Rad, U., Schulz, H., Khan, A. A., Ansari, M., Berner, U., Cepek, P., Cowie, G., Dietrich, P., Erlenkeuser, H., Geyh, M., Jennerjahn, T., Lückge, A., Marchig, V., Riech, V., Rösch, H., Schäfer, P., Schulte, S., Sirocko, F., Tahir, M. and Weiss, W.: Sampling the oxygen minimum zone off Pakistan: glacial-interglacial variations of anoxia and productivity (preliminary results, Sonne 90 cruise), Mar. Geol., 125, 7-19, 1995.

Wallace, P. J., Dickens, G. R., Paull, C. K. and Ussler, W.: Effects of core retrieval and degassing on the carbon isotope composition of methane in gas hydrate and free-gas bearing sediments from the Blake Ridge, Proceedings of the Ocean Drilling Program, Scientific Results, 164, 101-112, 2000.

Wallmann, K., Drews, M., Aloisi, G. and Bohrmann, G.: Methane discharge into the Black Sea and the global ocean via fluid flow through submarine mud volcanoes, Earth. Planet. Sci. Lett., 248, 545-560, 2006.

Wallmann, K., Linke, P., Suess, E., Bohrmann, G., Sahling, H., Schlüter, M., Dählmann, A., Lammers, S., Greinert, J. and von Mirbach, N.: Quantifying fluid flow, solute mixing, and biogeochemical turnover at cold vents of the eastern Aleutian subduction zone, Geochim. Cosmochim. Acta, 61, 5209-5219, 1997.

Wenzhöfer, F., Adler, M., Kohls, O., Hensen, C., Strotmann, B., Boehme, S. and Schulz, H. D.: Calcite dissolution driven by benthic mineralization in the deep-sea: in situ measurements of Ca^{2+}, pH, pCO_2 and O_2, Geochim. Cosmochim. Acta, 65, 2677-2690, 2001.

Wyrtki, K.: Physical oceanography of the Indian Ocean, in: The biology of the Indian Ocean. Ecological Studies, edited by: Zeitschel, B., Springer Verlag, Berlin, 18-36, 1973.

Chapter III – Manuscript 2

Evidence for earthquake-triggered hydrocarbon seepage at the Makran subduction zone

D. Fischer[1], J. M. Mogollón[2], M. Strasser[3], G. Bohrmann[1], S. Kasten[2]

[1] MARUM – Center for Marine Environmental Sciences and Department of Geosciences, University of Bremen, Klagenfurter Strasse, D-28334 Bremen, Germany

[2] Alfred Wegener Institute for Polar and Marine Research, Am Handelshafen 12, D-27570 Bremerhaven, Germany

[3] Geological Institute, Eidgenössische Technische Hochschule Zürich, Sonneggstrasse 5, CH-8092 Zürich, Switzerland

(Manuscript submitted to "Nature Geoscience")

Introductory paragraph

Methane has a high global warming potential and abundantly occurs in marine sediments (1, 2). Submarine seepage of methane-dominated hydrocarbons is heterogeneous in space and time and trigger mechanisms of episodic seep events are poorly understood (2-4). Hypothesized mechanisms consider critical gas pressures underneath gas hydrate-cemented sediments, implying that these are susceptible to mechanical failure and subsequent gas release (5, 6). Although gas hydrates often occur in seismically active regions, the role of earthquakes as triggers of methane seepage in gas hydrate-bearing sediments has been only superficially addressed (7, 8). Here we present solid phase and pore water geochemical data of sediment cores retrieved from the Makran convergent margin that evidence a significant increase in upward gas flux coinciding with a magnitude 8.1 earthquake in 1945. Our data suggest that co-seismic ground shaking induced mechanical fracturing of gas hydrate-cemented sediments. The event created pathways for free gas to migrate through the gas hydrate stability zone and into the water column, which condensed the geochemical zonation and substantially shifted the sulphate/methane transition towards the sediment surface. Our findings imply that seep events triggered by earthquakes demand consideration in local and global carbon budgets at other seismically active continental margins worldwide.

Main text

The Makran convergent margin is located offshore Pakistan, where the Arabian plate subducts underneath the Eurasian plate (9, 10) and it is prone to vigorous seismic activity (11). The tectonic regime established several East-West-striking near-parallel accretionary ridges, the youngest of which is termed Nascent Ridge (Fig. 13, ref. 9). Eight major earthquakes (Moment magnitude (M_W) >6.5) hit the Makran convergent margin since 1927 and the average frequency of M_W>8 earthquakes is 100-250 yrs (11). The only major earthquake that occurred near Nascent Ridge was the 1945 Balochistan event, being the strongest earthquake (M_W 8.1) recorded for the northern Arabian Sea (Fig. 13, refs 11, 12). Nascent Ridge is located within the gas hydrate stability zone and methane seepage related to gas buoyancy rather than to fluid advection is a common feature (9).

Gravity cores were retrieved from Nascent Ridge in 2007. Core GeoB 12306-1 (Hydrate-site, 3.8 m, 2861 m water depth, 24:11.761 N, 62:44.311 E) was characterized by degassing-cracks and a mousse-like sediment texture below 1.6 m pointing at the presence of gas hydrates prior to dissociation during core retrieval. A replicate core obtained from the same position, which was immediately opened upon retrieval, contained very abundant centimetre-scale gas hydrate chips below 1.6 m. At a distance of 5-10 m around Hydrate-site, vigorous gas discharge into the water column from fissures in the sediment was observed during remotely operated vehicle (ROV)-surveys. The sediment surface was hummocky with numerous mounds about 1 m in height and diameter (Fig. 13). Chemosynthetic fauna indicative of high hydrogen sulphide contents (13) merely appeared at the Hydrate-site as scattered, dm^2-scale agglomerations of vesicomyid clams and frenulate tubeworms. In contrast, very dense and >10^2 m^2-scale colonies of seep-fauna and microbial mats were reported from upper and mid-slope hydrocarbon seeps of the Makran convergent margin (14). Core GeoB 12331-2 (non-Hydrate-site, 5.3 m, 2831 m water depth, 24:11.507 N, 62:46.502 E) was obtained at a distance of 3.7 km east of the Hydrate-site. No indications of gas discharge into the water column were found at this site and although the core did not contain gas hydrates, these are likely to occur at greater depths (9). Massive authigenic carbonates, a ubiquitous feature at cold seeps in the Makran area and worldwide, were absent at both sites.

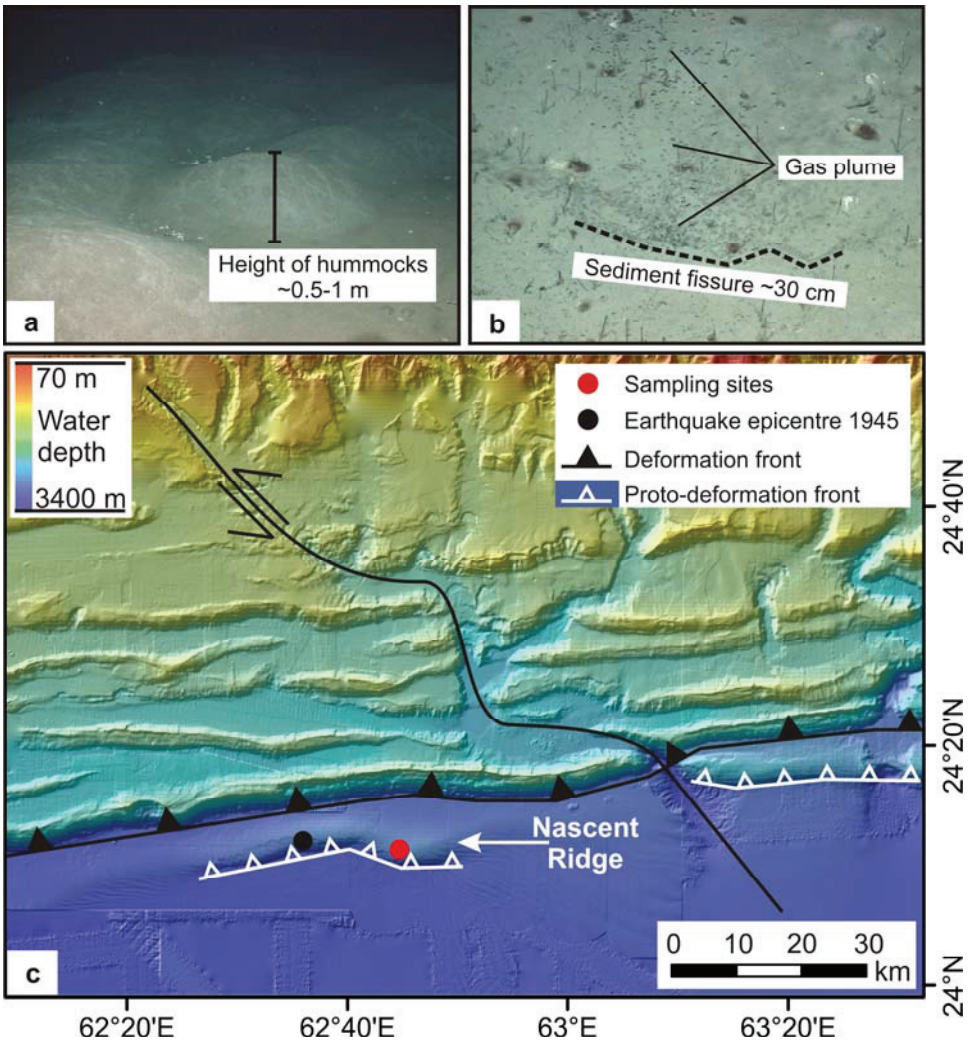

Figure 13: Sea floor images of the Hydrate-site (a and b) showing the hummocky sediment surface (a) and one of the observed gas bubble discharge sites (b). Scale is provided by black lines. (c) Bathymetric map of the Makran convergent margin and accretionary ridges. The tectonic architecture of the continental margin comprises the deformation front N of Nascent Ridge and the proto-deformation front S of Nascent Ridge (9). The epicentral location of the1945 earthquake is marked according to its first scientific description (12).

The sulphate/methane transition (SMT), where sulphate is consumed due to the anaerobic oxidation of methane (AOM; 15, 16), is located at a depth of 1.3 m at the Hydrate-site and at 4.7 m at the non-Hydrate-site (Fig. 14). Concentration profiles of bulk barium (Ba) and barium/aluminium (Ba/Al) ratios indicate Ba enrichments directly above the current depths of the SMT in both cores (Fig 14). The solid phase Ba enrichment at the Hydrate-site has a maximum concentration of 426 mg/kg at a depth of 1.25 m (Fig. 14a). The Ba enrichment at the non-Hydrate-site shows a peak concentration of about 471 mg/kg at a depth of 4.55 m (Fig. 14b). Below the SMT dissolved barium (Ba^{2+}) concentrations increase at

both sites. While Ba^{2+} displays a maximum of 94 µM at 1.9 m at the Hydrate-site, the maximum concentration at the non-Hydrate-site is distinctly lower (28 µM at 5.3 m, Fig. 14). Biogenic barite forms as microcrystallites in the water column (17) and Ba is diagenetically recycled in sulphate-depleted sediments below the SMT, where the pore water is undersaturated with respect to barite (18). Consequently, Ba^{2+} diffuses upward and reprecipitates as authigenic barite upon contact with sulphate above the SMT (18). Both examined sites exhibit not only bulk Ba enrichments just above the present depth of the SMT, but also concomitant peaks in Ba/Al ratios (Fig. 14), which together point at authigenic barite formation. Authigenic barite has previously been used reconstruct changes in upward methane flux (19). In this study, the time required to form the observed Ba enrichments was calculated following the approaches of Kasten and co-workers (20, 21), assuming constant upward diffusive Ba^{2+} fluxes. The Ba^{2+} fluxes into the respective diagenetic barite fronts range between 1.79-2.09 x 10^{-7} mol cm^{-2} yr^{-1} (Hydrate-site) and 6.14-7.17 x 10^{-8} mol cm^{-2} yr^{-1} (non-Hydrate-site), depending on assumed porosities (0.7 or 0.75). To exclude bubble-irrigation effects (22), which are likely in the upper 0.8 m at the Hydrate-site, we used the average concentration of total bulk Ba in the upper 1.25 m of the undisturbed non-Hydrate-site (374 mg/kg) to obtain the non-diagenetic background Ba concentration at the sediment surface for both cores

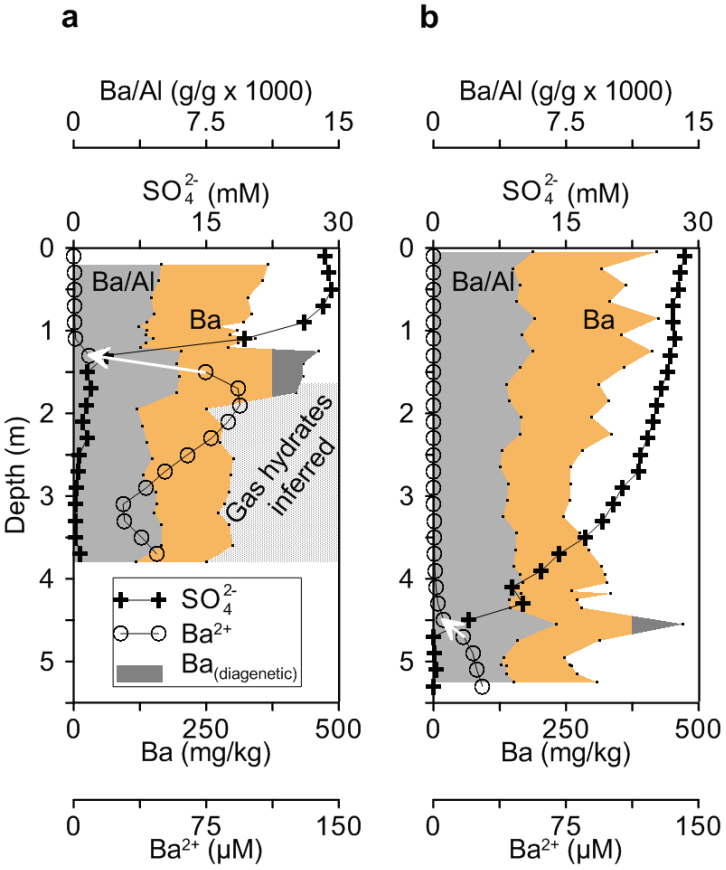

Figure 14: Concentration profiles of dissolved barium (Ba^{2+}), sulphate (SO_4^{2-}), bulk barium (Ba) and barium/aluminium (Ba/Al) obtained for the Hydrate-site (a) and non-Hydrate-site (b). White arrows indicate the gradient of the Ba^{2+} profiles used to calculate the diffusive Ba^{2+} fluxes.

(Fig .14). Consequently, the diagenetic Ba fraction near the SMT at both the Hydrate-site and at the non-Hydrate-site represents 217 mg/kg and 105 mg/kg, respectively. At the Hydrate-site, partial gas hydrate dissociation and associated release of hydrate-derived water due to depressurization during core retrieval could have diluted the in situ Ba^{2+} concentrations which would compromise the Ba^{2+} gradient used for the flux calculations. However, the used Ba^{2+} gradient is located above the inferred depth of in situ gas hydrate presence and thus an impact of gas hydrate dissociation on the Ba^{2+} gradient during core retrieval is considered negligible. Depending on the porosity chosen (0.7 or 0.75), the time required for the Ba enrichments to form at the Hydrate-site is circa 67-94 yrs, while at the non-Hydrate-site it is circa 56-79 yrs, which both compare well with the time elapsed since the 1945 earthquake (62 yrs).

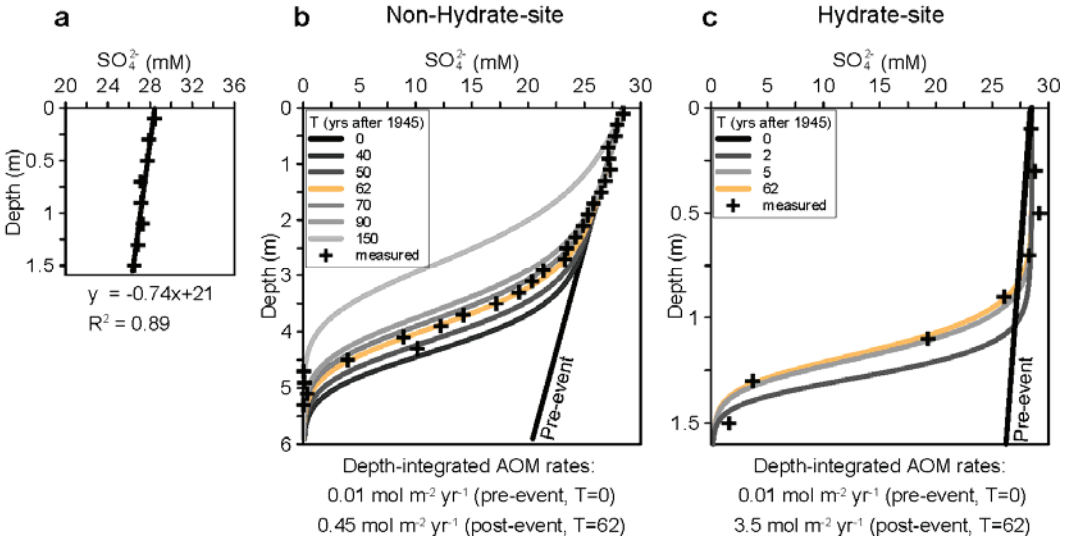

Figure 15: Simulated evolution of the sulphate depth profiles compared to measured profiles at both the examined sites. The slope of the upper 1.5 m of the sulphate concentration profile of the non-Hydrate-site indicates an approximate pre-event depth of the SMT at 21 m (a). Numerical simulations of sulphate profiles involving an upward shift of the SMT as a function of time (b and c). Using the selected model parameters (see Supplementary methods) the best fit of the modelled to the measured sulphate profiles in is achieved after 62 yrs (b and c). At the Hydrate-site steady-state conditions are reached after a mere 7 yrs. Thus, the evolution of the sulphate profiles is only shown for T=0, 2, 5, and 62 yrs. For a detailed description of the applied numerical model see Supplementary methods, figures and tables.

The sulphate concentration profile at the non-Hydrate-site shows a "concave-up" shape (Figs. 14b and 15) – a phenomenon that has previously been interpreted to reflect a (sub)recent increase in upward methane flux (23). The uppermost part of this profile (0-1.5 m) is almost linear and downward projection of the slope results in the approximate pre-earthquake sulphate gradient for both sites (Fig.

15a), which permits simulating the temporal evolution of the measured sulphate profiles using a nonsteady state 1-D diagenetic model (Fig. 15; Supplementary Figures 17 and 18 and Tables 1 and 2). The simulation reveals that the concave-up sulphate profile at the non-Hydrate-site can be correctly described by an upward shift of the methane source implying an increase in upward methane flux. Assuming that the SMT shifted from the downward-projected depth of 21 m ("pre-event", Fig. 15a) to 4.7 m ("post-event") due to a shoaling of the methane source to 5.9 m, where the methane equilibrium concentration with gas hydrates is 55.07 mM (ref. 24), the best fit of the simulated sulphate profile to the measured data is achieved 60-70 yrs after the 1945 earthquake (Fig. 15b) and involves an increase in the depth-integrated AOM rate from 0.01 mol m^{-2} yr^{-1} to 0.45 mol m^{-2} yr^{-1} (factor 45). At the Hydrate-site gas hydrates are inferred to have formed at depths below 1.6 m after the earthquake, where the methane equilibrium concentration with gas hydrates reaches 55.11 mM (ref. 24). The observed vigorous gas bubble discharge at this location is interpreted to irrigate sea water into the upper sediment as was previously shown at other locations (22). This process could lead to a steady-state sulphate profile a mere 7 yrs after the amplified methane flux triggered by the earthquake (Fig 15c). Here, the depth-integrated AOM rate increases from 0.01 mol m^{-2} yr^{-1} to 3.5 mol m^{-2} yr^{-1} (factor 350).

The two applied geochemical approaches independently evidence a significant increase in methane flux related to shoaling of the methane source circa 56-94 yrs before present. The absence of authigenic carbonates or mature chemosynthetic communities supports this interpretation and strongly suggests that the gas seeps at Nascent Ridge are relatively young features and reflect localized subsurface pathways of upward-migrating gas. Furthermore, high-resolution seismo-acoustic data reveal a bottom simulating reflector (BSR) at Nascent Ridge which points to the presence of free gas underneath the gas hydrate stability zone (9, 25, 26). Below the crest of Nascent Ridge, however, chaotic and tilted high-reflection anomalies considerably above the BSR suggest that the overlying sediments are fractured (26). This pattern contrasts the uniform and undisturbed sediment layering at the ridge-flanks (26). To explain both the observed geochemical data and conspicuous seismo-acoustic anomalies we argue that gas hydrate-cemented sediments overlying the BSR have been mechanically fractured as a consequence of the 1945 earthquake. High seismic ground accelerations during the M_W 8.1 earthquake exert additional shear-stress and lower the effective stress in the sediment, in which high pore pressures

resulting from dynamic earthquake loading cannot dissipate fast enough. Consequently, the sediment strength within the gas-hydrate stability zone falls below a threshold at which the excess gas pressure at the top of the free gas zone drives mechanical failure and fracturing (5, 6). This results in upward gas flux along localized fractures and eventually in hydrocarbon seepage from sea floor fissures (Fig. 13b). Before the event the SMT has been located at greater depth than today at both examined sites, because the upward methane flux had been controlled and compromised by gas hydrate-cemented sediments acting as a barrier for free gas (9). As soon as the sealing barrier is fractured due to the earthquake, free gas buoyantly intrudes into the gas hydrate stability zone above the BSR (Fig. 16). The gas dissolves thus enriching methane in the pore water and consequently induces the formation of shallow gas hydrates within the gas hydrates stability zone, in case the pore water is oversaturated with methane with respect to gas hydrates (27). As revealed by the numerical model for the non-Hydrate-site (Fig. 15) and by calculating the time of formation of the authigenic Ba enrichments for both sites, it is at this time that the SMT shifts from the pre-event depth to the present depths of 1.3 m (Hydrate-site) and 4.7 m (non-Hydrate-site) due to the increase in methane input (Fig. 15). Coevally, AOM rates

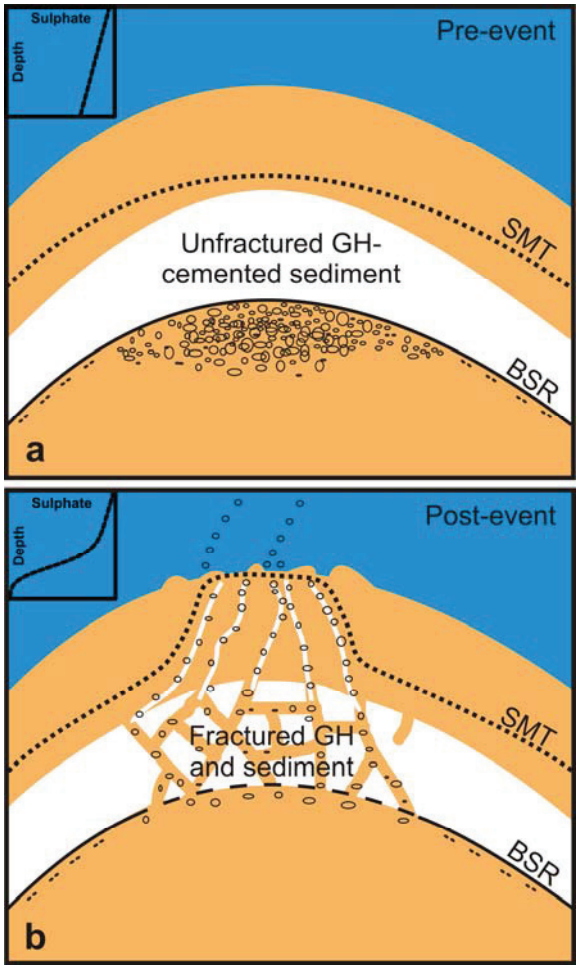

Figure 16: Conceptual model of pre-event (a) and post-event (b) conditions at Nascent Ridge and associated sulphate profiles. Before the earthquake (a), free gas was trapped underneath gas hydrate-cemented sediment which is documented by the prominent that the prominent BSR is still observed at ridge-flank sites today. After the event (b), earthquake ground-shaking caused mechanical fracturing of the sediment, and free gas intruded into the gas hydrate stability zone forming pristine gas hydrates and leading to gas escape into the water column. As a consequence, the BSR and sediment stratigraphy appears interrupted in seismo-acoustic data (26) and the SMT shifted towards the sediment surface at sites of gas migration, which leads to the nonsteady state sulphate depth profile.

significantly increase 350-fold (Hydrate-site) and 45-fold (non-Hydrate-site), which is due to steeper slopes of the methane (and sulphate) pore water profiles into the SMT after the earthquake (Fig. 15).

During the time of ROV observations in 2007, the gas flux has still been high enough to discharge free gas into the water column. The rate of gas emission into the water at the Hydrate-site at Nascent Ridge was quantified to be on the order of 10 mol_{CH4} min^{-1} with a large uncertainty of about ±60% (ref. 28). Assuming that this gas flux has been constant since the earthquake, about 3.26 $x10^8$ mol_{CH4} were discharged from Nascent Ridge between 1945 and 2007. This number almost certainly underestimates the assumed total gas discharge into the water column. Nevertheless, these considerations suggest that the earthquake-triggered export of free gas from the sediment into the hydrosphere may be as important as, or even more important than other, non-seismogenic seeps summarized elsewhere (29). Considering that gas discharge rates at other geological features, e. g. mud volcanoes, were reported to be very sensitive to seismicity (30), we propose that episodic seep events triggered by earthquakes constitute an important natural source of carbon to the hydrosphere and atmosphere that has not yet been accounted for in local or global carbon budgets (1).

Methods summary

A detailed description of the pore water model is given in the Supplementary. Pore water was extracted onboard ship close to in situ temperature using rhizons. Sulphate concentrations were determined by means of ion chromatography (Metrohm IC Advanced Compact 861) with a RSD <3 %. Dissolved barium (Ba^{2+}) was determined by means of inductively coupled plasma-optical emission spectroscopy (ICP-OES; IRIS Intrepid, Thermo Scientific) after acidification and 1:10 dilution of a pore water split with HNO_3 (RSD <7 %). Diffusive flux of Ba^{2+} into the precipitation zones was calculated for both sites according to Fick´s First Law based on assumed sediment porosities (0.7-0.75) and calculated diffusion coefficients corrected for tortuosity at ambient temperature. Bulk sediment barium and aluminium concentrations were determined by means of ICP-OES (RSD <5 %) after microwave acid digestion of dried and ground sediment (40-50 mg dry wt) in a mixed HCl (2 ml, 30%, suprapure), HNO_3 (3 ml, 65% subboiled), HF (0.5 ml, 40%, suprapure) solution. Analytical precision was controlled by measuring replicates (RSD <3 %) and accuracy was checked by measuring certified standard material provided by the National Institute of Standards and Technology (NIST 2702, Marine Sediment).

Supplementary Methods

A 1-D reactive transport model (eq.1) was developed in order to track the development of the methane and sulphate profiles after the M_W 8.1 earthquake. Two species were modelled, methane and sulphate, according to the following equation:

$$\varphi_i \frac{\partial C_{i,j}}{\partial t} = \frac{\partial D_{i,j} \varphi_i \left(\partial C_{i,j} / \partial z\right)}{\partial z} - \frac{\partial v_i \varphi_i C_{i,j}}{\partial z} - \varphi_i k_{AOM} C_{i,CH_4} C_{i,SO_4^{2-}} + \varphi_i \alpha \exp(-\beta z)(C_{0,j} - C_{i,j}) \qquad \text{(Eqn. 5)}$$

where t is time, z is the depth from the sediment-water interface, φ is the porosity, C is the concentration, D is the temperature- and tortuosity- corrected diffusion coefficient, v is the pore water velocity, k_{AOM} is the bimolecular rate constant for AOM, α is the irrigation coefficient (assumed to be the same for both species), β is the depth-attenuation coefficient for irrigation, and i, j represent subscripts depicting depth- and species- dependence, respectively. For constant and site-specific parameters see Supplementary Tables 1 and 2.

Organic matter degradation as a sink for sulphate or source for methane was neglected due to low organic carbon concentrations in the sediment (data not shown), which would render degradation rates negligible when compared to AOM at the considered decadal times scales. The model assumes that after the earthquake, the methane front (methane concentration at equilibrium with structure 1 pure methane hydrates) shifts upwards due to the movement of free gas within the hydrate stability zone through earthquake-induced fractures. This leads to saturation of ambient pore water with methane at shallow depths that were previously sulphate-rich.

Table 5: Constant parameters

Name	Symbol	Value	Unit	Reference
Porosity at sediment/water interface	φ_0	0.75		Assumed[a,b]
Porosity at depth	φ_∞	0.70		Assumed[a,b]
Porosity attenuation with depth	γ	0.003	cm^{-1}	Assumed[a,b]
1st constant for sulphate diffusion	m_0	$4.88*10^{-6}$	$cm^2\ s^{-1}$	Boudreau, 1997[c]
2nd constant for sulphate diffusion	m_1	$0.232*10^{-6}$	$cm^2\ s^{-1}\ °C^{-1}$	Boudreau, 1997[c]
Pre-exponential factor methane diffusion	A	$304.7*10^{-4}$	$cm^2\ s^{-1}$	Boudreau, 1997[d]
Activation energy for methane diffusion	E_a	18.36	$kJ\ mol^{-1}$	Boudreau, 1997[d]
Burial velocity at depth	v_∞	0.001	$cm\ yr^{-1}$	Assumed[a,e]
Temperature	T	2	°C	This study

[a] Parameter is insensitive relative to the bimolecular AOM rate constant.
[b] $\varphi = \varphi_\infty + (\varphi_0 - \varphi_0)\exp(-\gamma z)$
[c] $D_{SO_4^{2-}} = (m_0 + m_1 T)/(1 - 2\ln(\varphi))$
[d] $D_{CH_4} = A\exp(-E_a/(RT))/(1 - 2\ln(\varphi))$, where R is the universal gas constant.
[e] $v = v_\infty \varphi_\infty / \varphi$
[f] Boudreau, B. P. *Diagenetic models and their implementations* (Springer-Verlag, Berlin, 1997).

Table 6: Site Specific Parameters

Name	Symbol	Hydrate	Non-hydrate	Unit	Reference
Bimolecular AOM rate constant	k_{AOM}	0.4	0.007	$mM^{-1}\ yr^{-1}$	This study[a]
Model domain	L	1.6	5.9	m	Assumed
Bubble irrigation coefficient	α	10.0	0	yr^{-1}	Assumed
Irrigation attenuation with depth	β	0.028	0	cm^{-1}	Assumed
Top boundary condition sulphate	$C_{0,SO_4^{2-}}$	28.5	28.5	mM	This study
Bottom boundary condition sulphate	$\left.\frac{\partial C_{SO_4^{2-}}}{\partial z}\right\|_L$	0.0	0.0	$mM\ cm^{-1}$	Assumed
Top boundary condition methane	C_{0,CH_4}	0.0	0.0	mM	This study
Bottom boundary condition methane	C_{L,CH_4}	55.12	55.07	mM	This study[b]

[a] Parameter was adjusted until the sum of the error squared was minimized.
[b] Methane hydrate saturation value (after ref 23).

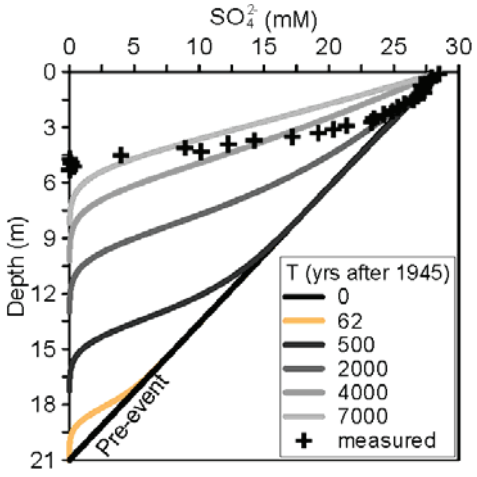

Figure 17: Numerical simulation of the sulphate profile of the non-Hydrate-site merely involving diffusion of dissolved methane from the pre-event source depth. Neither the depth of the SMT, nor the profile shapes in lead to a sufficient fit to the measured values. For a detailed description of the applied 1-D nonsteady state model and boundary conditions see methods section and Supplementary.

The initial conditions for sulphate were assumed to follow the linear trend of the first 5 points of the measured non-Hydrate-site sulphate profile, where the sulphate slope is near-constant. Initial conditions for methane were assumed to be the steady state solution leading to the initial sulphate conditions, i.e. a methane profile with an SMT at 21 m sediment. The methane front was then assumed to have shifted to 1.6 m and 5.9 m sediment depth at both the investigated sites after the earthquake. The AOM bimolecular rate constant was then varied in order to minimize the error with respect to the measured sulphate profiles. We tested our model by simulating the rise of the SMT at the non-GH-site merely considering diffusion, neglecting gas-phase transport and assuming an increase in methane concentrations to hydrate saturation values below the pre-event depth of the SMT. This approach neither leads to the observed depth of the SMT, nor to the correct sulphate profile shape (Fig.17).

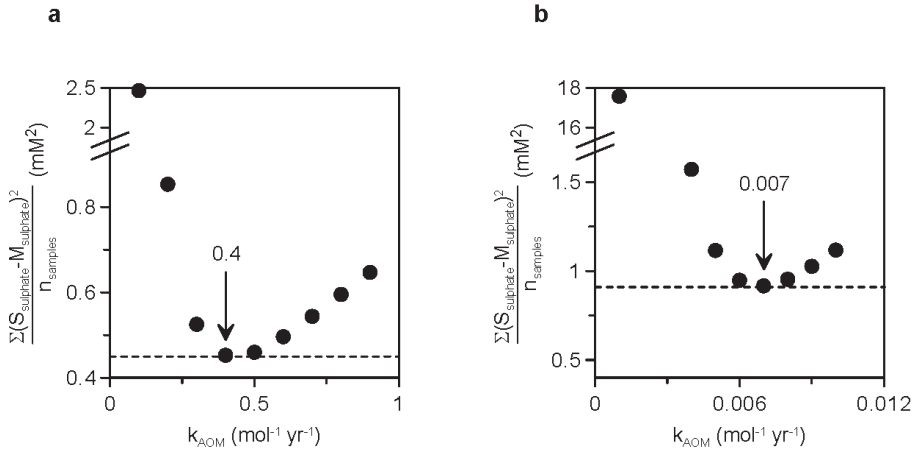

Figure 18: Average sum of square residuals (mM^2) for the (a) Hydrate and (b) non-Hydrate sites as a function of different k_{aom} values (mM^{-1} yr^{-1}). The average sum of squares were calculated by adding the square of the deviations between simulated ($S_{sulphate}$) and measured ($M_{sulphate}$) sulphate concentrations at T=62 years after the earthquake and dividing by the number of paired points. The minima indicate the best fit scenarios chosen for the simulation.

Acknowledgements

We thank M. Zabel for providing the sulphate data. We acknowledge comments by T. Goldhammer and J. Collins on an earlier version of the manuscript. M. Römer assisted in compiling the map and R. Alvaréz assisted in the laboratory ICP-OES analyses. This work was supported by the DFG Research Centre/Cluster of Excellence "The Ocean in the Earth System" (MARUM) with additional funding by the Helmholtz Association (Alfred Wegener Institute for Polar and Marine Research, Bremerhaven).

Author contributions

D.F. and S.K. designed the study and wrote the manuscript. D.F. conducted the laboratory sample analyses. J.M.M. developed the numerical simulation. J.M.M., M.S. and G.B. substantially contributed to writing the manuscript.

References

1 Denman, K.L. *et al.*, Couplings between changes in the climate system and biogeochemistry in *Climate Change 2007: The Physical Science Basis. Contribution of Working Group I to the Fourth Assessment Report of the Intergovernmental Panel on Climate Change*, edited by S. Solomon *et al.* (Cambridge University Press, Cambrige, New York, 2007).

2 Kvenvolden, K.A. & Rogers, B.W., Gaia's breath - global methane exhalations. *Mar. Pet. Geol.* **22,** 579-590 (2005).

3 Tryon, M.D., Brown, K.M., & Torres, M.E., Fluid and chemical flux in and out of sediments hosting methane hydrate deposits on Hydrate Ridge, OR, II: Hydrological processes. *Earth. Planet. Sci. Lett.* **201,** 541-557 (2002).

4 Tryon, M.D., Monitoring aseismic tectonic processes via hydrologic responses: An analysis of log-periodic fluid flow events at the Costa Rica outer rise. *Geology* **37,** 163-166 (2009).

[5] Flemings, P.B., Liu, X., & Winters, W.J., Critical pressure and multiphase flow in Blake Ridge gas hydrates. *Geology* **31,** 1057-1060 (2003).

[6] Hornbach, M.J., Saffer, D.M., & Holbrook, S.W., Critically pressured free-gas reservoirs below gas-hydrate provinces. *Nature* **427,** 142-144 (2004).

[7] Field, M.E. & Jennings, A.E., Seafloor gas seeps triggered by a northern California earthquake. *Mar. Geol.* **77,** 39-51 (1987).

[8] Halbach, P., Holzbecher, E., Reichel, T., & Moche, R., Migration of the sulphate-methane reaction zone in marine sediments of the Sea of Marmara--can this mechanism be tectonically induced? *Chem. Geol.* **205,** 73-82 (2004).

[9] Ding, F. *et al.*, Interaction between accretionary thrust faulting and slope sedimentation at the frontal Makran accretionary prism and its implications for hydrocarbon fluid seepage. *J. Geophys. Res.* **115,** B08106 (2010).

[10] Kukowski, N. *et al.*, Morphotectonics and mechanics of the central Makran accretionary wedge off Pakistan. *Mar. Geol.* **173,** 1-19 (2001).

[11] Heidarzadeh, M. *et al.*, Historical tsunami in the Makran Subduction Zone off the southern coasts of Iran and Pakistan and results of numerical modeling. *Ocean Eng.* **35,** 774-786 (2008).

[12] Pendse, C.G., The Mekran earthquake of the 28th November 1945. *India Meteorological Department Scientific Notes* **10,** 141-146 (1945).

[13] Sibuet, M. & Olu, K., Biogeography, biodiversity and fluid dependence of deep-sea cold-seep communities at active and passive margins. *Deep Sea Res. Part II* **45,** 517-567 (1998).

[14] von Rad, U. *et al.*, Gas and fluid venting at the Makran accretionary wedge off Pakistan. *Geo-Mar. Lett.* **20,** 10-19 (2000).

[15] Hoehler, T., Alperin, M.J., Albert, D.B., & Martens, C., Field and laboratory studies of methane oxidation in an anoxic marine sediment: evidence for a methanogen-sulfate reducer consortium. *Global Biogeochem. Cycles* **8,** 451-463 (1994).

[16] Boetius, A. *et al.*, A marine microbial consortium apparently mediating anaerobic oxidation of methane. *Nature* **407,** 623-626 (2000).

[17] Dehairs, F., Chesselet, R., & Jedwab, J., Discrete suspended particles of barite and the barium cycle in the open ocean. *Earth. Planet. Sci. Lett.* **49,** 528-550 (1980).

[18] Torres, M.E., Brumsack, H.J., Bohrmann, G., & Emeis, K.C., Barite fronts in continental margin sediments: a new look at barium remobilization in the zone of sulfate reduction and formation of heavy barites in diagenetic fronts. *Chem. Geol.* **127,** 125-139 (1996).

[19] Dickens, G.R., Sulfate profiles and barium fronts in sediment on the Blake Ridge: present and past methane fluxes through a large gas hydrate reservoir. *Geochim. Cosmochim. Acta* **65,** 529-543 (2001).

[20] Nöthen, K. & Kasten, S., Reconstructing changes in seep activity by means of pore water and solid phase Sr/Ca and Mg/Ca ratios in pockmark sediments of the Northern Congo Fan. *Mar. Geol.* **287,** 1-13 (2011).

[21] Kasten, S., Freudenthal, T., Gingele, F.X., & Schulz, H.D., Simultaneous formation of iron-rich layers at different redox boundaries in sediments of the Amazon deep-sea fan. *Geochim. Cosmochim. Acta* **62,** 2253-2264 (1998).

[22] Haeckel, M., Boudreau, B.P., & Wallmann, K., Bubble-induced porewater mixing: A 3-D model for deep porewater irrigation. *Geochim. Cosmochim. Acta* **71,** 5135-5154 (2007).

[23] Hensen, C. *et al.*, Control of sulfate pore-water profiles by sedimentary events and the significance of anaerobic oxidation of methane for the burial of sulfur in marine sediments. *Geochim. Cosmochim. Acta* **67,** 2631-2647 (2003).

[24] Tishchenko, P., Hensen, C., Wallmann, K., & Wong, C.S., Calculation of the stability and solubility of methane hydrate in seawater. *Chem. Geol.* **219,** 37-52 (2005).

[25] Minshull, T. & White, R., Sediment Compaction and Fluid Migration in the Makran Accretionary Prism. *J. Geophys. Res.* **94,** 7387-7402 (1989).

[26] Fekete, N. *et al.*, Seismic structure of shallow sediments at the Nasent Ridge vent site, Makran deformation front, offshore Pakistan. *Geophys. Res. Abstr.* **11,** EGU2009-10904 (2009).

[27] Haeckel, M., Suess, E., Wallmann, K., & Rickert, D., Rising methane gas bubbles form massive hydrate layers at the seafloor. *Geochim. Cosmochim. Acta* **68,** 4335-4345 (2004).

[28] Römer, M., Sahling, H., Spiess, V., & Bohrmann, G., The role of gas bubble emissions at deep-water cold seep systems: An example from the Makran continental margin, offshore Pakistan (extended abstract). *Proceedings of the 7th conference on gas hydrates (ICGH 2011)* (2011).

[29] Sahling, H. *et al.*, Vodyanitskii mud volcano, Sorokin trough, Black Sea: Geological characterization and quantification of gas bubble streams. *Mar. Pet. Geol.* **26,** 1799-1811 (2009).

[30] Manga, M., Brumm, M., & Rudolph, M.L., Earthquake triggering of mud volcanoes. *Mar. Pet. Geol.* **26,** 1785-1798 (2009).

Chapter IV – Manuscript 3

Impact of gas hydrates and methane seepage on the formation of authigenic iron sulfides at the Makran convergent margin

D. Fischer[1], S. W. Poulton[2], T. Frederichs[1], R. Alvarez[1], G. Bohrmann[1], S. Kasten[3]

[1] MARUM – Center for Marine Environmental Sciences and Faculty of Geosciences at the University of Bremen, Klagenfurter Strasse, 28359 Bremen, Germany

[2] School of Civil Engineering and Geosciences, Newcastle University, Newcastle upon Tyne, NE1 7RU, UK

[3] Alfred Wegener Institute for Polar and Marine Research, Am Handelshafen 12, 27570 Bremerhaven, Germany

(Manuscript in preparation for "Chemical Geology")

Abstract

Three sediment cores obtained from two sites at the top of Nascent Ridge, the youngest accretionary ridge located at the Makran convergent margin, were analyzed for pore water geochemistry, magnetic susceptibility and solid phase Fe-species distribution. Although the sediment cores were located within 3.5 km of each other and were assumingly prone to comparable sedimentation conditions, both the solid phase and pore water records differ considerably. Replicate cores GeoB 12303-1 and GeoB 12306-1 ("Hydrate-site") contained finely disseminated gas hydrates (GH) and showed positive ex situ chloride (and potassium) anomalies in the pore water, which is indicative of recent gas hydrate formation. In contrast, core GeoB 12331-2 ("non Hydrate-site") contained neither GHs, nor an ex situ pore water chloride anomaly over the sampled sediment interval.

In 1945 an earthquake hit Nascent Ridge that triggered gas migration into the GH stability zone and seepage across the sediment/water interface. The event significantly increased the upward methane flux and shifted the sulfate/methane transition (SMT) towards the sediment surface at both sites. At the Hydrate-site, GH formation below 160 cm established a steep upward methane gradient, leading to a very shallow SMT at about 130 m. Hydrogen sulfide released in the SMT created an upward migrating sulfidization front at both sites. At the Hydrate-site, the sulfidization front has reached the core-top, as indicated by sulfidic pore water conditions and the occurrence of authigenic pyrite throughout the core, coupled with a relatively constant and low magnetic susceptibility signal. In contrast, at the non Hydrate-site, the SMT is located at a depth of 470 cm and the sulfidization front has not reached the core-top. Here, the sulfidization front, is located at a depth of 150 cm, coinciding with a pronounced drop in magnetic susceptibility, indicative of the reductive dissolution of Fe-(oxyhydr)oxides by hydrogen sulfide. Although dissolved hydrogen sulfide reacts with solid phase Fe-species at both sites and with dissolved iron at the non Hydrate-site, Fe-monosulfides were not detected, which is likely due to fast pyritization by the abundant hydrogen sulfide.

1 Introduction

Early diagenetic processes have been shown to significantly alter the Fe-mineralogy and rock-magnetic properties of sediments, both due to microbial processes such as dissimilatory Fe(III)-reduction, and abiotic processes, such as the reaction of Fe-oxy(hydr)oxides with hydrogen sulfide (e.g. Fu et al., 2008; Kasten et al., 1998; Novosel et al., 2005; Riedinger et al., 2005; Wehrmann et al., 2011). Hydrogen sulfide and bicarbonate are produced during sulfate reduction via either organic matter degradation (organoclastic sulfate reduction OSR; Froelich et al., 1979) or the anaerobic oxidation of methane (AOM; Hoehler et al., 1994). OSR is decoupled from sulfate reduction via AOM (Ferdelman et al., 1999; Fossing et al., 2000) and usually occurs in marine sediments below the zones of dissimilatory metal (Fe, Mn) reduction, with an ultimate dependence on the availability of chemically stored energy in the form of fresh organic matter (Froelich et al., 1979). AOM with sulfate as the terminal electron acceptor (Hoehler et al., 1994) typically leads to the establishment of a sulfate/methane transition (SMT). In general, the depth of the SMT depends on the upward flux of methane, the downward flux of sulfate, and the sedimentation rate (Borowski et al., 1996; Riedinger et al., 2005), but may be shifted downwards by processes irrigating bottom water into the sediment, such as bioirrigation (Fischer et al., submitted-b) or bubble-irrigation (Haeckel et al., 2007).

Typical authigenic minerals that precipitate in relation to AOM are carbonates (e.g., Ritger et al., 1987), barite (e.g., Torres et al., 1996b), and iron sulfides (e.g. Kasten et al., 1998). While carbonate and barite authigenesis has been investigated frequently in marine sediments, including gas hydrates (GHs) and seep-sites (e.g., Bohrmann et al., 1998; Dickens, 2001; Greinert et al., 2002; Peckmann et al., 2001; Teichert et al., 2003; e.g. Torres et al., 1996a), the formation of iron sulfides in association with hydrocarbon seepage has only been studied sporadically (e.g., Larrasoaña et al., 2007; Novosel et al., 2005; Wehrmann et al., 2011). A close relationship between hydrogen sulfide contents (depending on the rate of AOM), the speciation of Fe-sulfides and GH occurrence (or methane flux) was shown by Housen and Musgrave (1996) and Larrasoaña et al (2007). The distribution and speciation of authigenic Fe-sulfides, which constitute a major marine sulfur sink, may serve as a proxy for methane flux and GH distribution.

Formation of pyrite due to reduction of Fe-(oxyhydr)oxides has been shown to strongly reduce the magnetic susceptibility of the sediment, because pyrite is paramagnetic (e.g., Larrasoaña et al., 2007; März et al., 2008; Riedinger et al., 2005; Rowan et al., 2009). However, several of the precursor minerals in pyritization, such as greigite (Fe_3S_4) and pyrrhotite ($Fe_{1-x}S$), are ferromagnetic and can thus produce a strong magnetic signal (Fu et al., 2008; Larrasoaña et al., 2007). However, these metastable minerals are only preserved in the sediment if pyritization is incomplete, for example, due to limitation by hydrogen sulfide or elemental sulfur (cf. review by Rickard and Luther, 2007). Techniques for the direct determination of greigite have been developed based on its ferromagnetism, in contrast to paramagnetic mackinawite and pyrite (Larrasoaña et al., 2007; Roberts and Weaver, 2005; Rowan et al., 2009). X-ray diffraction (XRD) has also been used to identify greigite (Holmkvist et al., 2011; Kasten et al., 1998), however, quantitative XRD analyses require a minimum concentration of 1 wt% of the target mineral.

In a recent study, Fischer et al. (submitted-a) proposed that the 1945 Balochistan earthquake offshore Pakistan caused a substantial upward shift of the SMT and triggered methane seepage across the sediment/water interface and shallow GH formation at Nascent Ridge. This scenario implies that the depth of hydrogen sulfide production during AOM was shifted upwards and Fe-(oxyhydr)oxides, which were present above the sulfidic zone before the event, became exposed to hydrogen sulfide. Thus, Nascent Ridge provides an ideal setting to analyze the influence of hydrogen sulfide on more or less pristine, non-sulfidized Fe-(oxyhydr)oxides.

Here, we present pore water and solid phase geochemical data for sediment cores retrieved from Nascent Ridge – the youngest accretionary ridge developed at the deformation front of the Makran convergent margin in the Northern Arabian Sea. The purpose of this study was to gain insight into the formation of iron sulfides in relation to hydrocarbon seepage and the presence of gas hydrates. We use pore water profiles, sequential extraction techniques and magnetic susceptibility measurements to investigate the diagenetic transformation of Fe-(oxyhydr)oxides into Fe-sulfides. Although the investigated sediment cores are situated in close proximity to each other (~3.5 km), they show significantly different degrees of Fe-sulfide authigenesis. Likely explanations for these differences appear to be the heterogeneous distribution of hydrogen sulfide and

gas hydrates, caused by local and temporal heterogeneity in upward methane fluxes induced by the Balochistan earthquake.

2 Geological setting

The convergent continental margin off the coast of Pakistan is characterized by a broad accretionary prism that has been forming since the late Miocene (Platt et al., 1985). Multi-channel seismic surveys show that tectonic activity currently forms the youngest accretionary ridge (hereafter Nascent Ridge) north of the deformation front (Ding et al., 2010; Kukowski et al., 2001; Schlüter et al., 2002; von Rad et al., 2000). Geochemistry, chemosynthetic communities, as well as authigenic precipitates from numerous cold seeps distributed along the Makran convergent margin have been investigated in earlier studies (Fischer et al., submitted-a; Fischer et al., submitted-b; Himmler et al., 2010; Römer et al., submitted; von Rad et al., 2000; von Rad et al., 1996).

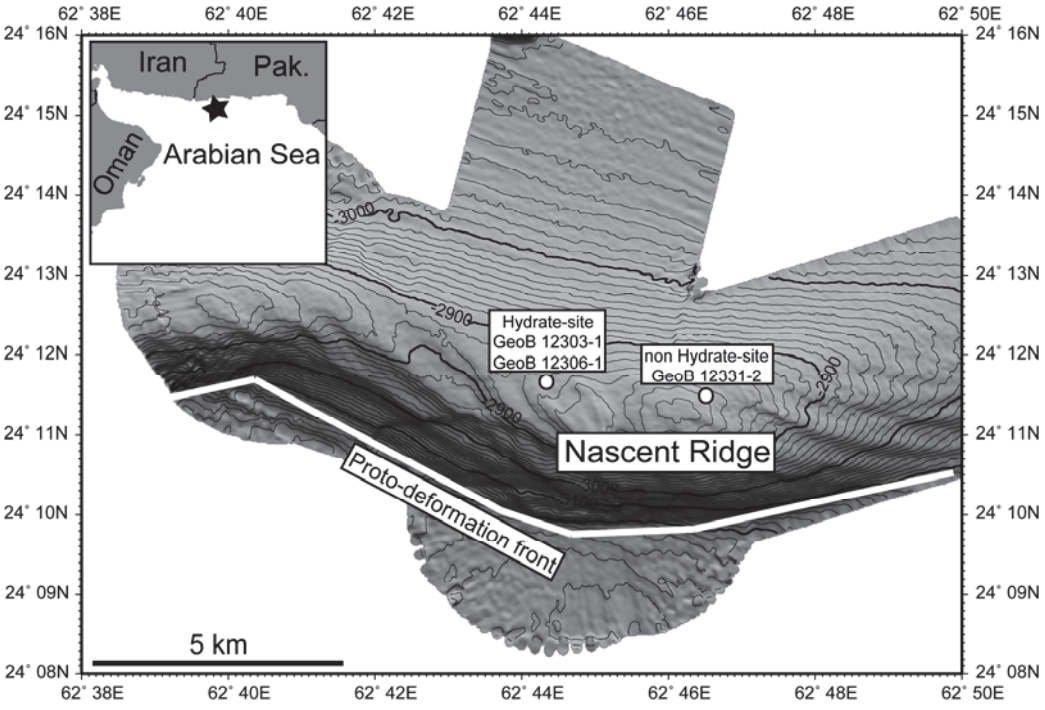

Figure 19: Map of the study area Nascent Ridge. The ridge is located just N of the proto-deformation front. Core locations are indicated. Upper left: Overview map of the Northern Arabian Sea.

3 Material and methods

Three gravity cores were obtained from the top of Nascent Ridge during cruise M 74/3 of RV METEOR in fall 2007 (Fig. 19, Table 7). Cores GeoB 12303-1 and GeoB 12306-1 (2861 m water depth) were recovered from a site of gas venting and contained GHs, whereas gravity core GeoB 12331-2 (2831 m water depth) was obtained from a site unaffected by gas seepage or GHs (Bohrmann et al., 2008). Examination of the gas vents with the remotely operated vehicle (ROV) "MARUM-QUEST 4000m" showed that gas bubbles escaping from the sediment were surrounded by a GH-skin. The gas vents were sparsely colonized by chemosynthetic communities including scattered vesicomyid clams and frenulate tubeworms (Fischer et al., submitted-a). Massive authigenic carbonates, which are typical of cold seeps at shallower water depths offshore Pakistan (von Rad et al., 1996), were neither observed in the examined cores, nor were they visually identified as outcrops or sea floor pavements during ROV dives.

Core GeoB 12303-1 was intended to recover GHs. It was thus equipped with a plastic hose instead of a plastic liner in order to provide rapid access to the sediment and gas hydrates. The core was immediately opened after retrieval and we observed degassing cracks, a mousse-like sediment structure, and very active gas release from abundant dissociating cm-scale GH chips below 160 cm (Fig. 20). Core GeoB 12306-1 was obtained as a replicate from the same site and was used for solid phase and pore water sampling. It was cut in half after pore water sampling was completed (within ~ 3 hours after retrieval) and showed abundant degassing cracks below 160 cm (Fig. 20). It is thus assumed that GHs in core GeoB 12306-1 were similarly distributed as in core GeoB 12303-1, but had not dissociated until opening of the core. Based on the occurrence of GHs, sites GeoB 12303-1 and GeoB 12306-1 will collectively be called

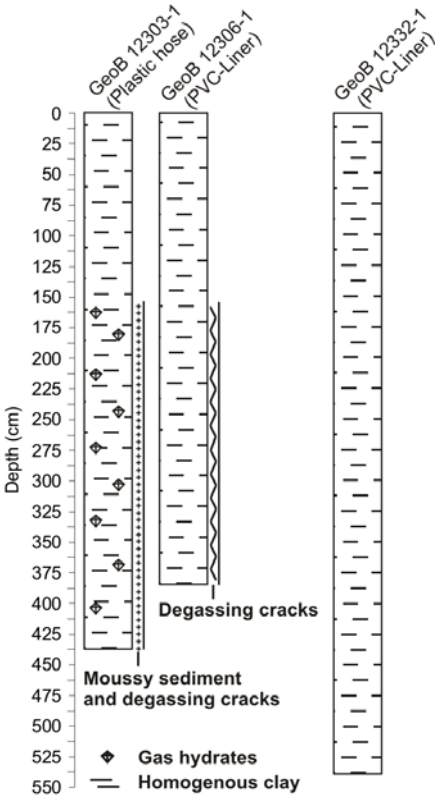

Figure 20: Simplified core descriptions of three examined cores from the Hydrate-site and from the non Hydrate-site. Stratigraphic details are given with respect to the presence of gas hydrates.

"Hydrate-site" in the following. Gravity core GeoB 12331-2 was retrieved within a distance of about 3.5 km to the East of the Hydrate-site, where no gas escape was observed. It showed no indication of GHs and will thus be referred to as "non Hydrate-site" in the following. However, we assume that GHs occur at greater depth below the cored sediment interval at this site.

3.1 Pore water analyses

Pore water was extracted at in situ temperature (~ 4°C) in the cold room of the ship at a resolution of 20 cm from cores GeoB 12306-1 and GeoB 12331-2, by means of rhizons attached to 10 ml syringes (Seeberg-Elverfeldt et al., 2005). To avoid pore water oxidation either within the rhizon, the plastic connector, or the syringe, we discarded the first ~ 0.5 ml of extracted pore water and immediately reattached the rhizons to the syringes. For Fe^{2+} determination, 1 ml of pore water was complexed with 50 µl of Ferrospectral solution and measured spectrophotometrically at a wave length of 565 nm. Sulfate and chloride aliquots were diluted 1:100 with deionized water, immediately frozen onboard, and analyzed in the home laboratory by means of ion chromatography (Metrohm IC Advanced Compact 861) at a flow rate of 0.7 ml min^{-1}. 1.5 ml of pore water was fixed in 0.6 ml of a 5 % zinc-acetate solution for hydrogen sulfide determination in the home laboratory by means of spectrophotometry after Cline (1969). Dissolved potassium was determined by inductively coupled plasma-optical emission spectroscopy (ICP-OES; IRIS Intrepid, Thermo Scientific) after acidification and 1:10 dilution with HNO_3. Analytical accuracy and precision were within 5 % RSD.

Table 7: Core locations, water depths, stratigraphic details, and occurrence of gas hydrates of the three examined cores.

Core ID	Location	Water depth (m)	Stratigraphic details	Gas hydrates
GeoB 12303-1	62:44.308 E 24:11.749 N	2861	Homogenous silty clay, degassing cracks and moussy sediment below 160 cm	yes
GeoB 12306-1	62:44.311 E 24:11.761 N	2861	Homogenous silty clay, degassing cracks below 160 cm	Inferred (see text)
GeoB 12331-2	62:46.502 E 24:11.507 N	2831	Homogenous silty clay	no

3.2 Solid phase

Solid phase samples were obtained onboard from core GeoB 12331-2 at a resolution of 10-20 cm and were immediately stored anoxically and frozen at -20°C. Core GeoB 12306-1 was sampled at a resolution of 5-20 cm in summer 2010 after storing the core at 4°C, and samples were immediately freeze-dried and ground with an agate mortar. Samples were kept frozen at -20°C until measurement. The core partially oxidized during storage, as indicated by a few mm-thick oxidation front (color changes) at the core-rim. Thus, sediment sampling for this core was conducted in the center of the core-liner in order to exclude contamination of samples with sediment oxidized during storage.

Table 8: Extraction scheme for Fe-species determination.

Step	Reagents/extraction time	Target Fe-species
Fe-HCl	0.5 M HCl for 1 hour	a: Amorphous Fe-oxides, ferrihydrite → $Fe_{ferrihydrite}$ b: Fe^{2+} adsorbed to mineral surfaces → Fe_{surf}
Fe-dith	Sodium dithionite/sodium citrate solution (pH ~4.8) for 2 hours	Goethite, hematite →Fe_{g+h}
Fe-oxal	Ammonium oxalate/oxalic acid solution (pH ~2.8) for 6 hours	Magnetite → $Fe_{magnetite}$
Fe- AVS	6 M HCl for min. 0.5 hours	(Amorphous) Fe monosulfide, ~ 30% greigite (Cornwell and Morse 1987) → Fe_{AVS}
Fe- CRS	Boiling $CrCl_2$ (2 M) solution in 10% HCl for min. 1 hour	Pyrite, ~ 70 % greigite (Cornwell and Morse 1987) → Fe_{pyrite}

We used a sequential extraction procedure to quantify different operationally-defined Fe pools that are broadly related to different mineral phases, including various Fe-(oxyhydr)oxides and Fe-sulfides (Table 8), and we combine these analyses with magnetic susceptibility measurements and total inorganic (TIC) and total organic carbon (TOC) contents. Total carbon content was determined using an Elementar Vario EL III element analyzer, where freeze-dried sediment samples were ground and then combusted in tin-cups at a temperature of 950°C. Subsamples were acidified with 6 N HCl to remove inorganic carbon and measured as described above. TOC was calculated as the difference between total carbon and TIC. Concentrations are given in wt% C with a RSD < 4%. Fe-(oxyhydr)oxide species were determined on about 70 mg of dried and ground sediment following a modified sequential extraction procedure (Poulton and Canfield, 2005). Ferric iron concentrations in the extracts were determined by atomic absorption spectroscopy (Varian SpectrAA 400), with all steps having a

RSD of <5%. Ferrous iron extracted during the HCl-step (Table 8) was determined by spectrophotometry (Stookey, 1970). Applying this method we were able to discriminate different Fe-(oxyhydr)oxide fractions dominated by distinct Fe-minerals, as summarized in Table 8. Fe-sulfides were extracted from about 1 g of sediment following a two-step extraction method (Canfield et al., 1986). This method extracts Fe-monosulfides first (acid volatile sulfur, AVS), and then Fe bound in pyrite (Fe_{pyrite}) in the chromium reducible sulfur (CRS)-step (Table 8). Greigite is not quantitatively recovered during the AVS-step of this method. The reported extraction efficiency for greigite is ~30 %, while the remaining 70 % is expected to be extracted in the CRS-step (Cornwell and Morse, 1987). Concentrations obtained from the extraction procedures are given as wt% Fe of the respective iron species. Magnetic susceptibility (□) was determined with a custom-made, automated split-core scanner using a Bartington MS2 susceptometer as reported by Funk et al. (2004). We use here the diagenesis proxy □/Fe (Funk et al., 2004) to support the interpretation of the magnetic susceptibility profiles.

To calculate this ratio we used the concentration of bulk Fe in g/kg. Total solid phase iron and aluminum concentrations were determined by means of ICP-OES after microwave acid digestion of dried and ground sediment (40-50 mg) in a mixed HCl (2 ml, 30%, suprapure), HNO_3 (3 ml, 65% subboiled), HF (0.5 ml, 40%, suprapure) solution. Analytical precision was controlled by measuring replicates (RSD <6%), and accuracy was checked relative to certified standard material provided by the National Institute of Standards and Technology (NIST 2702, Marine Sediment). We used a punch-in electrode to determine pH values in the sediment.

4 Results

4.1 Pore water

Pore water profiles obtained for cores GeoB 12306-1 (Hydrate-site) and GeoB 12331-2 (non Hydrate-site) are shown in Figs. 21 and 22. The concentration profile of sulfate at the Hydrate-site indicates a shallow zone of sulfate depletion at about 150 cm (Fig. 21), which represents the SMT. The sulfate profile at this site shows a pronounced kink at a depth of 80 cm, where near-constant concentrations of around 28 mM are followed by a very steep gradient towards

values around 1 mM in and below the SMT (Fig. 21). Dissolved ferrous iron (Fe^{2+}) was below detection limits and the pore water was sulfidic throughout (Fig. 21).

The hydrogen sulfide profile at the Hydrate-site is asymmetric over depth with a very steep upward concentration gradient from 7.5 mM at the SMT, to 0.6 mM at a depth of 80 cm and a much shallower downward gradient below 150 cm, to about 3.5 mM at the core bottom (Fig. 21). The pH profile at the Hydrate-site shows a gradual decrease from ~7.75 at the core-top to ~7.45 below 125 cm (Fig. 21). Although relatively constant between the core-top and 80 cm, chloride and potassium concentrations gradually increase at the Hydrate-site, from sea water values of around 555 mM and 10.5 mM, respectively, to maximum concentrations of 661 mM and 11.4 mM at a depth of 370 cm (Fig. 21).

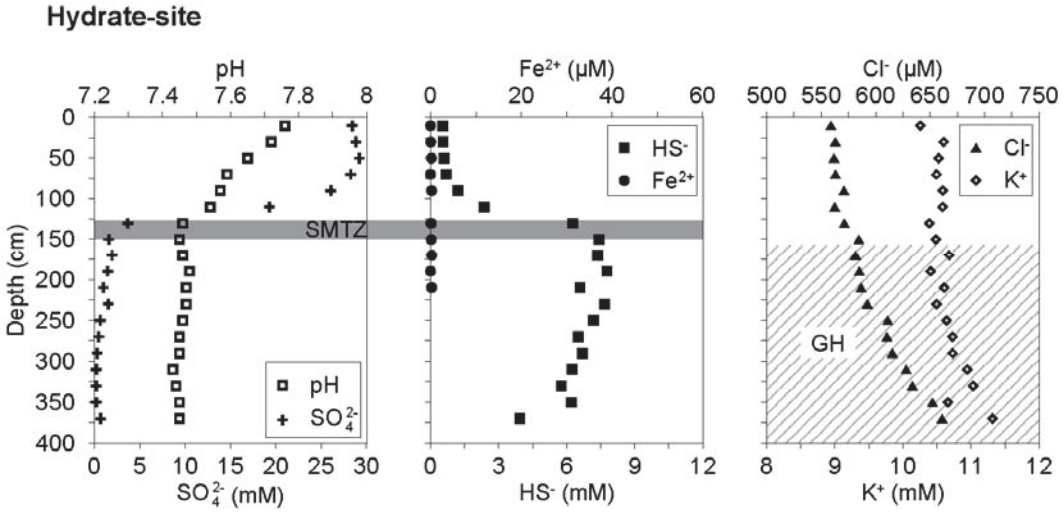

Figure 21: Pore water data of core GeoB 12306-1 retrieved from the Hydrate-site. The hatched area marks the distribution of cm-scale chips of gas hydrates.

Core GeoB 12331-2 retrieved from the non Hydrate-site is characterized by a deeper SMT at about 470 cm where sulfate is depleted (Fig. 22). The sulfate profile shows a concave-up shape. Hydrogen sulfide contents are below detection limit above 150 cm, and then gradually increase to a pronounced peak of 10.1 mM at the SMT (Fig. 22). The pH profile at the non Hydrate-site displays a distinct peak of ~7.8 at a depth of 150 cm, with a gradual decrease to values of ~7.5 above and below (Fig. 22). Chloride and potassium concentrations at the non Hydrate-site do not change throughout the sampled interval and stay around 550 mM and 10.4 mM, respectively (Fig. 22). Dissolved ferrous iron was detected

with a peak concentration of ~53 µM at the core-top, with a decrease towards depletion at a depth of 150 cm (Fig. 22), where a distinct sulfidization front is established.

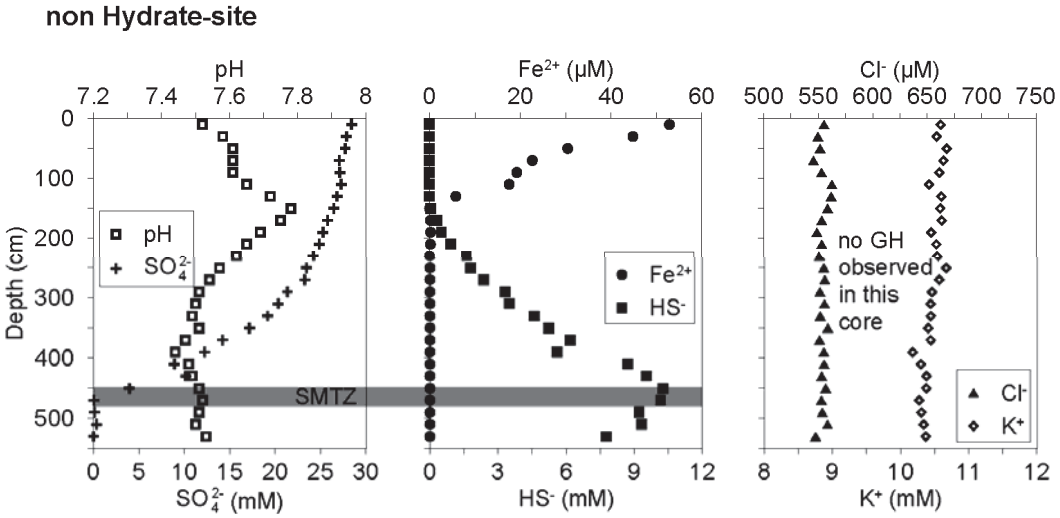

Figure 22: Pore water data of core GeoB 12331-2 retrieved from the non Hydrate-site. The core was devoid of gas hydrates or degassing cracks.

4.2 Magnetic susceptibility and solid phase

Magnetic susceptibility shows distinctly different patterns at the two sites (Fig. 23). The Hydrate-site is characterized by values of 100-150*10^{-6} SI units and a minor downward decrease. In contrast, the non Hydrate-site shows a near-constant magnetic susceptibility of around 200*10^{-6} SI units between the core-top and a depth of 130 cm. Below this, there is a distinct drop in susceptibility between 130 cm and 150 cm, to values of 100-150*10^{-6} SI units. The diagenesis proxy □/Fe mimics the magnetic susceptibility profiles in both cores (Fig. 23). TOC decreases from 0.8-1 wt% C at the core-top, to 0.3-0.5 wt% C below 100 cm at both sites (Fig. 24). TIC increases at both sites from 1.3 wt% C near the core-top,

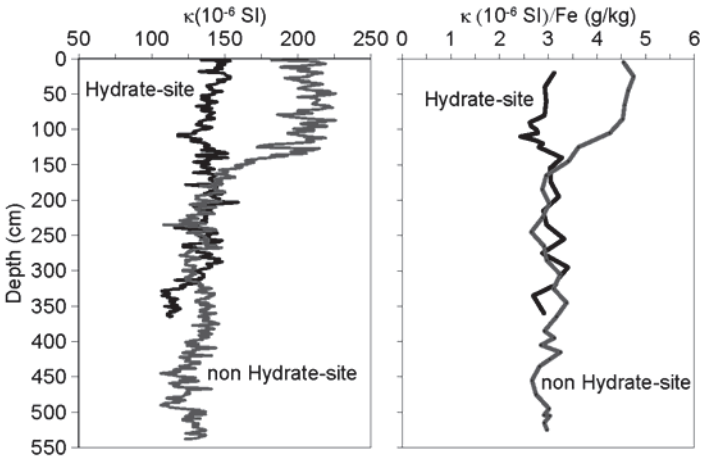

Figure 23: Depth profiles of magnetic susceptibility and the diagenesis proxy κ/Fe after (Funk et al. 2004).

to maximum contents of 3-3.5 wt% C at depth. At both investigated sites, Fe/Al ratios are relatively constant with depth (Fe/Al = ~0.58, Fig. 24) and the quantitatively dominant Fe-species is $Fe_{magnetite}$, whereas Fe-monosulfides (AVS-step) were not detected. XRD-analyses revealed that Fe_{pyrite} (CRS-step) is below the detection limit of 1 wt% in both cores (data not shown). This is well in accordance with the results of the chemical extractions, where the amount of Fe extracted in the CRS-step did not exceed 0.4 wt% in either core, which represents 0.86 wt% pyrite if this fraction contains exclusively pyrite. At the Hydrate-site, $Fe_{ferrihydrite}$ concentrations (0.03-0.2 wt%) and Fe_{surf} concentrations are low (0.11-0.2 wt%, Fig. 25).

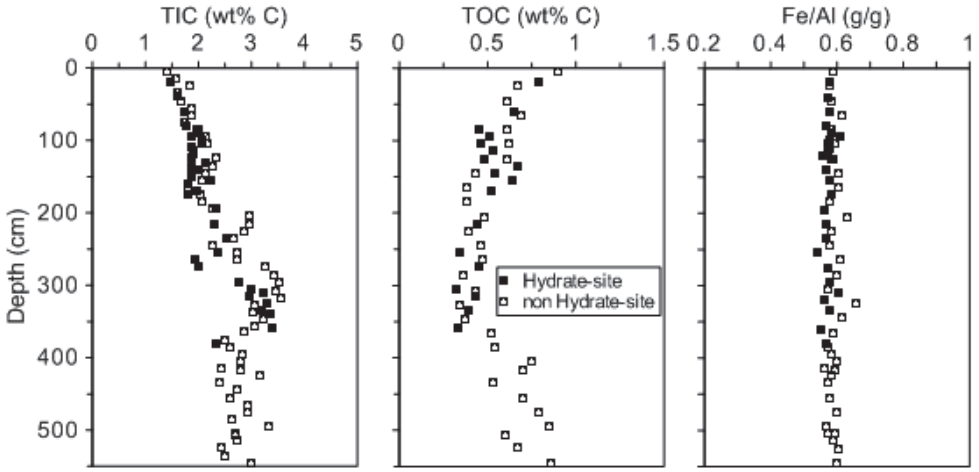

Figure 24: Downcore distribution of TIC, TOC and Fe/Al ratios for both investigated sites.

Fe_{g+h} (dominantly goethite and hematite; 0.12-0.28 wt%) and $Fe_{magnetite}$ (0.5-0.75 wt%) concentrations decrease downwards in this core (Fig. 25). Fe_{pyrite} concentrations are relatively low and constant at the Hydrate-site, fluctuating around 0.2 wt % (Fig. 25). There are, however, distinct horizons somewhat enriched in Fe_{pyrite} (Fig. 25). At the non Hydrate-site, Fe_{pyrite} contents gradually increase with depth from ~0.1 wt% close to the core-top, to maximum concentrations of ~0.36 wt% below 310 cm (Fig. 26). $Fe_{ferrihydrite}$ was detected only in the upper 130 cm, at concentrations below 0.05 wt%, while Fe_{surf} concentrations (0.16-0.2 wt%) decrease very slightly with depth at this site (Fig. 26). The Fe_{g+h} and $Fe_{magnetite}$ pools are variable throughout the cored interval, but do show distinct enrichments with maximum concentrations of 0.4 wt% (Fe_{g+h} at 110 cm) and 1.1 wt% ($Fe_{magnetite}$ at 185 cm).

5 Discussion

AOM consumes sulfate in the SMT at both sites. At the Hydrate-site the SMT is located at a depth of 130 cm, whereas at the non Hydrate-site the SMT is located at a depth of 470 cm (Figs. 21 and 22). The pore water profiles at both the Hydrate-site and the non Hydrate-site are not in steady state which is indicated by non-linear profile shapes (Figs. 21 and 22). Fischer et al. (submitted-a) showed that this nonsteady state situation is due to a recent upward shift of the SMT, caused by an increase in upward methane flux during or shortly after the earthquake in 1945. In the following sections we discuss whether, and to what extent, the SMT-shift altered the pore water and solid phase records, focusing on the distribution, formation, and preservation of Fe-species. Pore water data that are relevant and which are included in the interpretation and discussion are hydrogen sulfide, dissolved iron (Fe^{2+}), chloride and potassium, as well as pH values.

5.1 Gas hydrate distribution and spatial heterogeneity in upward methane flux

The sampling sites are located well within the GH stability zone (Bohrmann et al., 2008). Despite the close proximity of both examined sites, GH distribution differs considerably. Apparently, the upward methane flux at the Hydrate-site is, or has been, high enough to form and preserve shallow GHs, which is not the case within the sampled sediment interval at the non Hydrate-site (Fischer et al., submitted-a). Here, GHs likely occur below the depth of core penetration (Fischer et al., submitted-a).

We found a distinct downward increase in dissolved chloride and potassium at the Hydrate-site (Fig. 21). Deep-seated brines associated with evaporites or salt diapirism could cause an increase in pore water chlorinity (Aharon et al., 1992). However, such deposits were neither described nor expected in the study area. During GH formation, salt ions are excluded from the clathrate lattice (Hesse and Harrison, 1981) and are consequently enriched in the surrounding pore water leading to a positive in situ chloride anomaly. This phenomenon has been shown for a few sites (ex situ), for example Hydrate Ridge (Haeckel et al., 2004; Torres et al., 2004) and Umitaka Spur (Hiruta et al., 2009). In contrast, a negative ex situ anomaly can be found, if GH dissociate during core retrieval, provided that the initial positive in situ anomaly created by GH formation had been leveled-out due

to diffusion prior to coring. The extent of ex situ pore water anomalies depends on the amount of GHs in situ, on the time that has elapsed since GH formation, and on the amount of GHs that dissociated ex situ due to pressure release and warming during core recovery (Bohrmann and Torres, 2006; Haeckel et al., 2004). It is mostly a function of time elapsed since the recovery of a core containing GHs that controls whether the pore water contains a negative, positive, or no chloride anomaly (Haeckel et al., 2004). Core GeoB 12306-1 recovered from the Hydrate-site was sampled close to in situ temperature within one hour after retrieval and almost certainly contained GHs during pore water sampling that had not yet dissociated. Thus, the positive chloride and potassium anomalies shown in Fig. 21 are likely to represent the signal of ion exclusion from the GH lattice, and have probably been much more accentuated under in situ conditions, suggesting that GH-formation has recently occurred. Apparently, the proposed injection of methane into the shallow (> 150 cm) sediment after the 1945 earthquake (Fischer et al., submitted-a) led to formation of GHs below 160 cm at the Hydrate-site. In accordance with the interpretation of the nonsteady state sulfate profiles by Fischer et al. (submitted-a), this leads us to conclude that the upward methane flux was very high at the time of coring to form and preserve GHs, which is corroborated by the observed gas ebullition at this site in 2007.

5.2 Magnetic susceptibility and Fe-minerals influenced by a sulfidization front

The question as to whether the Fe mineralogy of sediments may serve as a proxy indicator for the dynamics of GHs and methane flux has been addressed in the recent literature (Dickens, 2011; Fu et al., 2008; Nöthen and Kasten, 2011; Novosel et al., 2005; Snyder et al., 2007). Fischer et al. (submitted-a) proposed that the release of free gas formerly sealed by massive GHs occurred during the 1945 Balochistan earthquake near Nascent Ridge. This scenario implies that the depth of the SMT shifted towards the sediment surface and that AOM rates were amplified due to the increased methane input, which led to increased hydrogen sulfide production. Here, we consider the effects of the amplified hydrogen sulfide release, the migration of the SMT, and the formation of GHs, on the distribution of Fe-(oxyhydr)oxides and Fe-sulfides in the sediment.

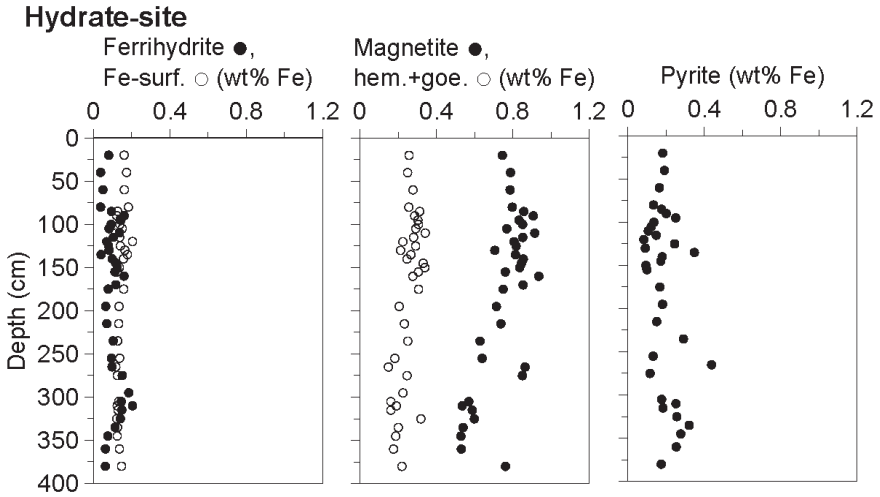

Figure 25: Downcore distribution of Fe-species at the Hydrate-site. Fe bound as goethite, or hematite is abbreviated "hem.+goe.", whereas Fe adsorbed to mineral surfaces is abbreviated "Fe-surf ", respectively.

The examined cores significantly differ in their downcore distribution of Fe-(oxyhydr)oxides and Fe-sulfides, as well as in the depth profile of magnetic susceptibility (Figs. 25-27). Reductive dissolution of ferrimagnetic magnetite by hydrogen sulfide ultimately leads to the formation of paramagnetic pyrite in a multi-step reaction summarized in Eqn. 6, if hydrogen sulfide is not the limiting factor (Canfield and Berner, 1987; Novosel et al., 2005; Poulton et al., 2004):

$$Fe_3O_4 + 2HS^- + 6H^+ \rightarrow 2Fe^{2+} + 4H_2O + FeS_2 \qquad \text{Eqn. 6}$$

Eqn. 6 involves a loss in magnetic susceptibility, which was found in both investigated cores for sediment intervals containing hydrogen sulfide (Figs. 23 and 27). Furthermore, at both the investigated sites, the □/Fe depth profiles mimic the magnetic susceptibility profiles (Fig. 23). This shows that the distinct drop in magnetic susceptibility at the non Hydrate-site is related to diagenetic reduction of Fe-(oxyhydr)oxides by hydrogen sulfide and is not due to, for example, dilution by carbonates or silicates (Funk et al., 2004). The $Fe_{magnetite}$ depth profile obtained by the sequential extraction method at the non Hydrate-site (Fig. 26) resembles the magnetic susceptibility depth profile (Fig. 23) of this core, suggesting that the main carrier of magnetism in the sediment is magnetite. The Fe(II)/Fe(III) redox boundary can be pinpointed very close to, or at, the core-top at the non Hydrate-site, because the Fe^{2+}-source is above the uppermost data point in Fig. 22. It should be stressed that gravity cores usually lack the uppermost 20-30 cm of sediment.

At the Hydrate-site, where the pore water is sulfidic throughout, $Fe_{magnetite}$ concentrations and magnetic susceptibility are fairly low compared to the hydrogen sulfide-free interval near the core-top at the non Hydrate-site (Fig. 27). This points to the conversion of the abundant magnetite to pyrite by hydrogen sulfide according to the multi-step reaction in Eqn. 6. Indeed, Fe_{pyrite} occurs at elevated concentrations without a major change over depth throughout the Hydrate-site, whereas Fe_{pyrite} contents at the non Hydrate-site gradually increase below the sulfidization front, which is currently located at a depth of 150 cm. In the interval from 30-110 cm, i.e. above the present depth of the sulfidization front, there is a slight enrichment in Fe_{pyrite}. According to Froelich et al. (1979) the zone of OSR is located below the zones of metal (Fe, Mn) reduction in marine sediments. We attribute the low Fe_{pyrite} contents above the present sulfidization front at the non Hydrate-site to reduction of reactive Fe-(oxyhydr)oxides by hydrogen sulfide released during OSR (Poulton, 2003; Poulton et al., 2004; Pyzik and Sommer, 1981; Yao and Millero, 1996).

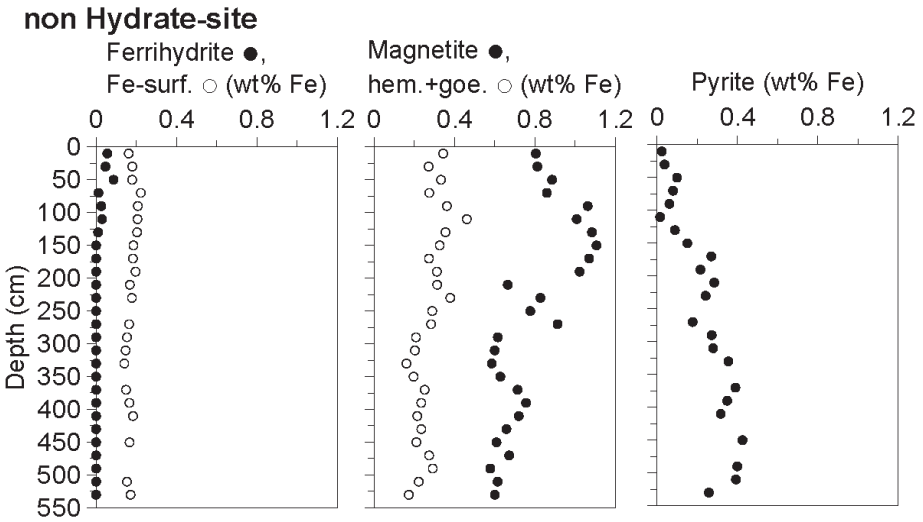

Figure 26: Downcore distribution of Fe-species at the non Hydrate-site. See caption of fig. 25 for further details.

It is striking that both $Fe_{magnetite}$ and $Fe_{ferrihydrite}$ are enriched near the core-top at the non Hydrate-site and that $Fe_{ferrihydrite}$ is in fact depleted below 130 cm. This shows that both these species preferably react with abundant hydrogen sulfide to form pyrite (Poulton et al., 2004). In fact, $Fe_{ferrihydrite}$, which reacts very quickly with hydrogen sulfide, is completely depleted in the sulfidic core-interval, whereas $Fe_{magnetite}$, which is a little less reactive towards hydrogen sulfide, persists to a

certain extent below the sulfidization front. On the other hand, the goethite/hematite fraction represented by the Fe_{g+h}-depth profile shows only a slight decrease in concentration with depth at both sites (Figs. 25 and 26) suggesting that the goethite/hematite fraction is not as sensitive as the ferrihydrite and magnetite fractions to reduction by hydrogen sulfide (see also Poulton et al., 2004). A likely explanation for this could be an unusually high degree of crystallinity of the goethite/hematite fraction (Poulton et al., 2004). As reported by von Rad et al. (1999), terrigenous material deposited offshore Pakistan is dominated by two fractions: (1) fluvially transported fine-grained sediment, and (2) eolian dust from the (semi-)arid Makran coastal- and Arabian deserts. The wind-blown dust may represent a possible source for the highly crystalline goethite/hematite fraction.

We expected to detect Fe_{AVS} associated with Fe-monosulfides precipitating from solution at or around the sulfidization front at the non Hydrate-site, according to Eqn. 7 (Berner, 1970; Rickard and Morse, 2005):

$$Fe^{2+} + HS^{-} \Leftrightarrow FeS + H^{+} \qquad \text{Eqn. 7}$$

The absence of Fe-monosulfides at the non Hydrate-site is a striking feature which is not easy to explain. Oxidation of Fe-monosulfides by atmospheric oxygen is excluded, because the samples were stored and transported frozen and under anoxic conditions. The absence of Fe-monosulfides at the non Hydrate-site could be a problem of sensitivity of the applied extraction method compared to very sensitive rock-magnetic methods, as presented by Larrasoaña et al. (2007), or due to the sampling resolution (> 10 cm) if we assume that the sulfidization front is a very confined and thin interval only several cm thick. While Wehrmann et al. (2011) also did not detect Fe_{AVS} in sediments prone to methane seepage and sulfidization fronts in the Gulf of Cadiz, Jørgensen et al. (2004) and Neretin et al. (2004) reported distinct Fe-monosulfide-rich horizons at sulfidization fronts in sediments of the Black Sea. These layers were several decimeters thick and hydrogen sulfide concentrations below the sulfidization front were significantly lower (< 1 mM) than those presented here. According to Eqn. 7, the formation of Fe-monosulfides from solution depends on the diffusive supply of reduced iron and sulfur, and depletes both these pools at the sulfidization front. Comparing the diffusive fluxes of hydrogen sulfide and dissolved ferrous iron into

the front, Jørgensen et al. (2004) concluded that Fe-monosulfide formation was limited by dissolved iron and hence sulfidization additionally depleted the solid phase iron pool. At the non Hydrate-site investigated here, hydrogen sulfide concentrations are very high and exceed dissolved ferrous iron concentrations by two orders of magnitude (Fig. 21), which demonstrates that the system is clearly limited by dissolved iron. Thus, any Fe-monosulfide that presumably precipitated from solution at the sulfidization front is prone to very high concentrations of hydrogen sulfide and rapidly undergoes pyritization according to the "hydrogen sulfide pathway" proposed by Rickard (1997). Furthermore, Fe-(oxyhydr)oxides, particularly magnetite, which are present even below the sulfidization front at the non Hydrate-site (see discussion below), provide further iron available for Fe-monosulfide formation and pyritization (cf. Jørgensen et al., 2004).

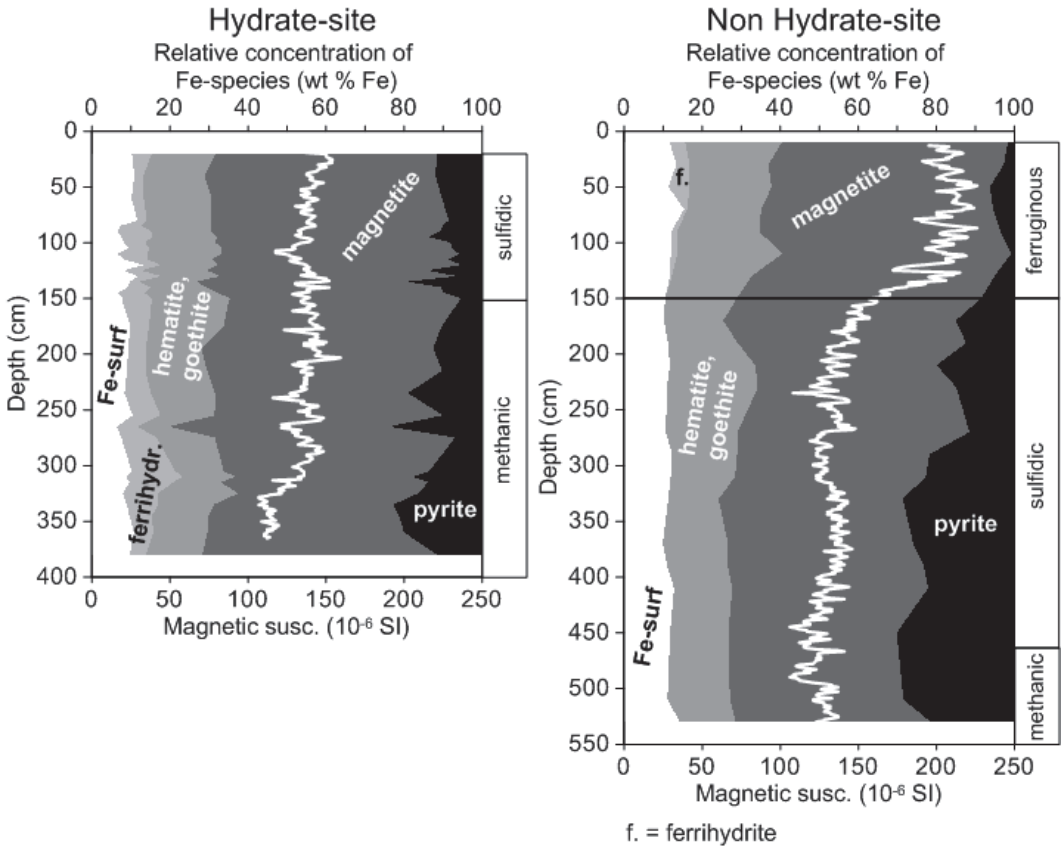

Figure 27: Relative downcore distribution of Fe-species at both examined sites given as per cent of the total sum of all extracted species. The white, thick lines denote the downcore magnetic susceptibility. At the non Hydrate-site the horizontal black line indicates the depth of the sulfidization front which separates the sulfidic (below) from the ferruginous intervals. Pore water redox zonation (Ferruginous, sulfidic, and methanic zones) is indicated in the white bars to the right of both graphs and was adopted from Canfield and Thamdrup (2009).

According to Berner (1970; 1984) and recent reviews by Rickard and Morse (2005) and Rickard and Luther (2007), the formation of the Fe-monosulfide

mackinawite from solution at the sulfidization front releases protons leading to a decrease in pore water pH, if hydrogen sulfide is the dominant sulfur species (Eqn. 7). In contrast, the hydrogen sulfide-promoted reduction of magnetite, which is suggested by the drop in magnetic susceptibility at the non Hydrate-site (Fig. 27), consumes protons according to Eqn. 6. Although very likely to occur based on the observed sulfidization front (Fig. 22), precipitation of Fe-monosulfides from solution (Eqn. 7) contradicts the measured pH profile at the non Hydrate-site. Considering Eqns. 6 and 7, the excess consumption of protons at the non Hydrate-site suggested by the maximum in pH at 150 cm (Fig. 22) can be sufficiently explained with the conversion of Fe-(oxyhydr)oxides (mainly magnetite) into pyrite by reaction with hydrogen sulfide (Eqn. 7). We therefore conclude that the quantitatively dominant Fe-sulfide-forming process is the reaction of hydrogen sulfide with Fe-(oxyhydr)oxides. These observations show that the precipitation of Fe-monosulfides from solution plays only a minor role in the early diagenetic cycling of iron and sulfur at the study sites.

The Fe-monosulfide, greigite, has been suggested as a proxy indicator for the occurrence of GHs in sediments (Housen and Musgrave, 1996; Larrasoaña et al., 2007). With the applied sequential extraction method for Fe-sulfides, about 30 % of greigite (if present) should have been extracted in the AVS-step, whereas about 70 % would be expected in the CRS-step (Cornwell and Morse, 1987; Jørgensen et al., 2004). Housen and Musgrave (1996) reported that greigite can be present in GH-bearing sediment if the GHs themselves incorporate hydrogen sulfide in the clathrate lattice and thereby remove it from the pore water, leading to stabilization of greigite at the expense of pyrite. Furthermore, Larrasoaña et al. (2007) showed that greigite formation suggests the presence of finely disseminated GHs and a moderate methane flux (SMT below 600 cm), whereas sediments containing massive GHs require a high methane flux (i.e. a high rate of AOM and hydrogen sulfide release) and favor pyrite formation (SMT above 200 cm). This interpretation may apply to the data presented here, because both investigated sites are considered as sites of relatively high upward methane flux induced by the 1945 earthquake and show SMTs at depths of 130 cm and 470 cm. However, in contrast to the non Hydrate-site, the GH-bearing core was not sampled for solid phase analyses onboard. Therefore, solid phase samples obtained in the home laboratory onshore were exposed to hydrogen sulfide during storage, since this core was not stored frozen. Consequently, if Fe-monosulfides (including greigite) had formed in association with finely dispersed

GHs at the Hydrate-site, they may possibly have been converted to pyrite prior to sampling of this core in 2010.

5.3 Co-occurrence of hydrogen sulfide and Fe-(oxyhydr)oxides – temporal control on pyritization?

In the presence of hydrogen sulfide, Fe-(oxyhydr)oxides are usually rapidly converted into pyrite, if sulfate reduction rates are high enough to produce sufficient amounts of hydrogen sulfide (Berner, 1970). Thus, a scenario is necessary which led to the preservation of Fe-(oxyhydr)oxides in the sulfidic intervals in both examined cores (Figs. 25, 26 and 27). The kinetics of reductive dissolution of Fe-(oxyhydr)oxides have been investigated in detail (Canfield and Berner, 1987; Canfield et al., 1992; Poulton et al., 2004). For example, magnetite is considered to react with hydrogen sulfide with a half-life of tens of days, whereas fresh amorphous Fe-oxides and ferrihydrite have half-lives of only several minutes to hours (Poulton et al. 2004). However, Canfield and Berner (1987) showed that the reductive dissolution of large magnetite grains by hydrogen sulfide can be considerably hampered by formation of pyrite coatings, which may increase the half-life of magnetite in the presence of hydrogen sulfide. In this case, the reductive dissolution of magnetite would be controlled by the availability of surface sites for reaction; if pyrite coatings occur around individual magnetite grains, the availability of surface sites is reduced and hydrogen sulfide cannot complex onto surface sites to allow the reaction to proceed (Canfield and Berner, 1987). This process might, in part, be responsible for the observed relatively high concentrations of $Fe_{magnetite}$ within the sulfidic interval at the non Hydrate-site (Figs. 26 and 27). However, our data suggest that, even if some of the magnetite is shielded from reduction by hydrogen sulfide by pyrite coatings, its reductive dissolution is not stopped. This is shown for the non Hydrate-site, where a drop in $Fe_{magnetite}$ concentration and magnetic susceptibility is marked by the current depth of the sulfidization front, indicating that $Fe_{magnetite}$ does react with hydrogen sulfide. In this respect, it is necessary to stress that ferrihydrite, which is highly reactive towards hydrogen sulfide (Poulton et al., 2004) was only detected above the sulfidization front at this site, which shows that pyritization of Fe-(oxyhydr)oxides is indeed an ongoing process.

Riedinger et al. (2005) showed that high sedimentation rates (100-200 cm $kyrs^{-1}$) during the last glacial led to preservation of considerable amounts of magnetite in

hydrogen sulfide-containing sediments offshore Uruguay. The SMT kept a constant distance to the "ascending" sediment surface and reduction of Fe-(oxyhydr)oxides was thus temporally limited by the short period of time they were exposed to hydrogen sulfide. In fact, sedimentation rates were reported to be between 58-90 cm kyr^{-1} and governed by thick turbiditic sequences in the abyssal plain south of Nascent Ridge is (Bourget et al., 2011). This makes it very likely that sedimentation rates are distinctly lower at the top of the ridge, which is elevated compared to the abyssal plain S of the deformation front by about 350-400 m (Fig. 19). In fact, the bathymetric depression N of Nascent Ridge (150-200 m below ridge-top; Fig. 19) may act as a trap for turbidites originating from the continental slope. Furthermore, fairly similar TOC/TIC depth profiles at both the GH- and the non Hydrate-site indicate that sedimentation conditions did not change significantly in the time-span recorded by the cored intervals (Fig. 24) and we found no indication for turbidite-layers in open core segments.

The scenario reported by Riedinger et al. (2005) considers more or less constant fluxes of sulfate and methane into the SMT. This is generally true for sulfate because it diffuses into the sediment from the water column and may thus be considered inexhaustible. Methane flux, however, depends on the rate and depth of methanogenesis and the predominant transport mechanism (Borowski et al., 1996). We thus propose the following scenario to explain the high concentrations of Fe-(oxyhydr)oxides co-occurring with hydrogen sulfide. Pore water profiles at both sites indicate that the SMT has significantly migrated towards the sediment surface which is most likely due to the increase in upward methane flux induced by the earthquake in 1945 (Fischer et al., submitted-a). We thus suggest that the co-occurrence of appreciable amounts of hydrogen sulfide and Fe-(oxyhydr)oxides, particularly magnetite, in both cores is a function of time and is related to the ascending sulfidization front (and SMT) triggered by the injection of methane in 1945 (Fischer et al., submitted-a). Further evidence for this recent event comes from the chloride and potassium anomalies found at the Hydrate-site (Fig. 21), which suggest that the observed GHs are rather young and formed just prior to coring. An upward migrating sulfide front caused by the increase in methane flux (upward shift of the SMT) led to gradual pyritization of Fe-(oxyhydr)oxides (and Fe-monosulfides) by abundant hydrogen sulfide. However, the SMT depth is assumed to have rapidly adjusted to the increased methane flux (Fischer et al., submitted-a) which could explain why Fe-(oxyhydr)oxides are still present in large amounts even below the present day SMT depth. At the non

Hydrate-site, such a scenario is likely because pyrite concentrations display a gradient from the core-bottom to the core-top (Fig. 26 and 27). Furthermore, the overlapping depth profiles of magnetite and hydrogen sulfide in the interval from 150 cm to 180 cm provide further evidence for time-limitation of the suggested process, implying that in this interval a significant portion of the magnetite has not yet been reduced. At the Hydrate-site, however, the shift of the SMT may have occurred faster, or the SMT depth may have been located at a shallower depth prior to the increase in methane flux than at the non Hydrate-site, because the sulfidization front has apparently reached the sediment surface/core-top and pyrite is present over the whole core length.

6 Conclusions

Sediment cores retrieved from Nascent Ridge in the northern Arabian Sea were investigated with respect to pore water geochemistry, magnetic susceptibility, the distribution of solid phase Fe-species, and diagenetic overprinting by hydrogen sulfide. The gas hydrate-bearing core was characterized by sulfidic pore water and elevated concentrations of pyrite throughout, and showed a positive chloride and potassium anomaly, pointing to recent formation of gas hydrates. A substantial increase in methane flux triggered by the 1945 Balochistan earthquake led to formation of shallow gas hydrates and steep methane and sulfate gradients, and pushed the sulfate/methane transition (SMT) to the sediment surface, which initiated a sulfidization front to migrate towards the sediment surface. This front reached the core-top in the gas hydrate-bearing core. In contrast, the gas hydrate-free core showed a distinct sulfidization front separating Fe-(oxyhydr)oxide-rich sediment near the sediment surface from Fe-sulfide-rich sediment below. Perhaps unexpectedly, Fe-monosulfides such as greigite, which are common precursor iron species during pyritization, were not found in either core, which is most likely due to rapid pyritization of any Fe-monosulfides in situ due to high hydrogen sulfide concentrations. Magnetite is usually unstable in the presence of hydrogen sulfide but was detected at relatively high concentrations within the hydrogen sulfide-bearing intervals, i.e. below the SMT at both studied sites. This study supports earlier findings stating that the rise of the SMT and sulfidization front is related to methane injection into the shallow subsurface sediment during the Balochistan earthquake offshore

Pakistan in 1945. Our results suggest that a rapid increase in upward methane flux causing shallow gas hydrate formation can be recorded in sediments below the SMT by the co-occurrence of both reactive Fe-(oxyhydr)oxides (for example magnetite) and pyrite.

Acknowledgments

We are indebted to the captain and crew of RV Meteor during cruise M74/3 to the Arabian Sea. Karsten Enneking and André Gaßner supported us during shipboard sample processing and analyses. Matthias Zabel conducted sulfate measurements and Hella Buschhoff determined TIC/TOC contents. Heiko Sahling and Miriam Römer kindly provided the map. Christoph Vogt is thanked for XRD-measurements. For discussion of the Fe-extraction data we would like to thank Christian März and Tom Wagner. Akihiro Hiruta is acknowledged for insightful discussion of the chloride and potassium data. This study was funded through the DFG-Research Center/Cluster of Excellence ”The Ocean in the Earth System" (MARUM). We acknowledge further financial support from the Helmholtz Association (AWI, Bremerhaven). All data are available on the database Pangaea (http://www.pangaea.de).

References

Aharon, P., Roberts, H.H. and Snelling, R., 1992. Submarine venting of brines in the deep Gulf of Mexico: Observations and geochemistry. Geology, 20(6): 483-486.

Berner, R.A., 1970. Sedimentary pyrite formation. American Journal of Science, 268(1): 1-23.

Berner, R.A., 1984. Sedimentary pyrite formation: An update. Geochimica et Cosmochimica Acta, 48(4): 605-615.

Bohrmann, G. et al., 2008. Report and preliminary results of R/V Meteor cruise M74/3, Fujairah-Male, 30 October-28 November, 2007. Cold seeps of the Makran subduction zone (Continental margin off Pakistan). Berichte, Fachbereich 5, Universität Bremen, 266, Bremen, 161 pp.

Bohrmann, G., Greinert, J., Suess, E. and Torres, M., 1998. Authigenic carbonates from the Cascadia subduction zone and their relation to gas hydrate stability. Geology, 26(7): 647-650.

Bohrmann, G. and Torres, M.E., 2006. Gas hydrates in marine sediments. In: H.D. Schulz and M. Zabel (Editors), Marine geochemistry. Springer Verlag, Berlin, Heidelberg, New York, pp. 418–512.

Borowski, W.S., Paull, C.K. and Ussler, W., III, 1996. Marine pore-water sulfate profiles indicate in situ methane flux from underlying gas hydrate. Geology, 24(7): 655-658.

Bourget, J. et al., 2011. Turbidite system architecture and sedimentary processes along topographically complex slopes: the Makran convergent margin. Sedimentology, 58: 376-406.

Canfield, D.E. and Berner, R.A., 1987. Dissolution and pyritization of magnetite in anoxic marine sediments. Geochimica et Cosmochimica Acta, 51(3): 645-659.

Canfield, D.E., Raiswell, R. and Bottrell, S.H., 1992. The reactivity of sedimentary iron minerals toward sulfide. American Journal of Science, 292(9): 659-683.

Canfield, D.E., Raiswell, R., Westrich, J.T., Reaves, C.M. and Berner, R.A., 1986. The use of chromium reduction in the analysis of reduced inorganic sulfur in sediments and shales. Chemical Geology, 54(1-2): 149-155.

Canfield, D.E. and Thamdrup, B., 2009. Towards a consistent classification scheme for geochemical environments, or, why we wish the term ‘suboxic’ would go away. Geobiology, 7(4): 385-392.

Cline, J.D., 1969. Spectrophotometric determination of hydrogen sulfide in natural waters. Limnology and Oceanography, 14(3): 454-458.

Cornwell, J.C. and Morse, J.W., 1987. The characterization of iron sulfide minerals in anoxic marine sediments. Marine Chemistry, 22(2-4): 193-206.

Dickens, G.R., 2001. Sulfate profiles and barium fronts in sediment on the Blake Ridge: present and past methane fluxes through a large gas hydrate reservoir. Geochimica et Cosmochimica Acta, 65(4): 529-543.

Dickens, G.R., 2011. Down the Rabbit Hole: toward appropriate discussion of methane release from gas hydrate systems during the Paleocene-Eocene thermal maximum and other past hyperthermal events. Climate of the Past, 7: 831-846.

Ding, F. et al., 2010. Interaction between accretionary thrust faulting and slope sedimentation at the frontal Makran accretionary prism and its implications for hydrocarbon fluid seepage. Journal of Geophysical Research, 115(B8): B08106.

Ferdelman, T.G., Fossing, H., Neumann, K. and Schulz, H.D., 1999. Sulfate Reduction in Surface Sediments of the Southeast Atlantic Continental Margin between 15 'S and 27 'S (Angola and Namibia). Limnology and Oceanography, 44(3): 650-661.

Fischer, D., Mogollon, J.M., Strasser, M., Bohrmann, G. and Kasten, S., submitted-a. Nature Geoscience.

Fischer, D. et al., submitted-b. Interaction between hydrocarbon seepage, chemosynthetic communities and bottom water redox at cold seeps of the Makran accretionary prism: Insights from habitat-specific pore water sampling and modeling. Biogeosciences

Fossing, H., Ferdelman, T.G. and Berg, P., 2000. Sulfate reduction and methane oxidation in continental margin sediments influenced by irrigation (South-East Atlantic off Namibia). Geochimica et Cosmochimica Acta, 64(5): 897-910.

Froelich, P.N. et al., 1979. Early oxidation of organic matter in pelagic sediments of the eastern equatorial Atlantic: suboxic diagenesis. Geochimica et Cosmochimica Acta, 43(7): 1075-1090.

Fu, Y., von Dobeneck, T., Franke, C., Heslop, D. and Kasten, S., 2008. Rock magnetic identification and geochemical process models of greigite

formation in Quaternary marine sediments from the Gulf of Mexico (IODP Hole U1319A). Earth and Planetary Science Letters, 275(3-4): 233-245.

Funk, J.A., von Dobeneck, T. and Reitz, A., 2004. Integrated rock magnetic and geochemical quantification of redoxomorphic iron mineral diagenesis in late Quaternary sediments from the equatorial Atlantic. In: G. Wefer, S. Mulitza and V. Ratmeyer (Editors), The south Atlantic in the late Quaternary: Reconstruction of material budgets and current systems. Springer-Verlag, Berlin, Heidelberg, New York, Tokyo, pp. 237-260.

Greinert, J., Bollwerk, S.M., Derkachev, A., Bohrmann, G. and Suess, E., 2002. Massive barite deposits and carbonate mineralization in the Derugin Basin, Sea of Okhotsk: precipitation processes at cold seep sites. Earth and Planetary Science Letters, 203(1): 165-180.

Haeckel, M., Boudreau, B.P. and Wallmann, K., 2007. Bubble-induced porewater mixing: A 3-D model for deep porewater irrigation. Geochimica et Cosmochimica Acta, 71: 5135-5154.

Haeckel, M., Suess, E., Wallmann, K. and Rickert, D., 2004. Rising methane gas bubbles form massive hydrate layers at the seafloor. Geochimica et Cosmochimica Acta, 68(21): 4335-4345.

Hesse, R. and Harrison, W.E., 1981. Gas hydrates (clathrates) causing pore-water freshening and oxygen isotope fractionation in deep-water sedimentary sections of terrigenous continental margins. Earth and Planetary Science Letters, 55(3): 453-462.

Himmler, T., Bach, W., Bohrmann, G. and Peckmann, J., 2010. Rare earth elements in authigenic methane-seep carbonates as tracers for fluid composition during early diagenesis. Chemical Geology, 277(1-2): 126-136.

Hiruta, A., Snyder, G.T., Tomaru, H. and Matsumoto, R., 2009. Geochemical constraints for the formation and dissociation of gas hydrate in an area of high methane flux, eastern margin of the Japan Sea. Earth and Planetary Science Letters, 279(3-4): 326-339.

Hoehler, T., Alperin, M.J., Albert, D.B. and Martens, C., 1994. Field and laboratory studies of methane oxidation in an anoxic marine sediment: evidence for a methanogen-sulfate reducer consortium. Global Biogeochemical Cycles, 8: 451-463.

Holmkvist, L. et al., 2011. Sulfate reduction below the sulfateâ€“methane transition in Black Sea sediments. Deep Sea Research Part I: Oceanographic Research Papers, 58(5): 493-504.

Housen, B.A. and Musgrave, R.J., 1996. Rock-magnetic signature of gas hydrates in accretionary prism sediments. Earth and Planetary Science Letters, 139(3-4): 509-519.

Jørgensen, B.B., Böttcher, M.E., Lüschen, H., Neretin, L.N. and Volkov, I.I., 2004. Anaerobic methane oxidation and a deep H_2S sink generate isotopically heavy sulfides in Black Sea sediments. Geochimica et Cosmochimica Acta, 68(9): 2095-2118.

Kasten, S., Freudenthal, T., Gingele, F.X. and Schulz, H.D., 1998. Simultaneous formation of iron-rich layers at different redox boundaries in sediments of the Amazon deep-sea fan. Geochimica et Cosmochimica Acta, 62(13): 2253-2264.

Kukowski, N. et al., 2001. Morphotectonics and mechanics of the central Makran accretionary wedge off Pakistan. Marine Geology, 173(1-4): 1-19.

Larrasoaña, J.C. et al., 2007. Diagenetic formation of greigite and pyrrhotite in gas hydrate marine sedimentary systems. Earth and Planetary Science Letters, 261(3-4): 350-366.

März, C., Hoffmann, J., Bleil, U., de Lange, G.J. and Kasten, S., 2008. Diagenetic changes of magnetic and geochemical signals by anaerobic methane oxidation in sediments of the Zambezi deep-sea fan (SW Indian Ocean). Marine Geology, 255(3-4): 118-130.

Neretin, L.N. et al., 2004. Pyritization processes and greigite formation in the advancing sulfidization front in the upper Pleistocene sediments of the Black Sea. Geochimica et Cosmochimica Acta, 68(9): 2081-2093.

Nöthen, K. and Kasten, S., 2011. Reconstructing changes in seep activity by means of pore water and solid phase Sr/Ca and Mg/Ca ratios in pockmark sediments of the Northern Congo Fan. Marine Geology, 287(1-4): 1-13.

Novosel, I., Spence, G.D. and Hyndman, R.D., 2005. Reduced magnetization produced by increased methane flux at a gas hydrate vent. Marine Geology, 216(4): 265-274.

Peckmann, J. et al., 2001. Methane-derived carbonates and authigenic pyrite from the northwestern Black Sea. Marine Geology, 177(1-2): 129-150.

Platt, J.P., Leggett, J.K., Young, J., Raza, H. and Alam, S., 1985. Large-scale sediment underplating in the Makran accretionary prism, southwest Pakistan. Geology, 13: 507-511.

Poulton, S.W., 2003. Sulfide oxidation and iron dissolution kinetics during the reaction of dissolved sulfide with ferrihydrite. Chemical Geology, 202(1-2): 79-94.

Poulton, S.W. and Canfield, D.E., 2005. Development of a sequential extraction procedure for iron: implications for iron partitioning in continentally derived particulates. Chemical Geology, 214(3-4): 209-221.

Poulton, S.W., Krom, M.D. and Raiswell, R., 2004. A revised scheme for the reactivity of iron (oxyhydr)oxide minerals towards dissolved sulfide. Geochimica et Cosmochimica Acta, 68(18): 3703-3715.

Pyzik, A.J. and Sommer, S.E., 1981. Sedimentary iron monosulfides: Kinetics and mechanism of formation. Geochimica et Cosmochimica Acta, 45(5): 687-698.

Rickard, D., 1997. Kinetics of pyrite formation by the H2S oxidation of iron (II) monosulfide in aqueous solutions between 25 and 125 °C: The rate equation. Geochimica et Cosmochimica Acta, 61(1): 115-134.

Rickard, D. and Luther, G.W., 2007. Chemistry of Iron Sulfides. Chemical Reviews, 107(2): 514-562.

Rickard, D. and Morse, J.W., 2005. Acid volatile sulfide (AVS). Marine Chemistry, 97(3-4): 141-197.

Riedinger, N. et al., 2005. Diagenetic alteration of magnetic signals by anaerobic oxidation of methane related to a change in sedimentation rate. Geochimica et Cosmochimica Acta, 69(16): 4117-4126.

Ritger, S., Carson, B. and Suess, E., 1987. Methane-derived authigenic carbonates formed by subduction-induced pore-water expulsion along the Oregon/Washington margin. Geological Society of America Bulletin, 98(2): 147-156.

Roberts, A.P. and Weaver, R., 2005. Multiple mechanisms of remagnetization involving sedimentary greigite (Fe3S4). Earth and Planetary Science Letters, 231(3-4): 263-277.

Römer, M., Sahling, H., Pape, T., Spiess, V. and Bohrmann, G., submitted. Gas bubble emission from submarine hydrocarbon seeps at the Makran continental margin (offshore Pakistan). Journal of Geophysical Reseach.

Rowan, C.J., Roberts, A.P. and Broadbent, T., 2009. Reductive diagenesis, magnetite dissolution, greigite growth and paleomagnetic smoothing in marine sediments: A new view. Earth and Planetary Science Letters, 277(1-2): 223-235.

Schlüter, H.U. et al., 2002. The Makran accretionary wedge: sediment thicknesses and ages and the origin of mud volcanoes. Marine Geology, 185(3-4): 219-232.

Seeberg-Elverfeldt, J., Schlüter, M., Feseker, T. and Kölling, M., 2005. Rhizon sampling of porewaters near the sediment-water interface of aquatic systems. Limnology and Oceanography: Methods, 3: 361-371.

Snyder, G.T. et al., 2007. Pore water profiles and authigenic mineralization in shallow marine sediments above the methane-charged system on Umitaka Spur, Japan Sea. Deep Sea Research Part II: Topical Studies in Oceanography, 54(11-13): 1216-1239.

Stookey, L.L., 1970. Ferrozine - a new spectrophotometric reagent for iron. Analytical Chemistry, 42(7): 779-781.

Teichert, B.M.A. et al., 2003. U/Th systematics and ages of authigenic carbonates from Hydrate Ridge, Cascadia Margin: recorders of fluid flow variations. Geochimica et Cosmochimica Acta, 67(20): 3845-3857.

Torres, M.E., Bohrmann, G. and Suess, E., 1996a. Authigenic barites and fluxes of barium associated with fluid seeps in the Peru subduction zone. Earth and Planetary Science Letters, 144(3-4): 469-481.

Torres, M.E., Brumsack, H.J., Bohrmann, G. and Emeis, K.C., 1996b. Barite fronts in continental margin sediments: a new look at barium remobilization in the zone of sulfate reduction and formation of heavy barites in diagenetic fronts. Chemical Geology, 127(1-3): 125-139.

Torres, M.E. et al., 2004. Gas hydrate growth, methane transport, and chloride enrichment at the southern summit of Hydrate Ridge, Cascadia margin off Oregon. Earth and Planetary Science Letters, 226(1-2): 225-241.

von Rad, U. et al., 2000. Gas and fluid venting at the Makran accretionary wedge off Pakistan. Geo-Marine Letters, 20(1): 10-19.

von Rad, U. et al., 1996. Authigenic carbonates derived from oxidized methane vented from the Makran accretionary prism off Pakistan. Marine Geology, 136(1-2): 55-77.

von Rad, U. et al., 1999. Multiple monsoon-controlled breakdown of oxygen-minimum conditions during the past 30000 years documented in

laminated sediments off Pakistan. Palaeogeography, Palaeoclimatology, Palaeoecology, 152: 129-161.

Wehrmann, L.M. et al., 2011. The imprint of methane seepage on the geochemical record and early diagenetic processes in cold-water coral mounds on Pen Duick Escarpment, Gulf of Cadiz. Marine Geology, 282(1-2): 118-137.

Yao, W. and Millero, F.J., 1996. Oxidation of hydrogen sulfide by hydrous Fe(III) oxides in seawater. Marine Chemistry, 52(1): 1-16

.

Annex to Chapter IV

(not included in manuscript 3)

The effect of different storing techniques on Fe-species preservation

Routine solid phase sampling of anoxic sediments involves storage of subsamples frozen and under an inert gas atmosphere, in order to prevent secondary reactions during storage. However, sample quality may be lowered if samples are subject to discontinuous freezing or oxidation by atmospheric oxygen. We have tested the qualitative preservation potential of the Fe-mineralogy of samples obtained from core GeoB 12331-2 that were analyzed upon storing with different techniques. For that purpose one set of samples was taken onboard ship, i.e. immediately after core-retrieval in November 2007 and stored immediately under argon gas and frozen at -20°C until analysis in 2010/2011 (hereafter "stored under anoxic conditions"). This method prevents oxidation during storage and transport and hampers any secondary reaction. Another set of subsamples obtained from comparable, but not the same depths was obtained from the core in July 2010 and these samples were freeze-dried, ground and stored under oxic conditions at room temperature until analysis in January/February 2011 (hereafter "stored under oxic conditions"). The core had been stored at 4°C under oxic conditions between the two sampling campaigns in 2007 (at sea) and 2010 (onshore). We conducted the sequential extraction procedures described in the preceding chapter on both sample sets. The results are given in Fig. 28. General trends of the respective downcore profiles of the different Fe-species and involved diagenetic reactions are discussed in the preceding chapter.

Despite few outliers, we found a relatively good recovery of the $Fe_{goethite\ and\ hematite}$-(g.+h.), $Fe_{magnetite}$- and Fe_{pyrite}-fractions in both analyzed sample sets (Figs. 28 c, d and e). In contrast, in the fractions $Fe_{ferrihydrite}$ and Fe^{2+} adsorbed to minerals surfaces (Fe_{surf}), we detected distinctly different Fe concentrations in those samples stored anoxically, than in those stored under oxic conditions (Figs. 28 a and b). The concentrations of $Fe_{ferrihydrite}$ are generally higher in the samples stored oxic than in those stored anoxic (Fig. 28 b). In addition, only small

amounts of $Fe_{ferrihydrite}$ were found in the upper 150 cm of the "anoxic" samples (Fig. 28 b). Fe^{2+} is very sensitive to changes in the redox conditions, i.e. it is only stable in a reducing environment, which is essentially oxygen-free. This is very well reflected in the high Fe_{surf} concentrations in the samples that were stored anoxic (Fig. 28 a). On the other hand, this means that in the samples stored oxic a certain amount (~ 30%) of Fe_{surf} has been removed probably due to oxidation during storage, which results in a significantly lower recovery of this fraction (Fig. 28 a). If some of the Fe_{surf} has been oxidized from ferrous to ferric iron, where has the newly formed ferric iron gone?

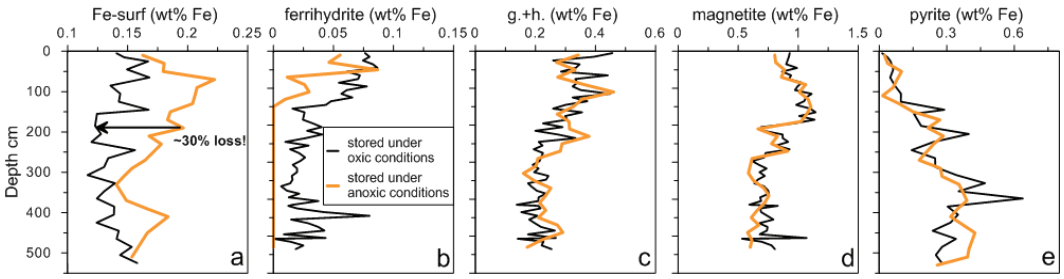

Figure 28: Results of the experimental comparison of different sediment storage techniques.

Apparently, Fe(III) derived from oxidation of the Fe_{surf}-pool has been added to the $Fe_{ferrihydrite}$-pool (Fig. 28 b), because in those samples stored oxic, more $Fe_{ferrihydrite}$ was found than in the samples stored anoxic. These observations lead to conclude that iron fractions with a higher degree of crystal order (goethite, hematite, magnetite, pyrite) are relatively unaffected by sample storage under oxic conditions over time periods of several years, whereas Fe^{2+} adsorbed to mineral surfaces is not stable under these conditions and is rapidly oxidized and apparently added to the $Fe_{ferrihydrite}$-pool. For investigations of the Fe-speciation in anoxic sediments it is thus strongly recommended to ensure that samples are stored under anoxic conditions and frozen. However, it is a striking feature that pyrite content is similarly high in samples stored oxic compared to those stored anoxic (Fig. 28 e). The expectation would be that pyrite is oxidized in the oxic sample set. A possible explanation for this observation is that pyrite in the samples stored oxic has been shielded from oxidation by a Fe-oxide-coating, which has similarly been described earlier (Morse, 1991).

Reference

Morse, J. W.: Oxidation kinetics of sedimentary pyrite in seawater, Geochim. Cosmochim. Acta, 55, 3665-3667, 1991.

Chapter V – Contribution to Co-Author Papers

Co-author paper 1:

Biogeochemistry of a low-activity cold seep in the Larsen B area, western Weddell Sea, Antarctica

H. Niemann, D. Fischer, D. Graffe, K. Knittel, A. Montiel, O. Heilmayer, K. Nöthen, T. Pape, S. Kasten,G. Bohrmann, A. Boetius, and J. Gutt

(Manuscript published in Biogeosciences 6, 2383–2395, 2009)

Abstract: First videographic indication of an Antarctic cold seep ecosystem was recently obtained from the collapsed Larsen B ice shelf, western Weddell Sea. Within the framework of the R/V Polarstern expedition ANTXXIII-8, we revisited this area for geochemical, microbiological and further videographical examinations. During two dives with ROV Cherokee (MARUM, Bremen), several bivalve shell agglomerations of the seep-associated, chemosynthetic clam *Calyptogena* sp. were found in the trough of the Crane and Evans glacier. The absence of living clam specimens indicates that the flux of sulphide and hence the seepage activity is diminished at present. This impression was further substantiated by our geochemical observations. Concentrations of thermogenic methane were moderately elevated with 2 µM in surface sediments of a clam patch, increasing up to 9 µM at a sediment depth of about 1m in the bottom sections of the sediment cores. This correlated with a moderate decrease in sulphate from about 28mM at the surface down to 23.4 mM, an increase in sulphide to up to 1.43 mM and elevated rates of the anaerobic oxidation of methane (AOM) of up to 600 pmol cm^{-3} d^{-1} at about 1m below the seafloor. Molecular analyses indicate that methanotrophic archaea related to ANME-3 are the most likely candidates mediating AOM in sediments of the Larsen B seep.

Co-author paper 2:

Distribution and abundance of gas hydrates in near-surface deposits of the Håkon Mosby Mud Volcano, SW Barents Sea

T. Pape, T. Feseker, S. Kasten, D. Fischer, G. Bohrmann

(Manuscript published in Geochemistry, Geophysics, Geosystems, 12, Q09009, 2011)

Abstract: The occurrence of gas hydrates at submarine mud volcanoes (MVs) located within the gas hydrate stability zone (GHSZ) is controlled by upward fluid and heat flux associated with MV activity. Determining the spatial distribution of gas hydrates at MVs is crucial to evaluate their sensitivity to known episodic changes in volcanic activity. We determined the hydrocarbon inventory and spatial distribution of hydrates at an individual MV structure. The Håkon Mosby Mud Volcano (HMMV), located at 1,250mwater depth on the Barents Sea slope, was investigated by combined pressure core sampling, heat flow measurements, and pore water chemical analysis. Quantitative pressure-core degassing revealed gas–sediment ratios between 3.1 and 25.7 corresponding to hydrate concentrations of up to 21.3% of the pore volume. Hydrocarbon compositions and physicochemical conditions imply that gas hydrates incipiently crystallize as structure I hydrate, with a dissociation temperature of around 13.8°C at this water depth. Based on numerous in situ measurements of the geothermal gradient in the seabed, pore water sulfate profiles and microbathymetric data, we show that the thickness of the GHSZ increases from less than 1 m at the warm center to around 47 m in the outer parts of the HMMV. We estimate the total mass of hydrate-bound methane stored at the HMMV to be about 102.5 kt, of which 2.8 kt are located within the morphological Unit I around the center and thus are likely to be dissociated in the course of a large eruption.

Chapter VI – Conclusions and Outlook

In chapter 2 we investigated the interaction of chemosynthetic communities, water column redox and seepage at four cold seeps located at the Makran continental margin. It was shown that on the one hand, water column redox, which determines if metazoan life is present, influences the geochemical zonation near the sediment surface at all investigated seeps: In case oxygen is present, metazoans including clams and polychaetes colonize the sediment surface and bioirrigate sulfate-rich bottom water into the sediment. Although the depth of the methane source is assumed to be fixed due to the occurrence of shallow gas hydrates at sites within the gas hydrate stability zone, bioirrigation shifts the SMT towards greater depths and thus steepens the gradients of sulfate and methane. As steeper gradients correspond to higher fluxes of these compounds into the reaction zone, higher rates of methane oxidation are fostered which increase the microbial filter-capacity of the sediment with respect to methane. On the other hand, seeps located within an oxygen-deficient environment lack any benthic metazoan life and hence bioirrigation. The depth of the SMT (i.e. the methane sink) is determined by the downward diffusive flux of sulfate and the upward advective transport of methane. Here, the microbial methane filter may be less efficient, because the SMT is usually located at shallower depth compared to seeps in oxygenated waters. In fact, the SMT may be pushed to the sediment surface by pore water advection which could allow methane to bypass the filter and escape into the bottom water. With regard to the scientific questions in chapter 1 this study shows how the interaction of bottom water redox, bioirrigation, and advection determines the depth of the SMT: Metazoans (indicative of oxic bottom water) bioirrigate the uppermost sediment with sulfate-rich water and thus exert control on the efficiency and depth at which the greenhouse gas methane is trapped and consumed within cold seep environments.

Chapter 3 dealt with the problem of an earthquake triggering and fostering hydrocarbon seepage at Nascent Ridge at the Makran continental margin. Pore water modeling and calculated ages of authigenic barite enrichments suggest a distinct increase in upward methane flux during an earthquake in 1945. The earthquake apparently led to the fracturing of gas hydrate-cemented sediments and thus induced the injection of large amounts of gas into the shallow sediment,

which has formerly been trapped underneath gas hydrates. The event very likely triggered the formation of cold seeps at the sediment surface. These seeps were still active 62 years after the eruption and we could show that the rate of gas released to the hydrosphere is similar to the rate at non-seismic cold seeps. Earthquakes triggering seepage should thus be considered in local and global carbon budgets. Referring to the scientific questions in chapter 1 it is clear that the time calculated to form authigenic barite in combination with nonsteady state pore water modeling is well suited to trace the upward migration of the SMT and to time single methane release events like the one in 1945. We suggest that seismic ground shaking can fracture gas hydrate-cemented sediments and thus represents a novel trigger of seepage in tectonically active regions, as for example subduction zones.

In chapter 4 the bulk Fe-species distribution and associated diagenetic processes were investigated for the sites described in chapter 3. We could show that the increase in gas flux in 1945 and the concomitant shift of the hydrogen sulfide-source (SMT) is as well recorded in the distribution of authigenic iron sulfides. Although the SMT has shifted upwards as a consequence of the earthquake, appreciable amounts of reactive iron phases were still present in sediments even below and within sulfidic intervals. This shows, that the iron in the sedimentary solid phase does belatedly respond to the changing redox regime in the pore water induced by the seismic event. It could not sufficiently be explained, however, why no Fe-monosulfides were detected, for example in the one core that showed a distinct sulfidization front. Transformation of Fe-(hydr)oxides involves a suite of intermediate Fe-monosulfides. We hypothesize that these are immediately pyritized by very abundant hydrogen sulfide. In order to study the effect of different storing techniques on the quality of anoxic sediment samples, an experimental investigation was conducted on two sample-sets obtained from comparable sediment depth of one of the cores investigated in chapter 4. The two sample-sets were stored under a) oxic or b) anoxic conditions, respectively. It was shown that those Fe-minerals that have a higher degree of crystal-order (goethite, hematite, magnetite, and pyrite) were not significantly affected by sample storage under oxic conditions. In contrast, the fractions of Fe^{2+} adsorbed to mineral surfaces (Fe-surf) and of ferrihydrite showed significantly different recoveries between the two sample-sets. While Fe-surf showed a clearly less well recovery in the samples stored under oxic conditions, ferrihydrite showed a significant increase in downcore concentrations in the oxic samples. This led to

the conclusion that secondary processes, as for example oxidation of reduced species by atmospheric oxygen, largely compromise the distribution and concentrations of low-crystallinity and highly reactive (towards hydrogen sulfide) minerals.

Although the above studies involve a suite of different inter-disciplinary approaches (geochemistry, numerical pore water modeling, geomicrobiology, geophysics), not all analyses that would be feasible to complete the picture could be done. For example, the sequential extraction of different iron phases conducted in chapter 4 could be improved and strengthened by also analyzing other species, for example different sulfur phases (for example elemental sulfur). In addition, the annex to chapter 4 shows that highly reactive iron species are very sensitive to inadequate sample storage. A detailed study assessing mineralogy alteration as a function of different storing techniques and time would be worthwhile. Furthermore, the habitat-specific sampling of cold seeps, as conducted in chapter 2, proved to be a powerful tool to evaluate the interplay of different pore water transport processes. A similarly high or even higher lateral coring/sampling resolution is desirable for cold seeps, in order to assess the habitat-specific transport regimes and solute fluxes.

Acknowledgements

This thesis would not have been possible without the constant support, faith and motivation I received from my principal supervisor Dr. Sabine Kasten. Sabine, you are not only a patient teacher but also a marvelous mentor. I will never forget these memorable days we shared in the cool-room of Meteor dissecting sediment cores in an environment characterized either by the delightful odor of hydrogen sulfide, or by the not always appealing appearance of Schnupsies (sp. nov; cf. tubeworms) and Mupfeln (sp.nov.; cf. clams), or a combination of these.

I am not less indebted to my second supervisor Prof. Gerhard Bohrmann. Gerhard, you agreed in "adopting" me in your group, which gave me the opportunity to talk to specialists in our field of research every time I had the feeling to drown in theoretical knowledge (or the lack thereof). Thanks for always having time for short discussions and jokes!

Did I say specialists? Well, this term goes together with the names Markus Brüning, Christian dos Santos Ferreira, Morten Hvitfeld Iversen, Tobias Himmler, Stefan Klapp, Jan-Hendrik Körber, Yann Marcon, Thomas Pape, Heiko Sahling, Michal Tomczyk, Jiangong Wei, Paul Wintersteller, and Ting Ting Wu. Not to mention our "science-managers" Greta Ohling and Angelika Rinkel. All of these united in the "Bohrmann Family" are a fantastic team!

I also dedicate a few words to a room: Ten-fifty! Thanks a lot to my office-mates Miriam, Morten and Ting Ting. We were quiet (if necessary); we were silly (most often); we were cynical (less, but still often); we shared the pleasure of being hung-over (regularly); we were friends (always).

What is a developing PhD-thesis without expeditions, discussions, coffee-breaks, conferences, co-authors, and a delightful stay abroad? Thank you Inka Meyer, Tobias Goldhammer, Tim Haarmann, Susann Henkel, Kara Bogus, Ludmila Baumann, Ingrid Stimac, Torben Gentz, Michael Schlüter, Luzie Schnieders, Jörn Peckmann, Matthias Zabel, Simon Poulton, Christian März, Lindi Lou Fryer, James Izon, José Mogollon, Akihiro Hiruta, Heide Schulz-Vogt, Petra Pop Ristova, Sven Kretschmer, Christoph Vogt, Ralle Rehage, Antje Boetius, Sarah Sokoll, my friends.

An honest "Thank you" goes to my parents Agnes and Ulrich Fischer, to my four lovely siblings and my cute niece. Didn´t meet you guys that often recently, but it felt all strange if it were too long breaks. Furthermore, I would have had utterly hard times, if I had not received your motivational (all) and monetary (parents) support throughout the years.

Maya: If your patience is a mountain and if your empathy is a rock, then your love must surely be a diamond. Tack så mycket for the often cited "everything"!

Erklärung

Erklärung gemäß § 6 Abs. 5 der Promotionsordnung der Universität Bremen für die mathematischen, natur- und ingenieurwissenschaftlichen Fachbereiche.

Hiermit versichere ich, dass ich

1. die vorliegende Arbeit ohne unerlaubte fremde Hilfe angefertigt habe,

2. keine anderen als die von mir angegebenen Quellen und Hilfsmittel benutzt habe,

3. die den benutzen Werken wörtlich oder inhaltlich entnommenen Stellen als solche kenntlich gemacht habe.

Bremen, den 29. November 2011

David Fischer